THESIS APPROVAL

GRADUATE SCHOOL, KASETSART UNIVERSITY

Doctor of Engineering (Mechanical Engineering)

DEGREE

Mechanical Engineering	Mechanical Engineering
FIELD	**DEPARTMENT**

TITLE: Study and Analysis of Engine Vibration, Effect of Using Hydrogen-diesel dual Fuel

NAME: Mister Boonthum Wongchai

THIS THESIS HAS BEEN ACCEPTED BY

THESIS ADVISOR

(Associate Professor Porranat Visuwan, Ph.D.)

THESIS CO-ADVISOR

(Assistant Professor Sathaporn Chuepeng, Ph.D.)

DEPARTMENT HEAD

(Associate Professor Chawalit Kittichaikarn, Ph.D.)

APPROVED BY THE GRADUATE SCHOOL ON _____

DEAN

(Associate Professor Gunjana Theeragool, D.Agr.)

THESIS

STUDY AND ANALYSIS OF ENGINE VIBRATION, EFFECT OF USING HYDROGEN-DIESEL DUAL FUEL

BOONTHUM WONGCHAI

A Thesis Submitted in Partial Fulfillment of
the Requirements for the Degree of
Doctor of Engineering (Mechanical Engineering)
Graduate School, Kasetsart University
2013

Boonthum Wongchai 2013: Study and Analysis of Engine Vibration, Effect of Using Hydrogen-diesel Dual Fuel. Doctor of Engineering (Mechanical Engineering), Major Field: Mechanical Engineering, Department of Mechanical Engineering. Thesis Advisor: Associate Professor Porranat Visuwan, Ph.D. 126 pages.

Hydrogen is one of the promising alternative fuels that can be used in internal combustion engines in order to reduce fossil fuel consumption and engine-out emissions. In this work, hydrogen is fumigated in to a diesel engine as hydrogen-diesel dual fuel operation with usual diesel fuel injected adjacent to the top dead center. The hydrogen addition is found to change the cylinder pressure characteristics and affect the engine vibration. In effects, the cylinder pressure and the engine vibration in terms of engine acceleration were studied. The single cylinder Kubota RT100 direct injection diesel engine was tested on the engine test bed equipped with engine indicating system and arrays of accelerometers. Hydrogen at various quantities of 0, 5, 10, 15, and 20 lpm was added and mixed with the air at the intake manifold before induced in to the cylinder. The cylinder pressure and the accelerations in x, y, and z directions installed beneath the engine base are measured at constant speeds and various torques.

The experimental results show that the maximum cylinder pressure, the average peak acceleration in all directions, and the peak of the magnitude of the difference between the acceleration vector summations at the engine supports with the hydrogen percentage of i% and the hydrogen percentage of 0% reduced with the increasing hydrogen percentage addition while the coefficient of variation of the maximum pressure increased. Consequently, the needs for optimization between the engine vibration reduction and the maximum pressure variation are prospectus for future work.

_____ _____ __ / __ / ____

Student's signature Thesis Advisor's signature

ACKNOWLEDGEMENTS

I would like to grateful thank to Assoc. Prof. Dr. Porranat Visuwan my thesis advisor and Asst. Prof. Dr. Sathaporn Chuepeng my thesis co-advisor for advice and every things for completely writing of thesis.

The present study was conducted at Kasetsart University Si Racha Campus. The authors would like to thank the Kasetsart University Research and Development Institute (KURDI) for the provision of the research grant to this project under the contract number V-T(D)173.53. The Kasetsart University Center for Advanced Studies in Industrial Technology under the National Research University (NRU) project is also acknowledged for the support to this study.

I would like to thank Buddha's Dhamma for guiding my life to solve every problems.

Boonthum Wongchai

February 2013

TABLE OF CONTENTS

Page

LIST OF TABLES

LIST OF FIGURES

LIST OF FIGURES (Continued)

LIST OF FIGURES (Continued)

LIST OF FIGURES (Continued)

LIST OF FIGURES (Continued)

LIST OF FIGURES (Continued)

LIST OF FIGURES (Continued)

LIST OF FIGURES (Continued)

LIST OF FIGURES (Continued)

Appendix Figure

LIST OF ABBREVIATIONS

A	=	the area of a piston head
a_0	=	the magnitude of the acceleration vector summation at the engine supports with the hydrogen percentage of 0%
a_A	=	the acceleration at point A
APA	=	average peak acceleration
Δa	=	The magnitude of the different between the acceleration vector summation at the engine supports with the hydrogen percentage of i% and the hydrogen percentage of 0%
Δa_{peak}	=	The peak of the magnitude of the different between the acceleration vector summation at the engine supports with the hydrogen percentage of i% and the hydrogen percentage of 0%
$\left(\frac{A}{F}\right)_s$	=	stoichiometic air/fuel ratio
c	=	damping constant
$COV_{P_{max}}$	=	coefficient of variation of the maximum pressure
f	=	frequency
F	=	the pressure force at a piston head
F_{0_4}	=	the inertia force of a piston
F_{23}	=	reaction force of a crank rod act on a connecting rod
F_{43}	=	reaction force of a piston act on a connecting rod
F_{A_3}	=	the inertia force of a connecting rod at point A
F_{B_3}	=	the inertia force of a connecting rod at point B
F_c	=	viscous force
F(t)	=	force
$\%H_2$	=	hydrogen percentage
k	=	spring constant
ℓ	=	the length of a connecting rod
ℓ_A	=	the length from point A to point g_3

LIST OF ABBREVIATIONS (Continued)

ℓ_B	=	the length from point A to point g_3
λ_x	=	a unit vector in the direction x
λ_y	=	a unit vector in the direction y
m	=	mass
m_3	=	the mass of a connecting rod
m_{A_3}	=	the separated mass of a connecting rod at point A
m_{B_3}	=	the separated mass of a connecting rod at point B
m_{Diesel}	=	diesel mass flow rate
m_f	=	fuel mass flow rate
m_{H_2}	=	Hydrogen mass flow rate
n	=	order of polynomial function
N	=	frequency in rpm
N_A	=	numbers of amplitude
ω	=	angular frequency/force frequency
ω_d	=	circular frequency of damped oscillation
ω_n	=	angular natural frequency
P	=	the pressure in a cylinder
P_{max}	=	average of the maximum pressure
ϕ	=	phase angle
T	=	shaft torque
τ	=	period
R_1, R_2	=	the reactive force at the support
R^2	=	coefficient of determination
RMS	=	root mean square
S	=	the shaking force due to the engine block
$S.D._{P_{max}}$	=	standard deviation of the maximum pressure
x	=	displacement

LIST OF ABBREVIATIONS (Continued)

$\dot{x}$	=	velocity
$\ddot{x}$	=	acceleration
X	=	Amplitude
$\ddot{x}_A$	=	average peak acceleration in x direction
$\ddot{x}_{peak}$	=	peak of the acceleration in x direction
$\ddot{y}_A$	=	average peak acceleration in y direction
$\ddot{z}_A$	=	average peak acceleration in z direction
ς	=	damping factor

STUDY AND ANALYSIS OF ENGINE VIBRATION, EFFECT OF USING HYDROGEN-DIESEL DUAL FUEL

INTRODUCTION

In the present day, compression ignition (diesel) engines are commonly used in vehicle transportations, industrials, electric power plants, and etc. Diesel engines are able to operate with a wide range of fuels, diesel oil, bio-diesel, and dual fuel. According to the global warming and energy problems, the alternative fuels are used to decrease the quantity of carbon dioxide (CO_2) in the atmosphere and diesel oil consumption. Hydrogen-diesel dual fuel is one choice of the alternative fuels. At the same output energy, the products from the combustion between hydrogen-diesel dual fuel and air produce lesser CO_2 than that of the combustion of diesel oil and air.

Hydrogen (H_2), the highly flammable gas which burns in air at a wide range of concentrations, can be produced from a wide variety of resources. Hydrogen-diesel dual fuel is the combination of hydrogen and diesel. In diesel engine applications, the chemical reaction will be started at the end of the compression stroke. The high-temperature, high-pressure, gases push the piston down and rotate the crank. The engine vibration is generated by the transmission force from the piston head to the crank support.

Engine vibration is the main topic in engineering problems. Hydrogen-diesel dual fuel may cause more engine vibration than diesel oil because of its highly combustion. In the present work, the effect of hydrogen on diesel engine vibration is the main object to study. However, cylinder pressure is the main factor of engine vibration. The relation of hydrogen quantity, cylinder pressure, and engine vibration must be studied.

OBJECTIVES

1. To study the cylinder pressure when using hydrogen-diesel dual fuel.
2. To study the diesel engine vibration when using hydrogen-diesel dual fuel.

Scope of thesis

1. This research proposes the study of the effect of hydrogen addition on the cylinder pressure and the engine vibration.

2. For elimination of the effect of multi piston on engine unbalance and engine vibration, a single cylinder Kubota RT100 direct injection diesel engine is used to test on the engine test bed with hydrogen-diesel dual fuel.

3. The hydrogen is added by fumigation with the flow rates are 0, 5, 10, 15 and 20 lpm at pressure of 1 bar and temperature of 25 °C.

4. The test conditions of the engine speeds and the engine torque are 2,000 rpm with 25% full load, 2,000 rpm with 50% full load, 1,600 rpm with 15% full load, and 1,600 rpm with 25% full load. The engine speed of 2,000 rpm is close to the maximum speed of the engine mean while the engine speed of 1,600 rpm is the common use of this engine.

5. The regression analysis is used to determine the equation of the graphs by linear equation (n = 1) and polynomial equation (n = 2).

LITERATURE REVIEW

This chapter presents diesel engine systems, hydrogen-diesel dual fuel and diesel engine vibrations.

1. Diesel engine

Compression ignition (diesel) engines are common used in cars, buses, ships, diesel power plants, and etc. Today, the economy saving of diesel fuel is the main topic of energy saving. Diesel engines are able to use a wide range of fuels, bio-diesel, and hydrogen-diesel dual fuel.

1.1 Four-stroke diesel Engines

In a diesel engine, fuel and air are mixed internally. The intake stroke; during the piston moves from top dead center (TDC) to bottom dead center (BDC) only air is inducted to the cylinder (Ferguson, 1986). The intake valve is opened and the exhaust valve is closed as shown in Figure 1 (A).

The compression stroke; the piston moves from BDC to TDC. The diesel injector(s) consists of a high pressure injection(s) of fuel when the air is at a high temperature. The auto-ignition of mixed fuel-air region initiates the combustion process. The intake valve and the exhaust valve are closed as shown in Figure 1 (B).

The power stroke; the piston moves from TDC to BDC. The high pressure from the chemical reaction of the mixed fuel-air region moves the piston and transfers the chemical energy to the engine torque. The intake valve and the exhaust valve are closed as shown in Figure 1 (C).

The exhaust stroke; the piston moves from BDC to TDC. The exhaust gas is ejected from the cylinder. The intake valve is closed and the exhaust valve is opened as shown in Figure 1 (D)

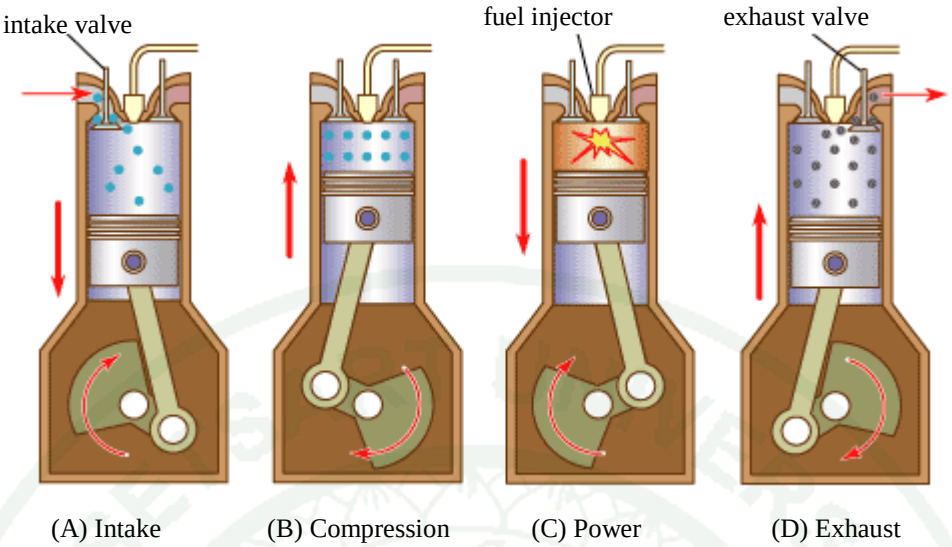

Figure 1 Four-stroke diesel engine

Source: Encyclopedia Britannica Inc (2007)

1.2 Two-stroke diesel engines

The compression stroke; the piston moves from BDC to TDC. The intake port is closed by the piston. The exhaust valve is closed. At the top of the stroke, fuel is injected into the cylinder as shown in Figure 2 (A). The combustion of the fuel-air region starts and generates the high pressure gases at the piston head.

The power stroke; the piston moves from TDC to BDC. The exhaust valve still closes until the piston head moves down to uncover the intake port. The burned gases are carried out and are taken place by the air as shown in Figure 2 (B).

2. The combustion stoichiometry

For a general hydrocarbon of a molecular composition C_aH_b combusted with air, the complete combustion equation is

$$C_aH_b + \left(a + \frac{b}{4}\right)(O_2 + 3.773N_2) = aCO_2 + \frac{b}{2}H_2O + 3.773\left(a + \frac{b}{4}\right)N_2 \qquad (1)$$

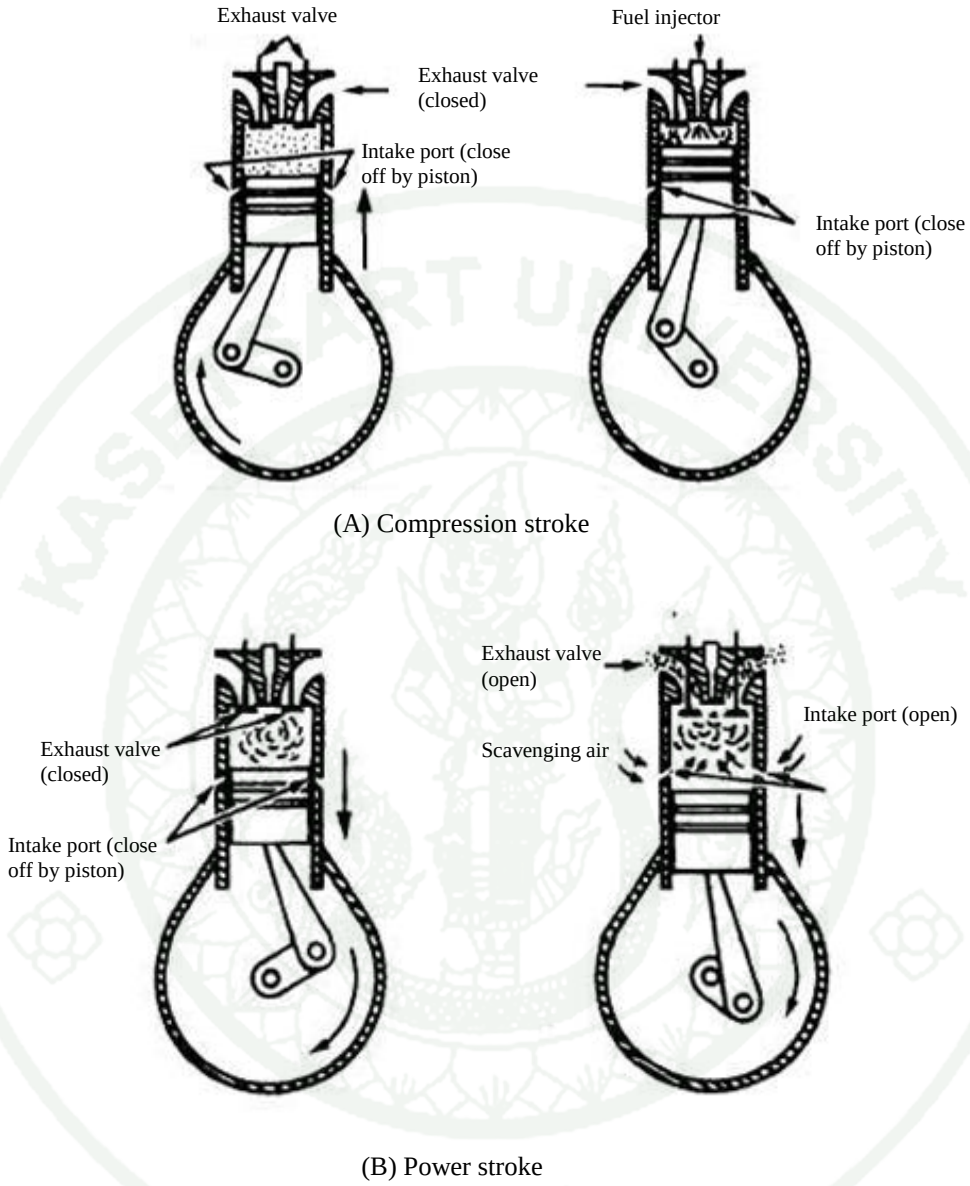

Figure 2 Two-stroke diesel engines

Source: Fireman (1987)

Equation (1) is the theoretical proportions of fuel and air. The complete chemical reaction of them requires at least air quantity in equation (1). The equation of the stoichiometic air/fuel ratio is

$$\left(\frac{A}{F}\right)_s = \frac{m_a}{m_f} = \frac{(a + b/4)(32 + 3.773 \times 28.16)}{12.011a + 1.008b} \quad (2)$$

where:

$\left(\frac{A}{F}\right)_s$ = stoichiometic air/fuel ratio.

For diesel oil $C_{15}H_{28}$ (is used in this research), the stoichiometric combustion equation is

$$C_{15}H_{28} + 22(O_2 + 3.773N_2) = 15CO_2 + 14H_2O + 83.006N_2 \quad (3)$$

From equation (2), the stoichiometic air/fuel ratio will be

$$\left(\frac{A}{F}\right)_s = 14.61 \quad (4)$$

Diesel engines are divided into two types: direct-injection (DI) engine and indirect-injection (IDI) engine. The direct-injection engines have a single combustion chamber where the fuel is injected directly into the combustion chamber. Meanwhile, the indirect-injection engines have the prechamber and the main chamber. The fuel is first injected into the prechamber and the combustion propagates into the main combustion chamber.

The combustion process of the direct-injection engine with one injection per engine can be identified on typical heat release-rate diagram as shown in Figure 3 (Heywood, 1988). Ignition delay (ab) is the period between the start of fuel injection into the combustion chamber and the start of combustion. Premixed combustion phase (bc) is the phase of combustion of fuel and air mixture occurs rapidly in a few crank angle degree and generate the high heat release rates. Mixing-controlled combustion phase (cd) is the phase of the heat release rate controlled by the fuel vapor-air mixing

process. Late combustion phase (de) is the phase of the heat release rate continuous at a lower rate because a small fraction of the fuel may not completely burn.

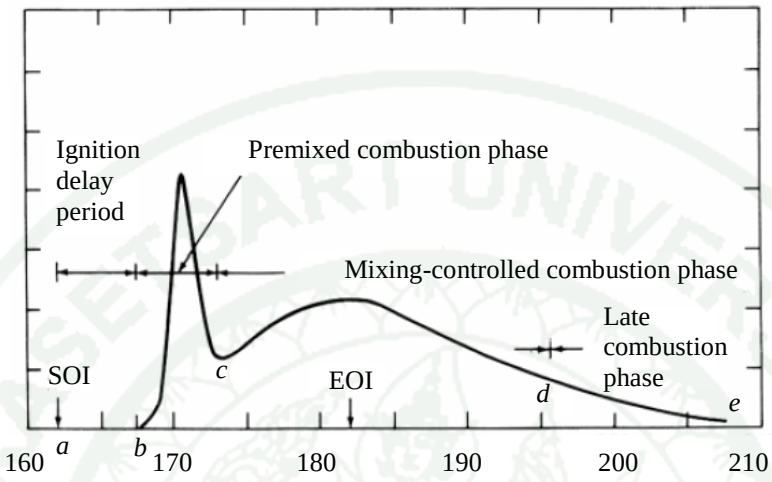

Figure 3 Typical direct injection heat-release rate diagram identifying different diesel combustion engine

Source: Heywood (1988)

3. Hydrogen production

Hydrogen is the most common element on earth; H_2 can be produced from various materials, e.g. water, fossil energy source, coal, biomass, hydrogen sulphide, anthropogemic waste, and etc. (Williams, 1980; Abbas and Daud, 2010; Sun *et al.*, 2012). Hydrogen production methods are categorized in six classes, electrochemical, thermochemical, photochemical, radiochemical, biochemical, and hybrid. From these methods can identify five sustainable hydrogen production, pathways, water splitting, hydrogen extraction from waste materials, fossil hydrocarbons decarbonizatoin, hydrogen sulfide decomposition, and biomass conversion (Eker and Kargi, 2010; Kargi *et al.*, 2011; Cai *et al.*, 2012; Dincer and Zamfirescu, 2012). Extraction of hydrogen requires energy. The main energy sources are fossil energy source, solar, hydro, biomass, geothermal, nuclear, wind, ocean thermal, and tidal. Water electrolysis

is a principally method for producing highly-pure hydrogen (Cox and Williamson; 1997).

Hydrogen production methods are several used in automotive applications. They are a combination of major reforming technique such as steam reforming, partial or complex oxidation, water-gas shift reaction, auto thermal reforming, and etc. (Tsolakis *et al.*, 2005)

Steam reforming (SR) is widely used and the most efficiency method to produce commercial hydrogen (Murdov, 2000; Profeti, 2009). Stream react with hydrocarbon to separate carbon oxides and hydrogen at high temperatures (700-1100°C) and in the suitable catalyst (Ahmed and Krumpelt, 2001). The equation of the stoichiometric reaction of the oxygenate fuel $C_xH_yO_z$ given by Garcia *et al.*, (2000) is

$$C_xH_yO_z + (x-z)H_2O \rightarrow xCO + (x+\frac{y}{2}-z)H_2, \ Q_{PR} > 0 \quad (5)$$

Q_{PR} = Heat of reaction (kcal or MJ)

The other commercial hydrogen production method is partial oxidation (PO). Equation (6) show that the sub-stoichiometric fuel/oxygen ratio of the PO. Oxygen limited restricts the fuel oxidation to separate carbon dioxide and water (Muradov, 2000). However this process is the inherently exothermal and the products are unstable products. Carbon dioxide and water, the products from complete oxidation of the PO in Equation (7) may also take place depending on the condition in the reactor. These are undesirable products.

$$C_xH_yO_z + \left(\frac{x}{2}-\frac{z}{2}\right)O_2 \rightarrow xCO + \frac{y}{2}H_2, \ Q_{PR} < 0 \quad (6)$$

$$C_xH_yO_z + \left(x+\frac{y}{4}-\frac{z}{2}\right)O_2 \rightarrow xCO_2 + \frac{y}{2}H_2O, \ Q_{PR} < 0 \quad (7)$$

The water gas-shift reaction (WGSR) use the product carbon monoxide from SR process in Equation (5). The product carbon monoxide can react with excess stream to produce hydrogen at temperature below 750°C (Grenoble *et al*, 1981).

$$CO + H_2O \rightarrow CO_2 + H_2, \quad Q_{PR} < 0 \tag{8}$$

The auto-thermal reforming (ATR) in Equation (9) is the combination of the SR and the PO. The reaction of the SR and the PO are generated by feeding the fuel, steam, and oxygen together into a catalytic reactor. The heat generated by the PO is absorbed by the SR reaction and the maximum temperature in the reactor is limited (Ahmed and Krumpelt, 2001).

$$C_xH_yO_z + \left(x - \frac{y}{4} - \frac{z}{2}\right)O_2 + H_2O \rightarrow xCO + \left(\frac{y}{2} + 1\right)H_2, \; Q_{PR} < 0 \tag{9}$$

4. Hydrogen storage

Hydrogen is an alternative energy and it is a gas in the earth's atmosphere. Hydrogen can be storaged as a gas, liquid, and in a solid material-hydrogen system (Cox and Williamson, 1997; Williams, 1980).

For the hydrogen gas storage, the high-pressure cylinder tanks are commonly used at pressures ranging from 150 to 400 bar and at a maximum pressure of 200 bar in commonly use (Williams, 1980; Langohr, 2007). High tensile strength metallic material can store hydrogen gas at high pressure more than 400 bar but they are usually associated with a weight penalty. The new light weight composite materials such as carbon-fiber compounds or others have been use to build the hydrogen gas storage tank.

Hydrogen has the low critical temperature of 33K to change from gas phase to liquid phase. For the hydrogen liquid storage, the cryogenic tanks are used at 21.1 K at ambient temperature. The simplest liquefaction proceed the Joule-Thomson cycle is

used to explain the hydrogen liquefaction process (Züttle, 2003). Firstly, Hydrogen gas is compressed and cooled in the heat exchanger. Secondly, in the expansion process, it pass through a throttle valve and change from the gas to the liquid-gas mixture. After expansion, the cool gas is separated from the liquid and return to the heat exchanger and it is compressed by the compressor again. The liquid nitrogen (78 K) is commonly used for pre-cool hydrogen before the first step.

Hydrogen can undergo physio-absorption on a high specific surface area. For solid material-hydrogen system, interaction in metals and complex hydrides is used (Cox and Williamson, 1997; Williams, 1980; Züttle, 2003; Demirci *et al.*, 2009; Luzan *et al.*, 2009; Pukazhselvan, 2012.) The resonant fluctuation in charge distributions (Val der Waals interactions) are the cause of the physio-absorption of hydrogen. The hydrogen molecule can interact at the surface of a solid carbon and increases with temperature and absorption temperature.

5. Hydrogen-diesel dual fuel

Hydrogen can use as dual fuel in SI engines (Houseman and Hoehn, 1974; Apostolescu and Chiriac, 1996; Ji, 2009; Escalante and Fernandez, 2010; Wang[1] *et al.*, 2010; Wang[2] *et al.*, 2012) and CI engines (Badr *et al.*, 1999; Tomita *et al.*, 2001; Saravanan *et al.*, 2007; Korakianitis *et al.*, 2010; Lata *et al.*, 2011; Shin *et al.*, 2011; Miyamoto *et al.*, 2011; Wu *et al.*, 2012).

In diesel engines, hydrogen is mixed with the air by direct mixing in the manifold or by injection directly into the cylinder (Badr, *et al.*, 1999; Escalante and Fernandez, 2010). The auto ignition occurs when diesel fuel is injected before TDC in the compression stroke. From the study of hydrogen-diesel dual fuel combustion, the results show that the emitted carbon oxides, hydrocarbon, and smoke are reduced (Tomita *et al.*, 2001; Escalante and Fernandez, 2010).

For hydrogen fuel, the stoichiometric combustion equation is

$$H_2 + 0.5(O_2 + 3.773N_2) = H_2O + 1.887N_2 \quad (10)$$

The equation of hydrogen percentage ($\%H_2$) on mass basis of hydrogen-diesel dual fuel is

$$\%H_2 = \frac{m_{H_2}}{m_f} \times 100 \quad (11)$$

where:

m_{H_2} = hydrogen mass flow rate (kg/s)

m_f = fuel mass flow rate (kg/s)

The fuel mass is the combination of hydrogen mass and diesel mass

$$m_f = m_{H_2} + m_{Diesel} \quad (12)$$

where:

m_{Diesel} = diesel mass flow rate (kg/s)

For hydrogen-diesel dual fuel with hydrogen percentage of $\%H_2$, Equation (3) and Equation (10) can be written as

$$(1-\%H_2)[C_{15}H_{28} + 22(O_2 + 3.773N_2) = 15CO_2 + 14H_2O + 83.006N_2] \quad (13)$$

and

$$\%H_2[H_2 + 0.5(O_2 + 3.773N_2) = H_2O + 1.887N_2] \quad (14)$$

The stoichiometric combustion is the combination of Equation (13) and Equation (14).The new stoichiometric combustion equation for the hydrogen-diesel

dual fuel will be

$$(1-\%H_2)[C_{15}H_{28}]+\%H_2[H_2]+\{22(1-\%H_2)+0.5(\%H_2)\}[O_2+3.773N_2]= 15(1-\%H_2)[CO_2]+\{14(1-\%H_2)+(\%H_2)\}[H_2O]+\{83.006(1-\%H_2) +1.887(\%H_2)\}[N_2] \quad (15)$$

The stoichiometric air/fuel ratio of the combustion of hydrogen-diesel dual fuel can be written as

$$\left(\frac{A}{F}\right)_s = \frac{\{22(1-\%H_2)+0.5(\%H_2)\}[O_2+3.773N_2]}{(1-\%H_2)[C_{15}H_{28}]+\%H_2[H_2]} \quad (16)$$

6. Fundamentals of Mechanical vibration

6.1 Mass-spring system

The foundation of mechanical vibration starts from mass-spring system (m-k) as shown in Figure 4. The mass m is supported by spring with the spring constant k and is acted by force F(t).

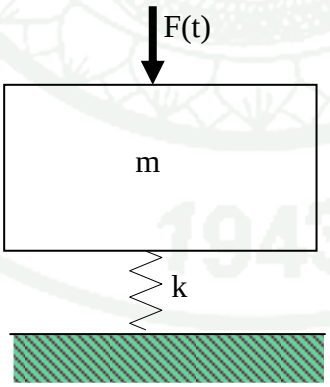

Figure 4 Mass-spring system (m-k)

The equation of motion (EOM) of the mass-spring systems is

$$m\ddot{x}+kx=F(t) \quad (17)$$

where:

m = mass (kg)

x = displacement (m)

$\ddot{x}$ = acceleration ($\frac{m}{s^2}$)

k = spring constant ($\frac{N}{m}$)

F(t) = force (N)

t = time (s)

Equation (17) can be written as

$$\ddot{x}+\omega_n^2 x=\frac{1}{m}F(t) \tag{18}$$

where:

ω_n = angular natural frequency ($\frac{rad}{s}$)

and

$$\omega_n=\sqrt{\frac{k}{m}} \tag{19}$$

In the case of F(t) =0, Equation (18) is linear and homogenous differential equation called free vibration. The general solution is

$$x=X\sin(\omega_n t+\phi) \tag{20}$$

where:

X = amplitude (m)

ϕ = phase angle (rad)

6.2 Mass-spring-damper system (m-k-c)

The mass-spring-damper system in Figure 5 is developed from the mass-spring system. Dampers are used to decrease the vibrations by damper forces e.g. viscous force, dry friction force, and internal friction force. The viscous dampers are commonly used in mechanical vibrations. When a piston moves in a cylinder through a viscous fluid, the viscous force always acts in a direction opposite to a piston velocity. The equation of the viscous force is

$$F_c = c\dot{x} \tag{21}$$

where:

F_c = viscous force (N)

c = damping constant ($\frac{N \cdot s}{m}$)

$\dot{x}$ = velocity ($\frac{m}{s}$)

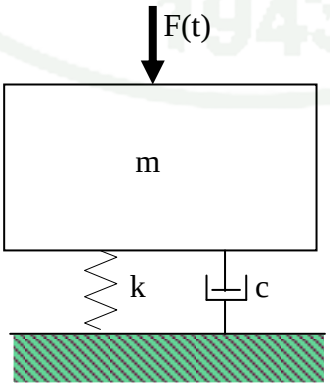

Figure 5 Mass-spring-damper system (m-k-c)

The equation of motion (EOM) of the mass-spring-damper systems is

$$m\ddot{x}+c\dot{x}+kx=F(t) \tag{22}$$

Equation (22) can be written as

$$\ddot{x}+2\varsigma\omega_n\dot{x}+\omega_n^2 x=\frac{1}{m}F(t) \tag{23}$$

where:

ς = damping factor

and

$$\varsigma=\frac{c}{2m\omega_n} \tag{24}$$

For free vibration (F(t)=0), oscillatory motion occurs when $\varsigma < 1$ called underdamped case. The general solution is

$$x = Xe^{-\varsigma\omega_n t}\sin(\omega_d t+\phi) \tag{25}$$

where:

ω_d = circular frequency of damped oscillation ($\frac{rad}{s}$)

and

$$\omega_d = \omega_n \sqrt{1-\varsigma^2} \tag{26}$$

If F(t) $\neq$ 0, Equation (18) and Equation (23) are called force vibration. F(t) are in the forms of harmonic functions (sine function and cosine function) and transient functions (step function, ramp function, rectangular function, haft sine function, and etc.).

For $F(t) = \sin(\omega t)$, the general solution of Equation (23) is

$$x = X_1 e^{-\varsigma\omega_n t} \sin(\omega_d t + \phi_1) + X_2 \sin(\omega t - \phi_2) \tag{27}$$

where

ω = force frequency ($\frac{\text{rad}}{\text{s}}$)

The first term in Equation (27) can be eliminated when the system becomes steady state vibration and the Equation (27) can be rewritten

$$x = X\sin(\omega t - \phi) \tag{28}$$

If function F(t) is transient, there are many cases of vibration system and many general solutions. Laplace transform technique is commonly used in transient function to find the general solution.

In addition, If function F(t) is in other forms, many functions may be the cause of nonlinear equations. If the analytical mathematics cannot solve these equations, the numerical method must be used.

7. Engine force analysis

In Figure 6, when fuel is burned in the cylinder, combustion pressure P is generated and pushes the piston downward with the force F which is transferred force to the connecting rod and crank. The vibration is generated by the forces (in vertical and horizontal direction) while the torsional vibration is generated by the shaft torque. The angular displacement and the angular velocity are used in torsional vibration analysis and vibration controlling (Li and Stone, 1999; Fredrik and Toivonen, 2008.)

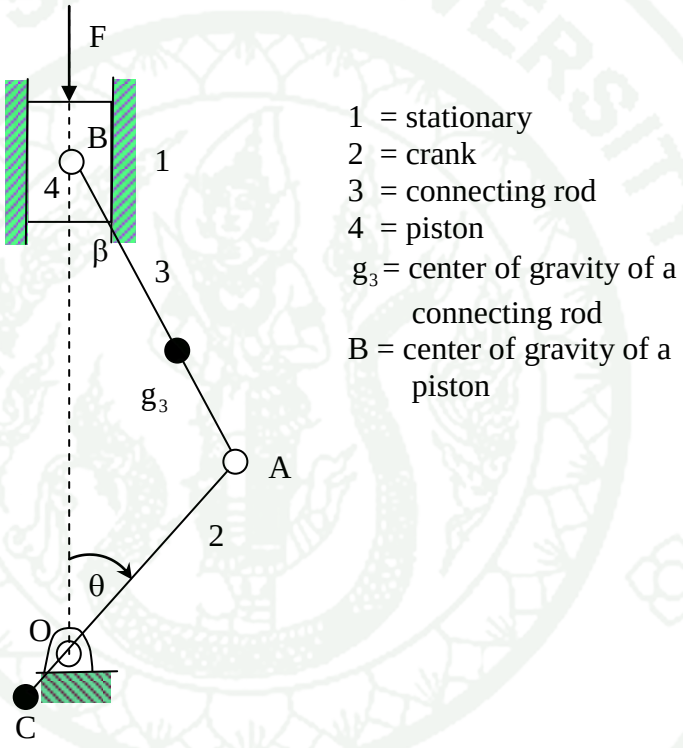

Figure 6 The slider crank mechanism

The relation of the force F and the pressure P in the cylinder is

$$F = PA \tag{29}$$

Where:

F = the pressure force at a piston head (N)

P = the pressure in a cylinder (Pa)

A = the area of a piston head (m^2)

The pressure P is the function of the crank angle θ as show in Figure 7. Thus F can be written

$$F = P(\theta) \tag{30}$$

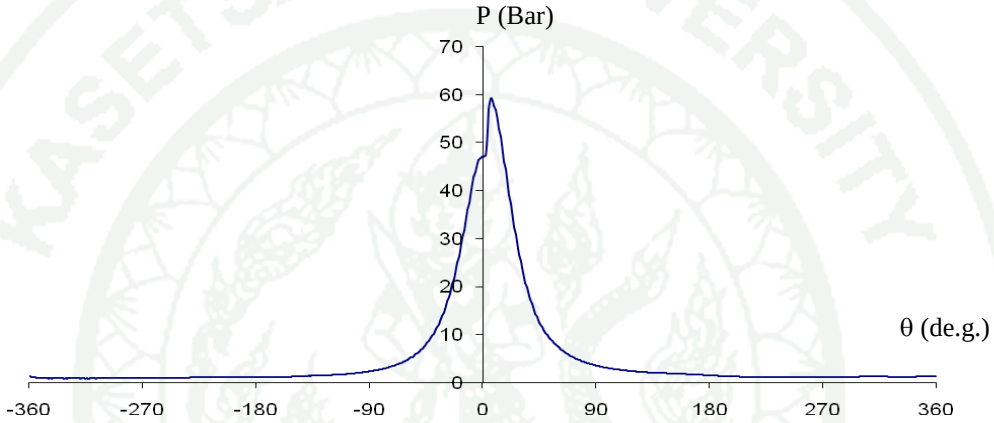

Figure 7 The cylinder pressure

In engine forces analysis, there are methods to determine the engine force related parameters; superposition analysis and point mass analysis are commonly used.

In the point mass analysis shown in Figure 8, the mass of the connecting rod is divided into two parts, at points A and B.

$$m_{A_3} = m_3 \frac{\ell_A}{\ell} \tag{31}$$

where:

m_3 = the mass of the connecting rod (kg)

m_{A_3} = the separated mass of the connecting rod at point A (kg)

ℓ_A = the length from point A to point g_3 (m)

ℓ = the length of the connecting rod (m)

and

$$m_{B_3} = m_3 \frac{\ell_B}{\ell} \tag{32}$$

where:

m_{B_3} = the separated mass of the connecting rod at point B (kg)

ℓ_B = the length from point B to point g_3 (m)

The inertia force (opposite direction of the acceleration) can be determined using Equation (33) to Equation (35)

$$F_{0_4} = m_4 a_B \tag{33}$$

$$F_{B_3} = m_B a_B \tag{34}$$

$$F_{A_3} = m_A a_A \tag{35}$$

where:

F_{0_4} = the inertia force of the piston (N)

F_{B_3} = the inertia force of the connecting rod at point B (N)

F_{A_3} = the inertia force of the connecting rod at point A (N)

a_A and a_B = the acceleration at point A and B ($\frac{m}{s^2}$)

The counterweight of the crank M_{CW} is added so that an inertia force F_{cw} is induced to balance the inertia force F_{A_3} as shown in Figure 8 (a).

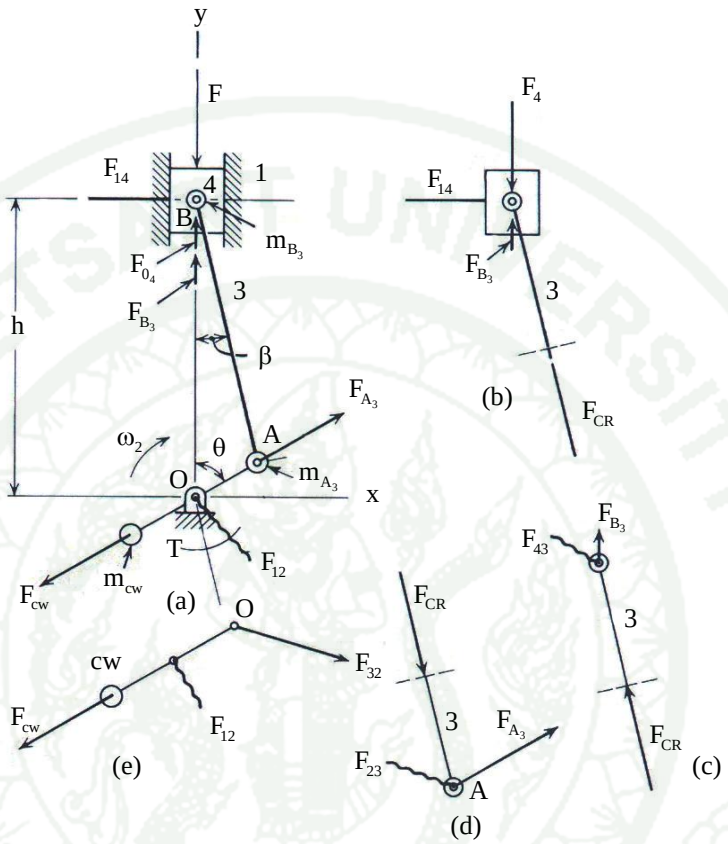

Figure 8 The point mass engine force analysis

Source: Mabie and Reinholtz (1987)

In Figure 8 (b), the piston and the upper part of the connecting rod are in dynamic equilibrium. F_4 is the resultant of the forces F and F_{0_4}. F_{14} and F_{CR} is determined using the sum of the force vectors which equals to zero.

$$\vec{F}_4 + \vec{F}_{B_3} + \vec{F}_{14} + \vec{F}_{CR} = 0 \qquad (36)$$

and

$$\vec{F}_{14} = F_{14}\vec{i} \quad (37)$$

$$\vec{F}_{CR} = F_{CR}(\sin\beta\ \vec{i} + \cos\beta\ \vec{j}) \quad (38)$$

For the upper part of the connecting rod as shown in Figure 8 (c), F_{43} can be determined by using Equation (39)

$$\vec{F}_{B_3} + \vec{F}_{43} + \vec{F}_{CR} = 0 \quad (39)$$

and

$$\vec{F}_{43} = F_{43}(\lambda_x\vec{i} + \lambda_y\vec{j}) \quad (40)$$

where:

λ_x and λ_y = a unit vector in the direction x and y

F_{43} = The reaction force of the piston acting on the connecting rod (N)

Figure 8 (d) shows the lower part of the connecting rod under the action of the force F_{CR}, F_{A_3}, and F_{23}. The force F_{23} can be determined using Equation (41).

$$\vec{F}_{A_3} + \vec{F}_{23} + \vec{F}_{CR} = 0 \quad (41)$$

and

$$\vec{F}_{23} = F_{23}(\lambda_x\vec{i} + \lambda_y\vec{j}) \quad (42)$$

where:

F_{23} = The reaction force of the crank acting on the connecting rod (N)

From Figure 8 (e), F_{12} can be determine by using Equation (43)

$$\vec{F}_{32} + \vec{F}_{12} + \vec{F}_{CW} = 0 \tag{43}$$

and

$$\vec{F}_{12} = F_{12}(\lambda_x \vec{i} + \lambda_y \vec{j}) \tag{44}$$

Finally, The shaft torque T can be calculated from the relation

$$T = F_{14}h \tag{45}$$

For the force analysis of the engine block shows in Figure 9, the forces from the slider crank mechanism are used for determination the shaking force and the shaking couple.

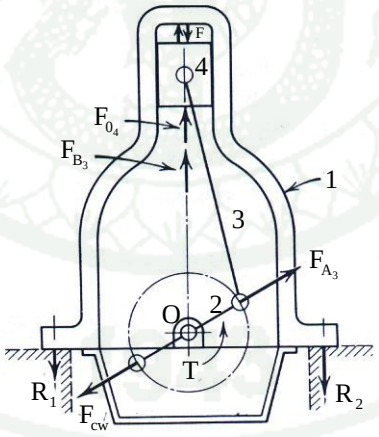

Figure 9 Force analysis of the engine block

Source: Mabie and Reinholtz (1987)

F_{A_3} is balanced by F_{cw} and the net result is zero. Only F_{0_4}, F_{B_3}, T, R_1 and R_2 act on the engine block. The resultant force of F_{0_4} and F_{B_3} is the shaking force and

they are balanced by the sum of R_1 and R_2.

$$\vec{S} = \vec{F}_{0_4} + \vec{F}_{B_3} = \vec{R}_1 + \vec{R}_2 \quad (46)$$

where:

S = the shaking force due to the engine block (N)

R_1, R_2 = the reactive force at the support (N)

The shaking torque of the engine block is T. The reactive force R_1 is not equal to R_2 when the torque T acts on the engine block.

8. Engine vibration

Engine vibrations are the important thing in engine design. The engineer must limits magnitude of engine vibration follow the ISO standards. There are many parts of vehicle mechanisms joint together with bolt, rod, linkage, and etc. When the driver drives a car, the vibration sources can be generated from engine shaking force and rough-road reaction force. These forces transmit to the driver's seat (Loutridis *et al*., 2011) and the steering wheel (Jeon *et al.*, 2009) and affect the driver uncomfortable.

In engine assembly process, the miss assembly can be a cause of engine vibrations (Yang and Gibson, 1996). The miss location and the unbalance mass of rotating parts must be strongly check.

From Equation (30), (36) and (46) found that the shaking force S is the function of the crank angle.

Because the pressure in a cylinder is the nonlinear function, so that S is the nonlinear function. The engine vibration equation from the mass-spring-damper system with the shaking force S cannot determines the general solution by using

analytical mathematic. The numerical method is used to determine the approximate equation of the engine vibration (Johnsson, 2006).

The engine vibration can be measured by commonly using the displacement transducer (Morris *et al.*, 2008), the velocity transducer (Wakui *et al.*, 2007; Cheng *et al.*, 2012), the accelerometer (Bohn *et al.*, 2004; Barelli *et al.*, 2009; Jeon *et al.*, 2009, Hafidi *et al.*, 2010). The acoustic measuring is an alternative method to measure the engine vibration with non-intrusive measurements (Li *et al.*, 2001; Barelli *et al.*, 2009). The acoustic signal is measured by the high quality microphone.

The signals from the combustion analysis and the vibration analysis are the periodic function. In four-stroke engines, they have period of 720 degree per cycle. There are many signal processing methods to analyze them e.g. statistical analysis, spectral analysis, time-frequency analysis, and wavelet transform (Li *et al.*, 1997; Li *et al.*, 2001).

In the statistical analysis, the four ways to express the vibration amplitude are peak, peak-to-peak, root mean square (RMS), and average.

Peak of the vibration amplitude is measured from zero to peak of the graph as shown in Figure 10. This type is used to describe the vibration level from the velocity transducer or the accelerometer.

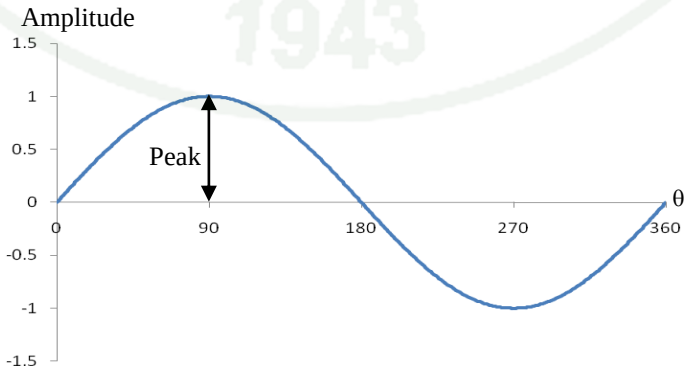

Figure 10 Peak of the vibration amplitude

Peak-to-peak of the vibration amplitude is measured from negative peak to positive peak as shown in Figure 11.

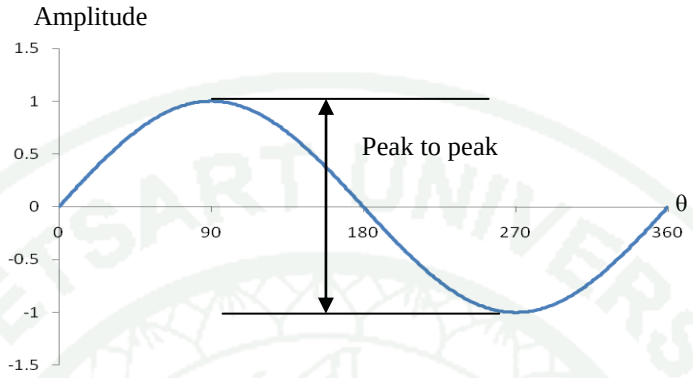

Figure 11 Peak-to-peak of the vibration amplitude

RMS of the vibration amplitude (show in Figure 12) can be expressed by Equation (47).

$$RMS = \sqrt{\frac{\sum x^2}{N_A}} \quad (47)$$

Where:

x = amplitude level

N_A = numbers of amplitude

RMS (shows in Figure 12) is commonly use in electrical for determination the power under the curve. But in engine vibration, peak and peak-to-peak are populate than RMS while average of the vibration amplitude is the basic value in general works.

In engine vibration and combustion analysis, 100 revolutions of the signal graphs are commonly used to determine the average of peak or the average of peak-to-peak (Liew *et al*., 2010).

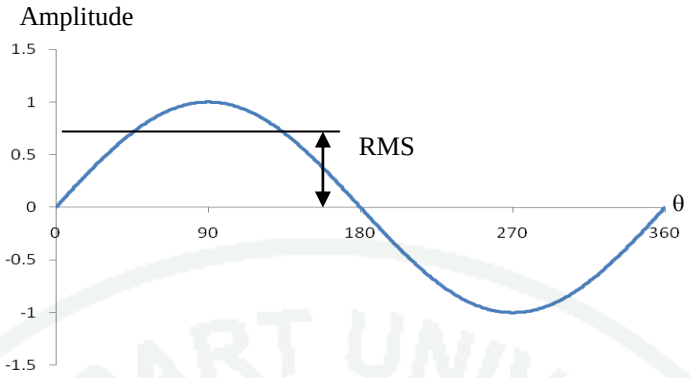

Figure 12 RMS of the vibration amplitude

The average peak acceleration (APA) is used in the present work. For 100 revolutions, the average peak acceleration in x direction can be written.

$$\ddot{x}_A = \frac{\sum_{i=1}^{100} \ddot{x}_{peak,i}}{100} \tag{48}$$

Where:

$\ddot{x}_A$ = average peak acceleration in x direction $(\frac{m}{s^2})$

$\ddot{x}_{peak,i}$ = peak of the acceleration in x direction $(\frac{m}{s^2})$

In spectral analysis, the vibration graph in time domain is the periodic function includes sine functions and cosine functions (called harmonic function) in varies frequency. The relation of angular velocity of the graph (or angular frequency) and frequency is

$$\omega = 2\pi f \tag{49}$$

Where:

ω = angular velocity ($\frac{\text{rad}}{\text{s}}$)

f = frequency ($\frac{1}{\text{s}}$ or Hz)

While period is the time that the graph use in one revolution, it can be written

$$\tau = \frac{1}{f} \tag{50}$$

Where:

τ = period (s)

The periodic function can be broken up into the harmonic component by using Fourier series.

$$f(t) = \frac{a_0}{2} + \sum_{i=0}^{\infty}[a_i \cos(i\omega t) + b_i \sin(i\omega t)] \tag{51}$$

and

$$a_i = \frac{2}{\tau}\int_0^T f(t)\cos(i\omega t)dt \tag{52}$$

$$b_i = \frac{2}{\tau}\int_0^T f(t)\sin(i\omega t)dt \tag{53}$$

Figure 13 (a) shows the sum of three harmonic functions each at a different frequency and amplitude in time domain. Figure 13 (b) shows the harmonic components can be plotted their amplitudes in frequency domain called Fourier transform (FT). Finally, Fourier transform is advanced to be fast Fourier transform (FFT) for signal processing by using the computer.

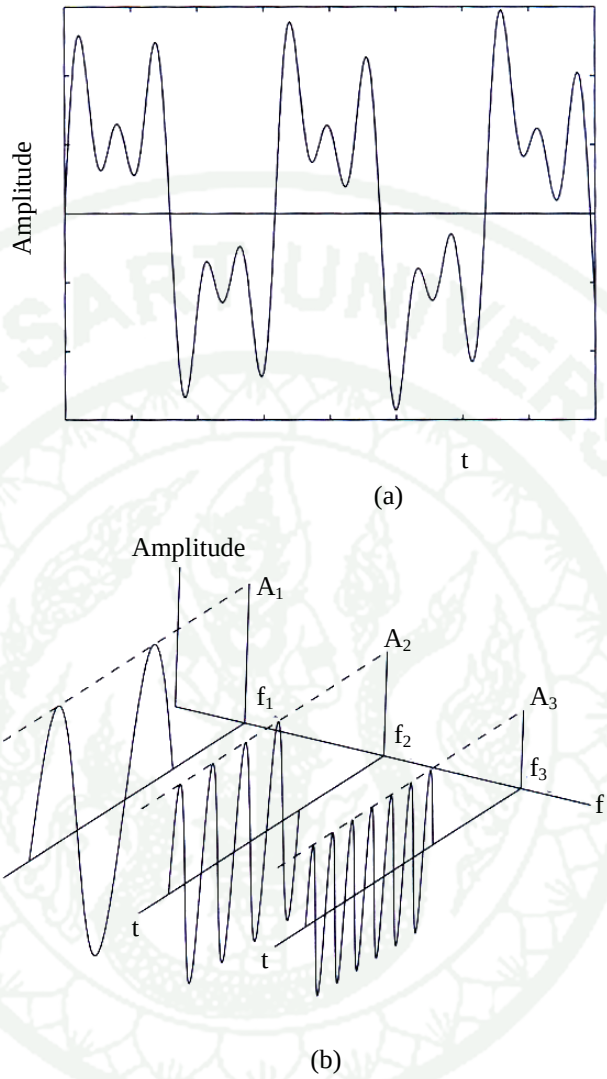

Figure 13 Time and frequency domain of the three harmonic functions (a) the sum of three harmonic functions (b) the harmonic components

Source: Balachandran and Magrab (2004)

9. Effect of hydrogen on diesel engine performance

Hydrogen can be added with diesel as hydrogen-diesel dual fuel. There are several three ways for hydrogen addition by fumigation, carburetion, and injection.

Fumigation (used in this study) is hydrogen addition by using hydrogen pressure and cylinder pressure during intake stroke. This is as the engine used in the test has a mechanical diesel injection pump. By this manner, hydrogen is mixed with air at an intake manifold and flow into a cylinder. In the end of compression stroke, diesel oil is injected at high pressure and mixed with hydrogen and air. The mixture is homogeneous and has smooth combustion. Additionally, fumigation cannot be used with turbocharger as its boost will resist the hydrogen addition.

For carburetion, air flows across a venturi of a carburetor and increases pressure when the cross area at a venturi is decreased. At a venturi, hydrogen is sucked pass a jet and mixes with air before flow into a cylinder.

For injection, hydrogen injected by the injector(s) directs into the cylinder at high pressure at the end of compression stroke. By injection, the mixture is heterogeneous and has non-smooth combustion.

When hydrogen-diesel dual fuel is used, the results from many research papers found that hydrogen affects the performance of diesel engine e.g. break thermal efficiency, heat release rate, NO_x, CO, the cylinder pressure, and etc.

For break thermal efficiency, Varde and Frame (1983) found that the brake thermal efficiency increased from 30.5 to 33.7% with the substitution of 12.5% diesel by hydrogen at full load operation. Saravanan *et al.* (2007) studied effect of hydrogen addition methods on break thermal efficiency and found that hydrogen addition by using manifold injection (fumigation) and port injection (injection) increased break thermal efficiency while carburetion decreased brake thermal efficiency. Lata *et al.* (2012) compared the break thermal efficiency at 10% load, 40% load and 80% load with the conditions at various hydrogen percentages. The results found that break thermal efficiency increased at low of hydrogen addition and decreased at high of hydrogen addition.

The heat release rate is important thing in diesel performance. Combustion characteristic will be changed by hydrogen addition. Liew *et al.* (2010) study on

hydrogen addition in a heavy-duty diesel and found that the peak of heat release rate increased and shifted toward by increasing hydrogen percentage. Shin *et al.* (2011) found that the peak of heat release rate increased by hydrogen addition like Liew *et al.* (2010) but it still began to rise at the same crank angle for different hydrogen supply levels if injected hydrogen into a cylinder. While Lata *et al.* (2012) found that the heat release rate in I phase is decreased by hydrogen addition.

The results from research papers (Lilik *et al.*, 2010; Miyamoto *et al.*, 2011; Lata *et al.*, 2012,) found that hydrogen addition increased NO_x. Meanwhile CO and HC are decreased by hydrogen addition.

For the cylinder pressure, the results from several research found that the maximum cylinder pressure increased by hydrogen addition (Szwaja *et al.*, 2009; Lilik *et al.*, 2010; Miyamoto *et al.*, 2011; Shin *et al.*, 2011;). Lata *et al.* (2012) found that the maximum cylinder pressure increased at low of hydrogen addition and decreased at high of hydrogen addition. McWilliam (2008) found that the maximum cylinder pressure decreased by hydrogen addition at low load.

10. Coefficient of variation of the maximum cylinder pressure

When hydrogen is added, the maximum pressure in a cylinder will be changed. The variance of the maximum pressure can be explained by using the coefficient of variation (Wu and Wu, 2012).

$$COV_{P_{max}} = \frac{S.D._{P_{max}}}{P_{max}} \tag{54}$$

where:

$COV_{P_{max}}$ = coefficient of variation of the maximum pressure

$S.D._{P_{max}}$ = standard deviation of the maximum pressure

P_{max} = average of the maximum pressure

11. Regression analysis

Often in the experiment, regression analysis is used to find relation between variables. There are many kinds of regression analysis. Linear regression and polynomial regression are commonly used for curve fitting. Equation of polynomial regression is

$$y = a_0 + a_1x + a_2x^2 + a_3x^3 + ... + a_nx^n \quad (55)$$

where:

n = order of polynomial function

In present work, regression analysis is used for curve fitting with n = 1 (linear regression) and n = 2.

For n = 1

$$y = bx + c \quad (56)$$

For n = 2

$$y = ax^2 + bx + c \quad (57)$$

where:

a, b, c = constant

The coefficient of determination R^2 is used to describe how about a curve fitting. R^2 is a number between 0 and 1. If R^2 approaches 1, a curve fitting is well. The equation of R^2 is

$$R^2 = \sum \frac{(y - \bar{y})^2}{(y_i - \bar{y})^2} \quad (58)$$

where:

y = approximate data from regression analysis

y_i = real data

$\bar{y}$ = average of real data

In this work, the relations between P_{max} and $\%H_2$, $COV_{P_{max}}$ and $\%H_2$, APA and $\%H_2$, and APA and P_{max} are constructed from real data by using Equation (56) and Equation (57).

For n = 1

$$P_{max} = a(\%H_2) + b \quad (59)$$

$$COV_{P_{max}} = a(\%H_2) + b \quad (60)$$

$$APA = a(\%H_2) + b \quad (61)$$

$$APA = a(P_{max}) + b \quad (62)$$

For n = 2

$$P_{max} = a(\%H_2)^2 + b(\%H_2) + c \quad (63)$$

$$COV_{P_{max}} = a(\%H_2)^2 + b(\%H_2) + c \quad (64)$$

$$APA = a(\%H_2)^2 + b(\%H_2) + c \quad (65)$$

$$APA = a(P_{max})^2 + b(P_{max}) + c \quad (66)$$

MATERIALS AND METHODS

Materials

This research is accomplished using the following materials which will be described in the next sub-topics.

	Quantity
1. Single-piston diesel engine	1 engine
2. Engine test base	1 unit
3. Brake system	1 unit
4. Torque meter	1 piece
5. Pressure transducer	1 piece
6. Hydrogen	1 cylinder
7. Revolution speed sensor	1 piece
8. Shaft encoder	1 piece
9. Hydrogen flow meter	1 piece
10. Diesel flow meter	1 piece
9. "G-link" wireless acceleration meter	5 pieces
10. “WADA base” base station	1 piece
11. Computer	2 unit
12. “Node Commander” software	1 unit
13. DEWESoft software	1 unit

Methods

1. Test condition

A single cylinder Kubota RT100 direct injection diesel engine is tested on the engine test bed. Hydrogen-diesel dual fuel is used in this present work. Hydrogen gas pressure is controlled at 1 bar by the valves. It flows through the flow meter before mixing with air at the intake manifold and flow into the cylinder. Hydrogen flow rates

are 0, 5, 10, 15 and 20 lpm. Diesel flows through the flow meter before it is injected into the cylinder by the injector.

The engine is tested at each conditions listed in Table 1. The cylinder pressure and the engine accelerations at the engine base are measured for the time duration of 100 revolutions of the engine consecutively.

Table 1 Test condition

Test condition	Engine revolution N (rpm)	Engine torque T (%)
Exp. 1	2,000	25
Exp. 2	2,000	50
Exp. 3	1,600	15
Exp. 4	1,600	25

2. Engine setup

In the present work, a single cylinder Kubota RT100 direct injection diesel engine with specification listed in Table 2 is used. Figure 14 shows its setup on the engine test bed. The engine base is supported by four springs with each spring constant of 35 kN/m. In Figure 14, the front view is x-z plane, the left view is y-z plane, and the top view is x-y plane.

Table 2 Test engine specification

Property	Value
Model	Kubota RT100 DI
Number of cylinder	1
Bore × Stroke	88 mm × 90 mm
Displaced volume and Compression ratio	547 cm^3, 18:1
Maximum power	7.4 kW @ 2,400 rpm
Maximum torque	3.4 kg·m @ 1,600 rpm

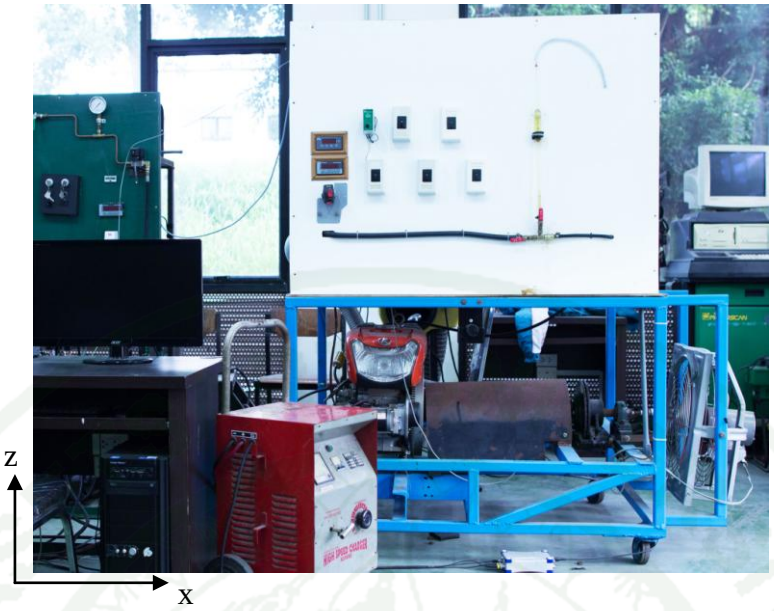

(a)

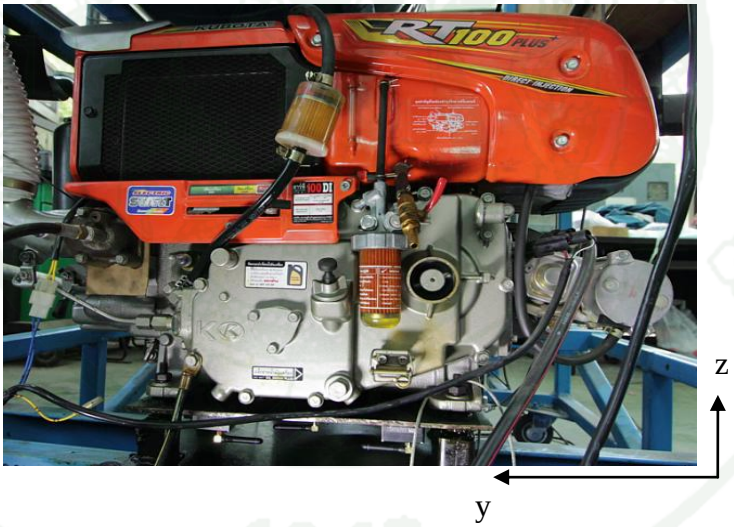

(b)

Figure 14 The setup of the engine test bed (a) front view (b) left view.

3. Measuring the cylinder pressure

Cylinder pressure traces as shown in Figure 15 (a) were acquired using Kistler 6052C piezo pressure transducers which are suited to applications where the bore is

smaller than 5 mm (this case). Key technical data of the transducer are listed in Table 3. An amplifier Dewetron DEWE-30-4 3066A03 as shown in Figure 15 (b) was employed for conditioning the charge signals from piezo-electric transducers.

Table 3 Cylinder pressure transducer specification

Property	Value
Measuring range	0 to 250 bar FSO
Sensitivity	19.90 pC/bar
Linearity	±0.4 % FSO
Natural frequency	160 kHz

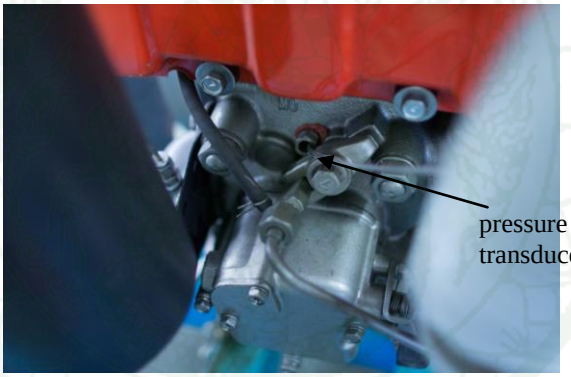

(a)

(b)

Figure 15 Pressure measurement (a) pressure transducer (b) amplifier

Crankshaft position was determined by an incremental shaft encoder model BDK 16.05A.0360-5-4 from Baumer Electric which was mounted in alignment with the engine crank shaft at the back of the engine as shown in Figure 16. The conditioned cylinder pressure signals from both channels of the charge amplifier corresponding to the engine crank shaft position signal from the shaft encoder were simultaneously collected using DEWESoft software.

Figure 16 Shaft encoder

The crank angle (CA) at top dead center (TDC) is detected before measuring the cylinder pressure and the pressure is measured every 1 degree of CA for the time duration of 100 revolutions of the engine consecutively.

4. Measuring the accelerations

Five G-Link wireless accelerometers are used to measure the engine acceleration at the engine base. Figure 17 and Figure 18 show accelerometer mounting positions. The accelerometers are controlled by Node Commander software through base station WADA base as shown in Figure 19. The main technical specifications are shown in Table 4.

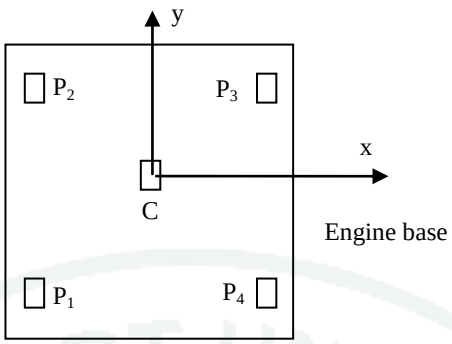

Figure 17 The accelerometer mounting allocations (top view)

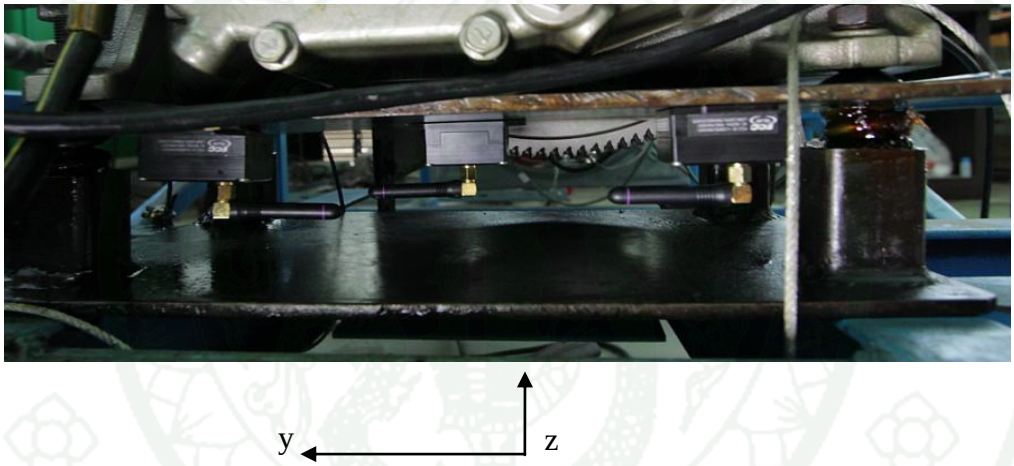

Figure 18 The accelerometer mounting allocations (left view)

Table 4 Acceleration meter specifications

Part	Specifications
G-link	Measuring acceleration X, Y and Z axes
	Sample rate 2048 samples per channel per second
	Range: ±2g or ±10g
	On-board flash memory: 2 MB
	Nonlinearity ±0.2%
WADA base	Power: usb
	Frequency: 2.405 GHz to 2.480 GHz.

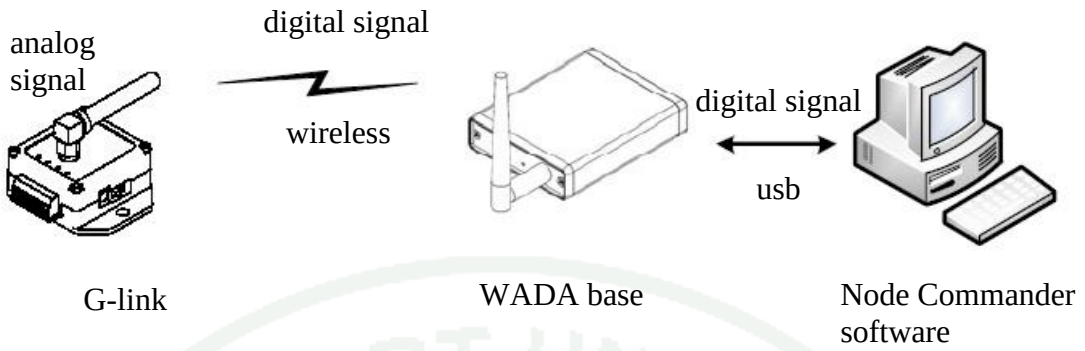

Figure 19 Wireless accelerometer G-link and base station WADA base connection

5. The schematic diagram of the experimental

The schematic diagram of the experimental is shown in Figure 20.

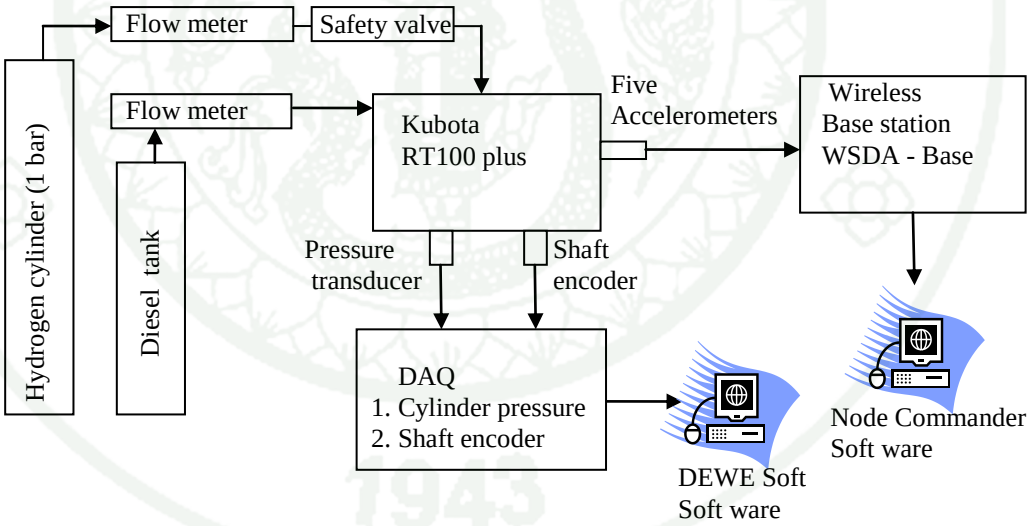

Figure 20 Schematic diagram of the experimental setup

RESULTS AND DISCUSSION

Results

1. Maximum cylinder pressure

Cylinder pressure characteristics corresponding to the crank angle in degree (CAD) at around the end of compression stroke and the beginning of the expansion stroke are shown in Figure 21 for different hydrogen percentages at 2,000 rpm speed and 25% torque (Exp. 1).

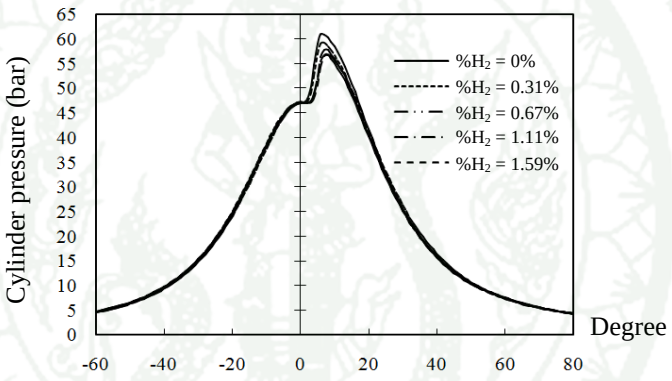

Figure 21 Average cylinder pressure at various hydrogen percentage for the test condition Exp. 1

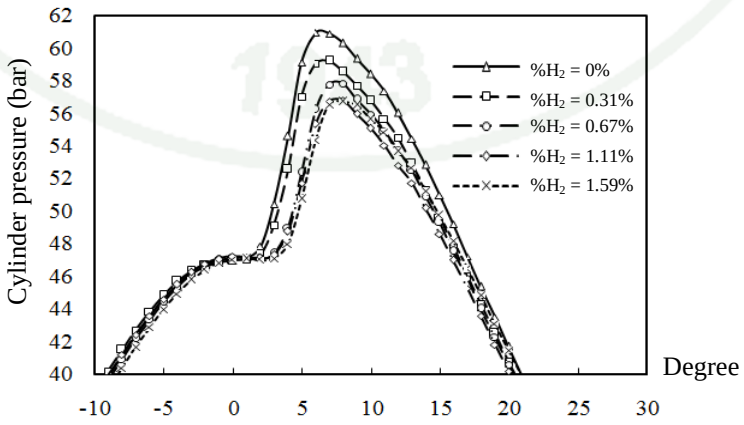

Figure 22 The magnification of maximum cylinder pressure for the test condition Exp. 1

Figure 22 shows the magnification of the maximum cylinder pressure illustrated in Figure 21 and numerated in Table 5.

Table 5 Maximum cylinder pressure (P_{max})

	Exp. 1		Exp. 2		Exp. 3		Exp. 4	
H_2 lpm	$\%H_2$	P_{max} bar	$\%H_2$	P_{max} bar	$\%H_2$	P_{max} bar	$\%H_2$	P_{max} bar
0	0	60.94	0	69.79	0	57.99	0	58.14
5	0.31	59.22	0.22	67.54	0.52	56.43	0.50	58.12
10	0.67	57.82	0.48	62.54	1.24	55.97	1.06	57.83
15	1.11	56.79	0.75	58.47	2.17	54.73	1.90	56.32
20	1.59	56.71	1.09	58.01	3.45	53.25	3.04	54.80

2. The correlation of maximum cylinder pressure and hydrogen percentage

The maximum cylinder pressure is plotted against the hydrogen percentage for all the test conditions. The first order and second order correlations between maximum cylinder pressure (P_{max}) and hydrogen percentage are shown in Figure 23 and 24, respectively.

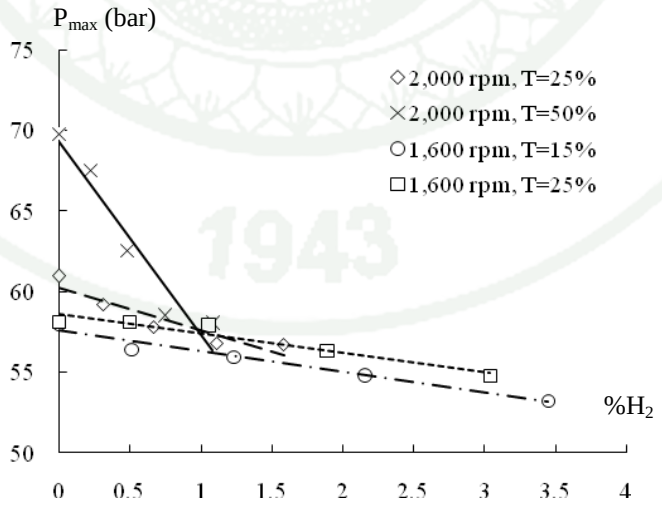

Figure 23 The first order correlation between maximum cylinder pressure (P_{max}) and hydrogen percentage

By using Equation (59) and Equation (63), the relationships between maximum cylinder pressure (P_{max}) and hydrogen percentage in first (n=1) and second (n=2) orders generate the correlation constants for regression analysis numerated in Table 6.

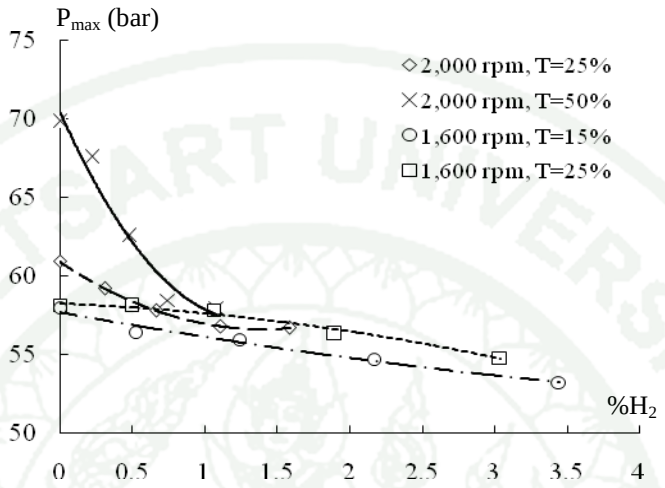

Figure 24 The second order correlation between maximum cylinder pressure (P_{max}) and hydrogen percentage

Table 6 Correlation constants for the relation between P_{max} and $\%H_2$

Order	Condition	a	b	c	R^2
1	Exp.1	-2.6515	60.248		0.8712
	Exp.2	-11.904	69.310		0.9242
	Exp.3	-1.2816	57.565		0.9690
	Exp.4	-1.1787	58.570		0.9401
2	Exp.1	2.2068	-6.1711	60.940	1.0000
	Exp.2	8.0564	-20.667	70.511	0.9689
	Exp.3	0.1138	-1.677	57.730	0.9767
	Exp.4	-0.2641	-0.366	58.272	0.9776

3. Coefficient of variation of the maximum cylinder pressure

From Equation (54), the coefficient of variation of the maximum cylinder are shown in Table 7.

Table 7 The coefficient of variation of the maximum cylinder pressure ($COV_{P_{max}}$)

	Exp. 1		Exp. 2		Exp. 3		Exp. 4	
H_2	$\%H_2$	$COV_{P_{max}}$	$\%H_2$	$COV_{P_{max}}$	$\%H_2$	$COV_{P_{max}}$	$\%H_2$	$COV_{P_{max}}$
lpm		bar		bar		bar		bar
0	0	1.22	0	1.40	0	1.07	0	1.05
5	0.31	1.22	0.22	1.55	0.52	1.26	0.50	1.09
10	0.67	1.23	0.48	2.30	1.24	1.39	1.06	1.16
15	1.11	1.27	0.75	4.38	2.17	1.41	1.90	1.37
20	1.59	1.39	1.09	4.49	3.45	1.58	3.04	1.37

The coefficient of variation of the maximum cylinder pressure is also plotted against the hydrogen percentage for all the test conditions. The first order and second order correlations between the coefficient of variation of the maximum cylinder pressure and hydrogen percentage are shown in Figures 25 and 26, respectively.

By using Equation (60) and Equation (64), the relationships between the coefficient of variation of the maximum pressure ($COV_{p_{max}}$) and hydrogen percentage in first (n=1) and second (n=2) orders generate the correlation constants numerated in Table 8.

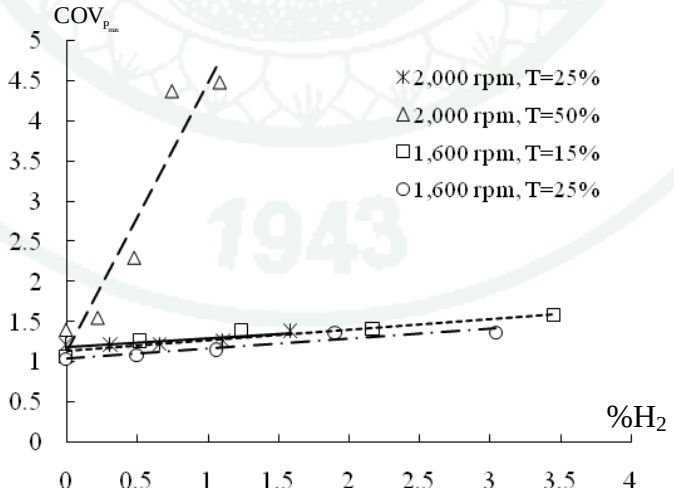

Figure 25 The first order correlation between coefficient of variation of maximum cylinder pressure ($COV_{P_{max}}$) and hydrogen percentage

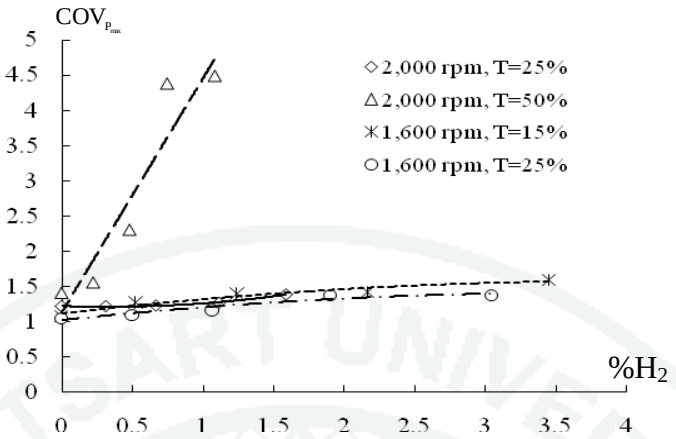

Figure 26 The second order correlation between coefficient of variation of maximum cylinder pressure ($COV_{P_{max}}$) and hydrogen percentage

Table 8 Correlation constants for the relation between $COV_{P_{max}}$ and $\%H_2$

Order	Condition	a	b	c	R^2
1	Exp.1	0.1023	1.1907		0.7964
	Exp.2	3.3334	1.132		0.8893
	Exp.3	0.1311	1.1484		0.8951
	Exp.4	0.1195	1.0525		0.8809
2	Exp.1	0.1091	-0.0718	1.225	0.9899
	Exp.2	-0.0106	3.345	1.1304	0.8893
	Exp.3	-0.0287	0.2308	1.1069	0.9387
	Exp.4	-0.0275	0.204	1.0207	0.9179

4. The average peak acceleration

Examples of the engine acceleration graphs at point C in Exp. 1 (engine speed 2,000 rpm, Torque 25%) with $\%H_2$ of 0.31% are shown in Figure 27 to Figure 29.

For other experiments, the results show that the engine accelerations are the periodic function for all directions with the period of 720° per revolution.

The average peak accelerations of 100 revolutions at point P_1, P_2, P_3, P_4 and C in x, y and z direction are shown in Table 9 to Table 12.

Figure 27 The engine acceleration at point C in x direction ($\ddot{x}_C$)

Figure 28 The engine acceleration at point C in y direction ($\ddot{y}_C$)

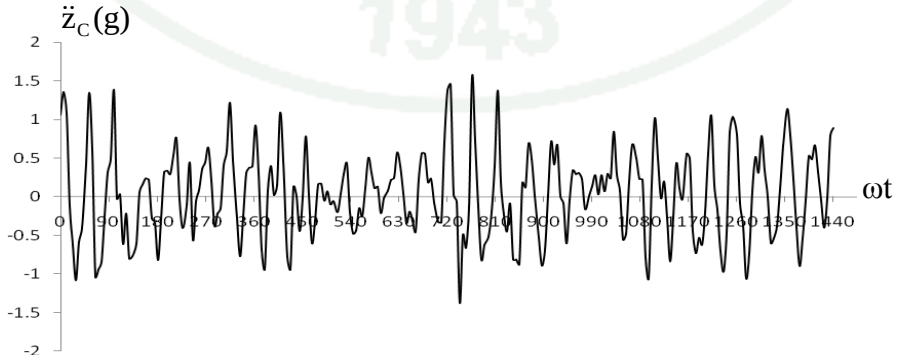

Figure 29 The engine acceleration at point C in z direction ($\ddot{z}_C$)

Table 9 The average peak accelerations in Exp. 1

%H	$\ddot{x}_{APA,1}$	$\ddot{y}_{APA,1}$	$\ddot{z}_{APA,1}$	$\ddot{x}_{APA,2}$	$\ddot{y}_{APA,2}$	$\ddot{z}_{APA,2}$	$\ddot{x}_{APA,3}$	$\ddot{y}_{APA,3}$	$\ddot{z}_{APA,3}$	$\ddot{x}_{APA,4}$	$\ddot{y}_{APA,4}$	$\ddot{z}_{APA,4}$	$\ddot{x}_{APA,C}$	$\ddot{y}_{APA,C}$	$\ddot{z}_{APA,C}$
0.00	2.40	2.08	1.82	2.64	1.76	2.04	2.37	1.46	2.34	2.40	2.01	1.93	2.37	1.41	1.58
0.31	2.25	1.89	1.81	2.62	1.70	1.83	2.16	1.15	1.90	1.78	1.76	1.90	2.13	1.23	1.33
0.67	2.03	1.59	1.67	2.61	1.52	1.60	1.85	1.13	1.42	1.69	1.56	1.85	1.60	1.12	1.28
1.11	1.79	1.45	1.65	2.12	1.39	1.58	1.61	1.09	1.35	1.32	1.45	1.79	1.40	1.08	1.14
1.59	1.65	1.26	1.36	2.03	1.21	1.38	1.55	0.95	1.28	1.26	1.15	1.74	1.31	0.91	0.99

Note: $\ddot{x}_{APA,i}$ = average peak acceleration in x direction at point i

$\ddot{y}_{APA,i}$ = average peak acceleration in y direction at point i

$\ddot{z}_{APA,i}$ = average peak acceleration in x direction at point i

Table 10 The average peak accelerations in Exp. 2

%H	$\ddot{x}_{APA,1}$	$\ddot{y}_{APA,1}$	$\ddot{z}_{APA,1}$	$\ddot{x}_{APA,2}$	$\ddot{y}_{APA,2}$	$\ddot{z}_{APA,2}$	$\ddot{x}_{APA,3}$	$\ddot{y}_{APA,3}$	$\ddot{z}_{APA,3}$	$\ddot{x}_{APA,4}$	$\ddot{y}_{APA,4}$	$\ddot{z}_{APA,4}$	$\ddot{x}_{APA,C}$	$\ddot{y}_{APA,C}$	$\ddot{z}_{APA,C}$
0.00	2.71	2.78	3.30	3.02	2.44	2.00	3.13	1.93	2.95	2.36	1.88	3.36	2.90	1.95	1.90
0.22	2.09	2.48	2.02	2.49	2.38	1.70	2.39	1.89	2.61	1.94	1.87	2.80	2.00	1.83	1.88
0.48	1.89	2.38	1.68	2.28	2.32	1.67	2.00	1.85	2.52	1.74	1.84	2.42	1.73	1.81	1.79
0.75	1.78	2.23	1.62	2.25	2.19	1.56	1.97	1.62	2.17	1.67	1.61	2.25	1.68	1.59	1.52
1.09	1.69	2.08	1.55	2.14	2.03	1.51	1.77	1.57	2.13	1.61	1.59	2.20	1.55	1.53	1.49

Table 11 The average peak accelerations in Exp. 3

%H	$\ddot{x}_{APA,1}$	$\ddot{y}_{APA,1}$	$\ddot{z}_{APA,1}$	$\ddot{x}_{APA,2}$	$\ddot{y}_{APA,2}$	$\ddot{z}_{APA,2}$	$\ddot{x}_{APA,3}$	$\ddot{y}_{APA,3}$	$\ddot{z}_{APA,3}$	$\ddot{x}_{APA,4}$	$\ddot{y}_{APA,4}$	$\ddot{z}_{APA,4}$	$\ddot{x}_{APA,C}$	$\ddot{y}_{APA,C}$	$\ddot{z}_{APA,C}$
0.00	1.79	2.43	2.02	2.61	2.35	1.82	2.28	1.47	2.37	1.70	1.21	2.02	1.74	1.54	1.18
0.52	1.79	2.29	1.88	2.13	1.89	1.46	2.12	1.34	2.20	1.61	1.12	1.88	1.42	1.15	0.94
1.24	1.75	2.20	1.77	2.07	1.76	1.39	1.93	1.23	2.16	1.53	1.10	1.80	1.34	1.01	0.88
2.17	1.74	2.01	1.68	1.84	1.49	1.36	1.83	1.04	1.86	1.42	0.98	1.69	1.30	0.87	0.81
3.45	1.66	1.70	1.47	1.73	1.27	1.33	1.64	0.93	1.64	1.35	0.92	1.61	1.18	0.70	0.69

Table 12 The average peak accelerations in Exp. 4

%H	$\ddot{x}_{APA,1}$	$\ddot{y}_{APA,1}$	$\ddot{z}_{APA,1}$	$\ddot{x}_{APA,2}$	$\ddot{y}_{APA,2}$	$\ddot{z}_{APA,2}$	$\ddot{x}_{APA,3}$	$\ddot{y}_{APA,3}$	$\ddot{z}_{APA,3}$	$\ddot{x}_{APA,4}$	$\ddot{y}_{APA,4}$	$\ddot{z}_{APA,4}$	$\ddot{x}_{APA,C}$	$\ddot{y}_{APA,C}$	$\ddot{z}_{APA,C}$
0.00	1.82	2.46	2.07	2.56	2.44	1.74	2.27	1.58	2.26	1.79	1.20	1.98	1.75	1.60	1.11
0.50	1.72	2.37	1.93	2.42	2.25	1.70	2.20	1.53	2.19	1.71	1.17	1.94	1.48	1.34	1.04
1.06	1.63	2.22	1.77	2.25	2.13	1.60	2.10	1.44	2.18	1.46	1.06	1.82	1.36	1.23	0.98
1.90	1.58	1.93	1.62	1.97	1.74	1.39	1.98	1.42	2.13	1.37	1.03	1.63	1.30	1.06	0.91
3.04	1.52	1.71	1.38	1.89	1.52	1.41	1.82	1.09	1.76	1.31	0.96	1.53	1.09	0.78	0.79

The hydrogen percentage is plotted against the average peak acceleration (APA) for the test condition Exp. 1 (N = 2,000 rpm, T = 25%). The first order (n = 1) and second order (n = 2) correlations between average peak acceleration and hydrogen percentage are shown in Figure 30 to Figure 39.

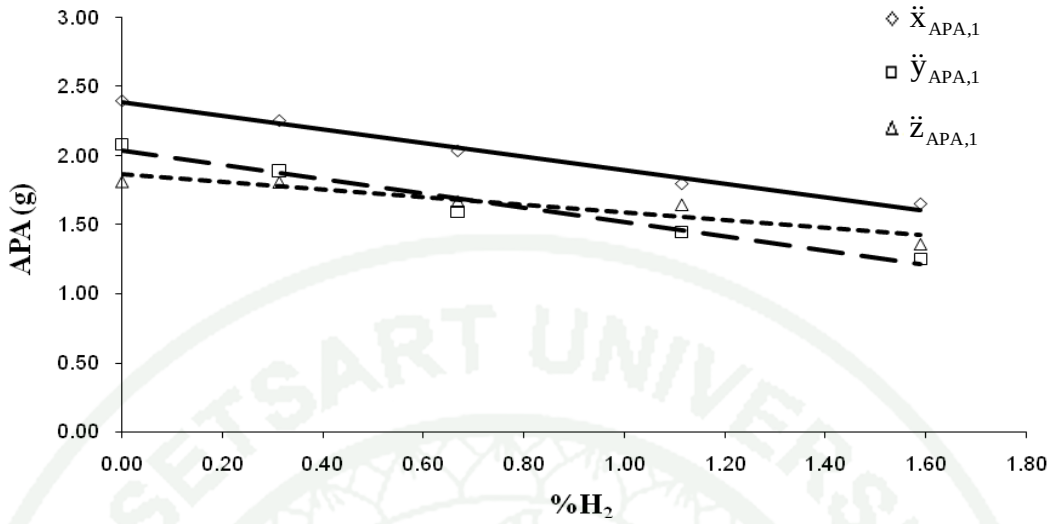

Figure 30 The correlation between APA at point 1 and $\%H_2$ (Exp. 1 and n = 1)

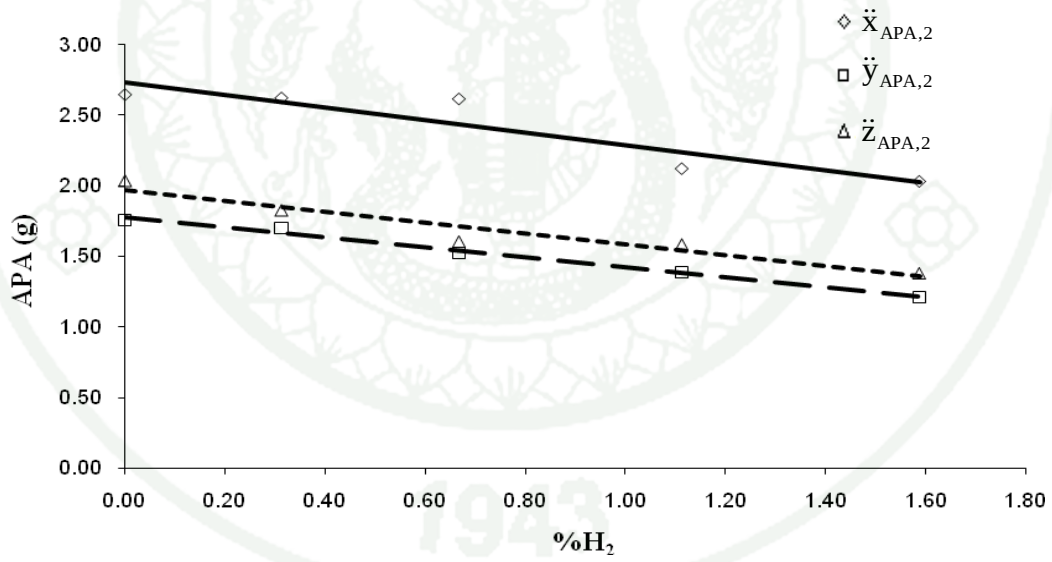

Figure 31 The correlation between APA at point 2 and $\%H_2$ (Exp. 1 and n = 1)

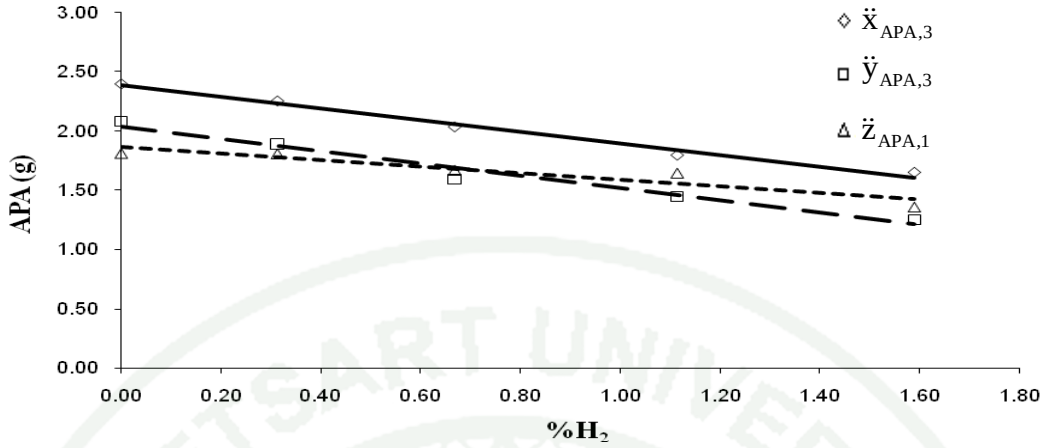

Figure 32 The correlation between APA at point 3 and $\%H_2$ (Exp. 1 and n = 1)

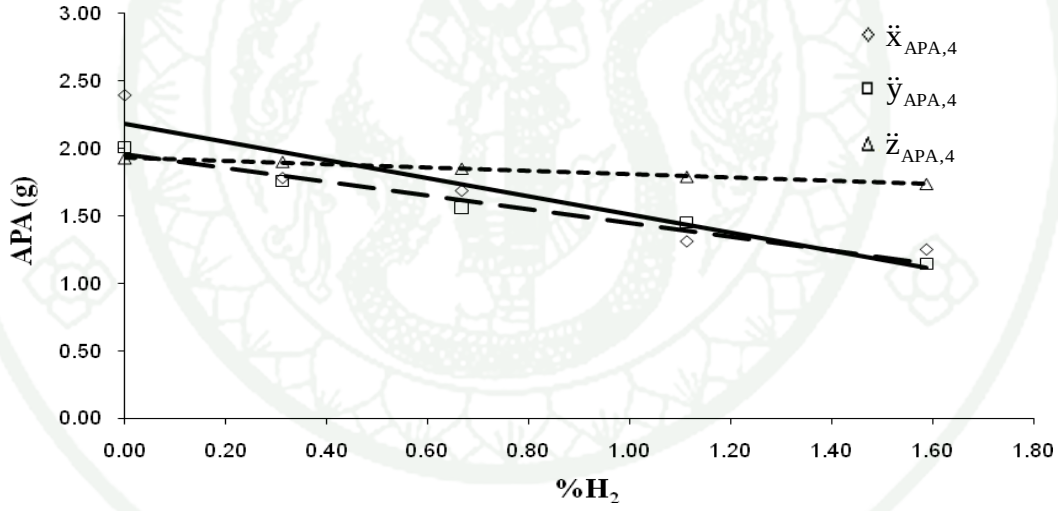

Figure 33 The correlation between APA at point 4 and $\%H_2$ (Exp. 1 and n = 1)

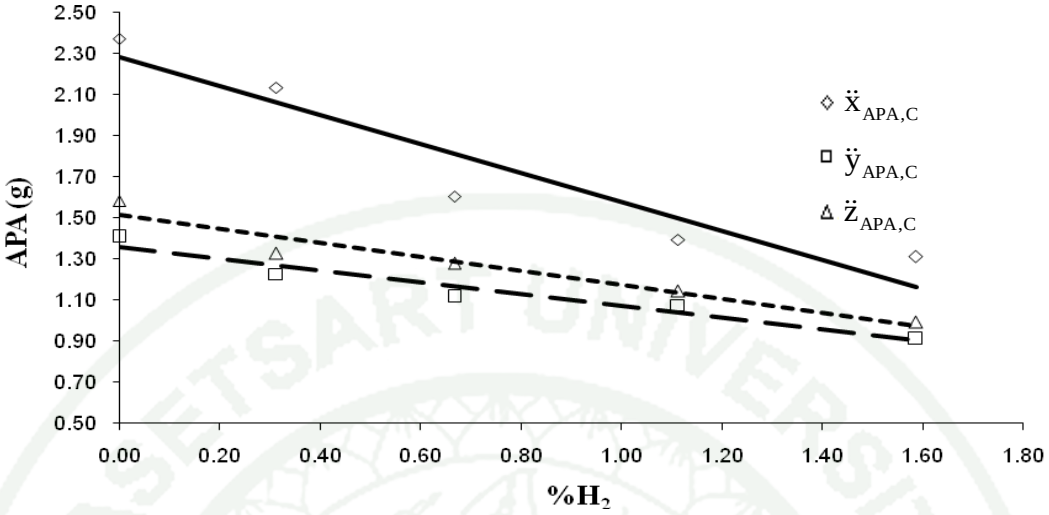

Figure 34 The correlation between APA at point C and $\%H_2$ (Exp. 1 and n = 1)

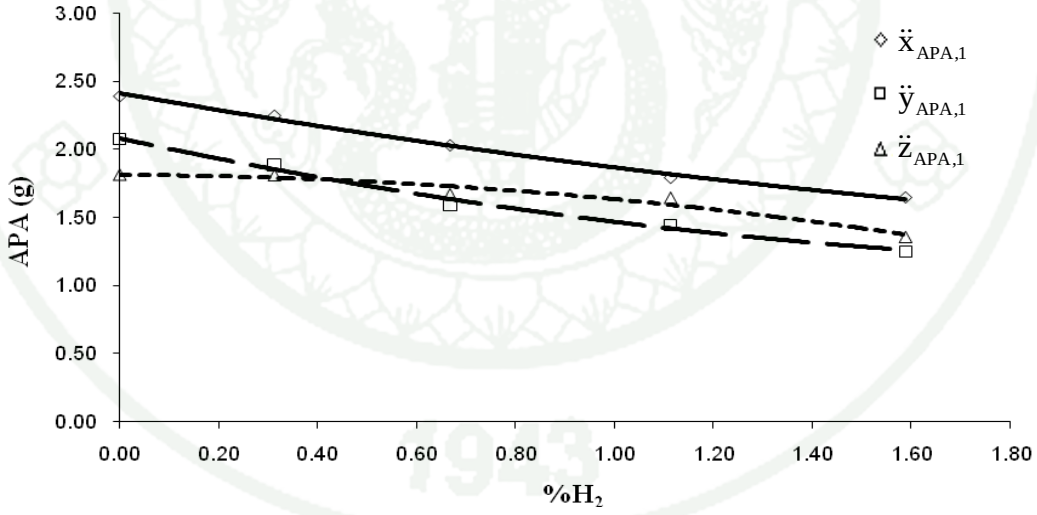

Figure 35 The correlation between APA at point 1 and $\%H_2$ (Exp. 1 and n = 2)

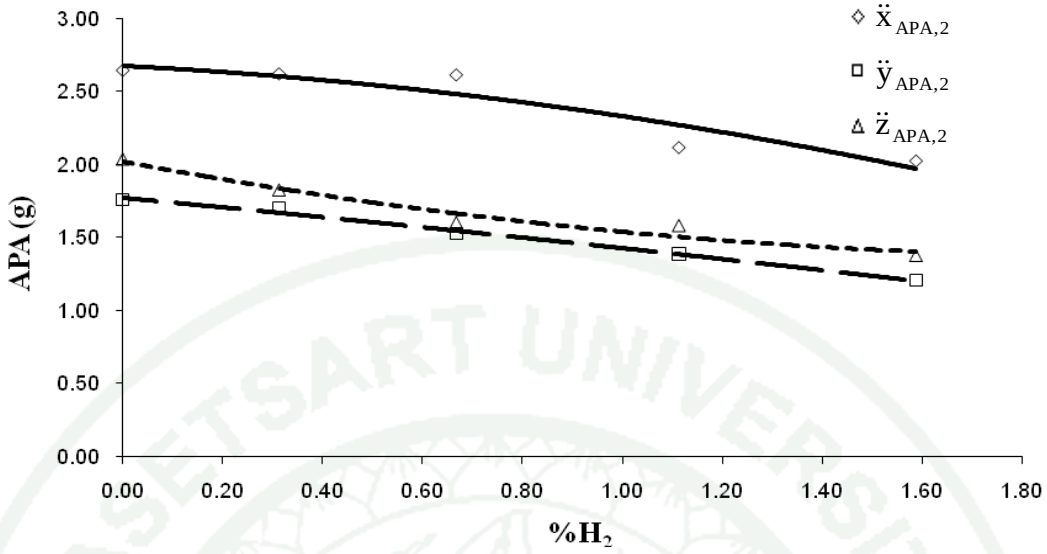

Figure 36 The correlation between APA at point 2 and $\%H_2$ (Exp. 1 and n = 2)

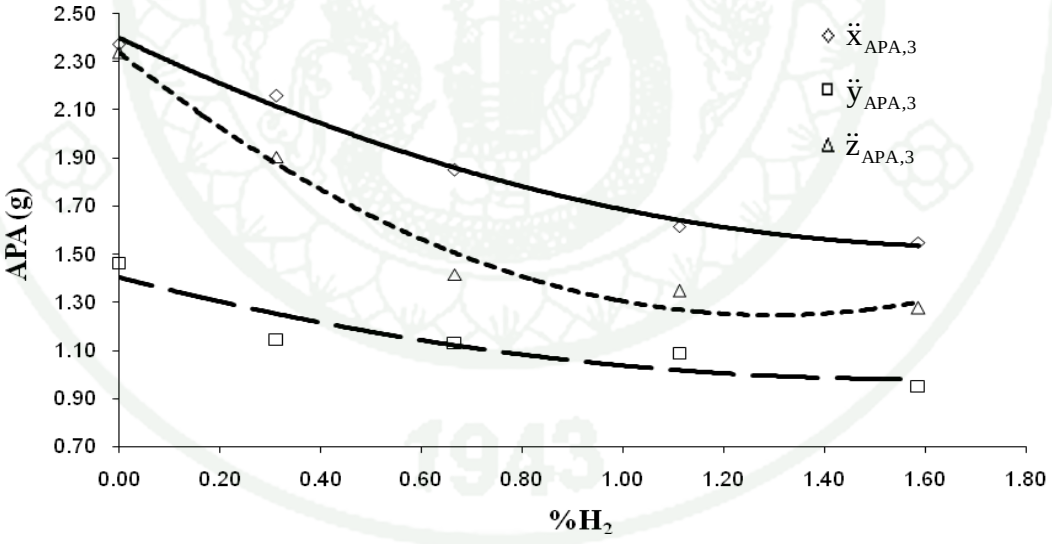

Figure 37 The correlation between APA at point 3 and $\%H_2$ (Exp. 1 and n = 2)

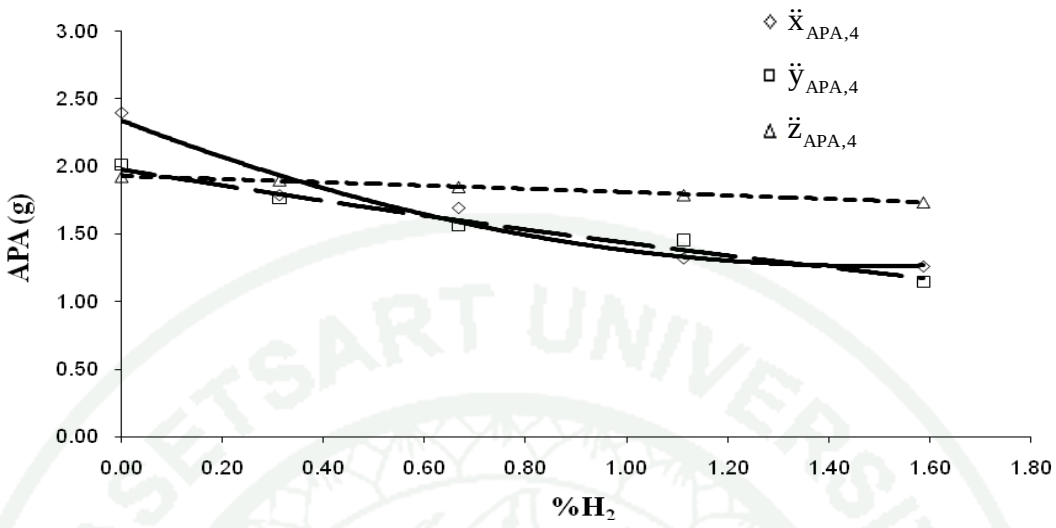

Figure 38 The correlation between APA at point 4 and $\%H_2$ (Exp. 1 and n = 2)

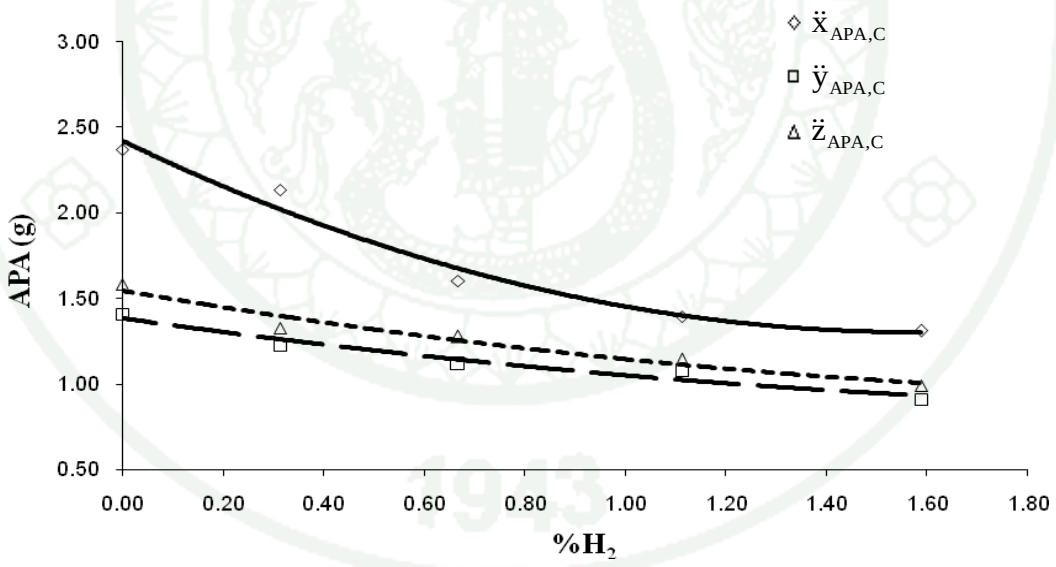

Figure 39 The correlation between APA at point C and $\%H_2$ (Exp. 1 and n = 2)

For the test condition Exp. 2 (N = 2,000 rpm, T = 50%) the average peak acceleration is plotted against the hydrogen percentage as shown in Figure 40 to Figure 49.

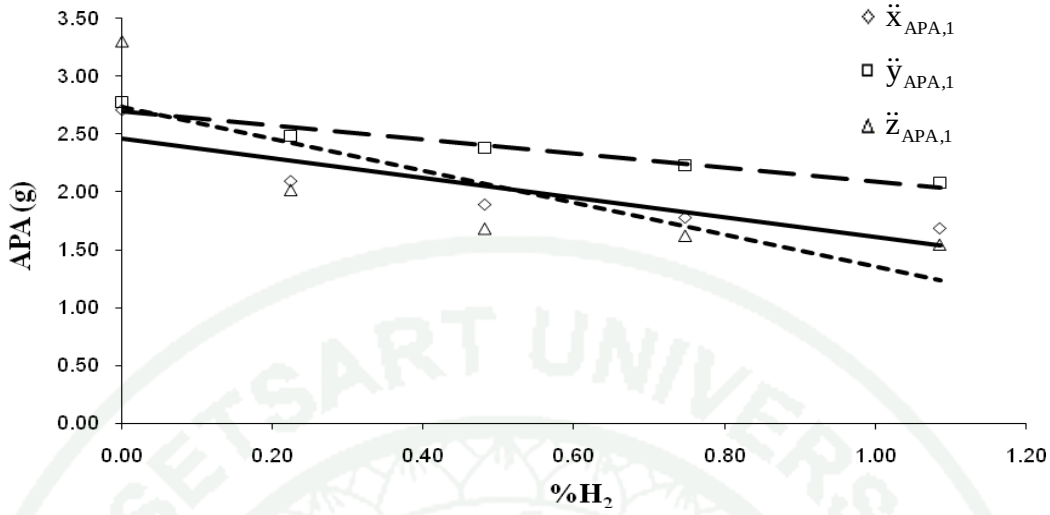

Figure 40 The correlation between APA at point 1 and $\%H_2$ (Exp. 2 and n = 1)

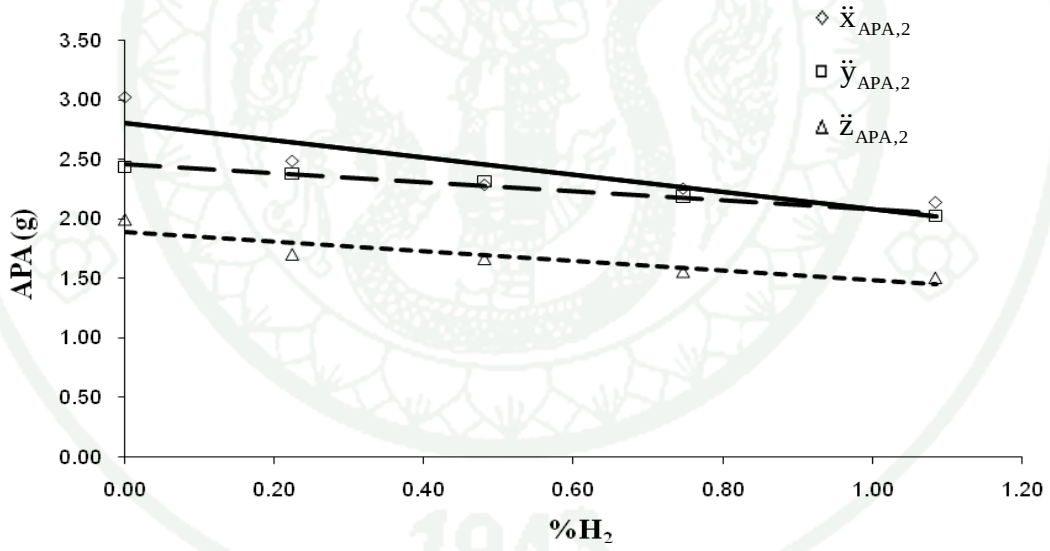

Figure 41 The correlation between APA at point 2 and $\%H_2$ (Exp. 2 and n = 1)

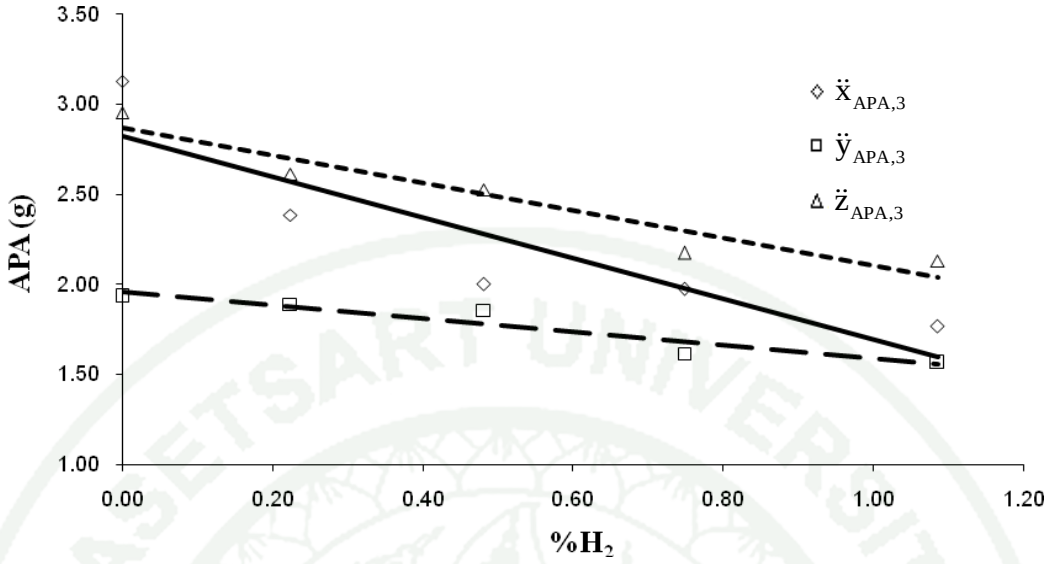

Figure 42 The correlation between APA at point 3 and $\%H_2$ (Exp. 2 and n = 1)

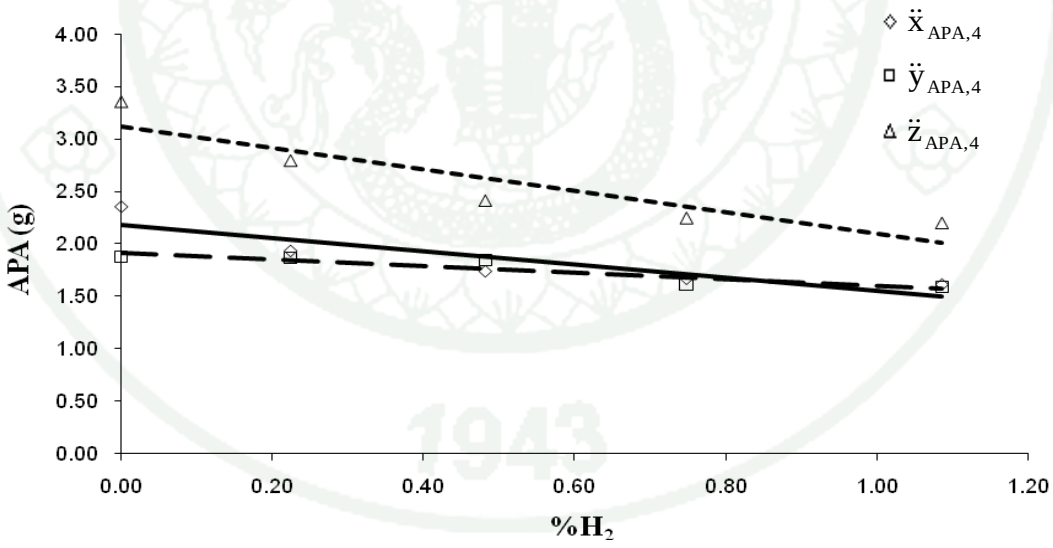

Figure 43 The correlation between APA at point 4 and $\%H_2$ (Exp. 2 and n = 1)

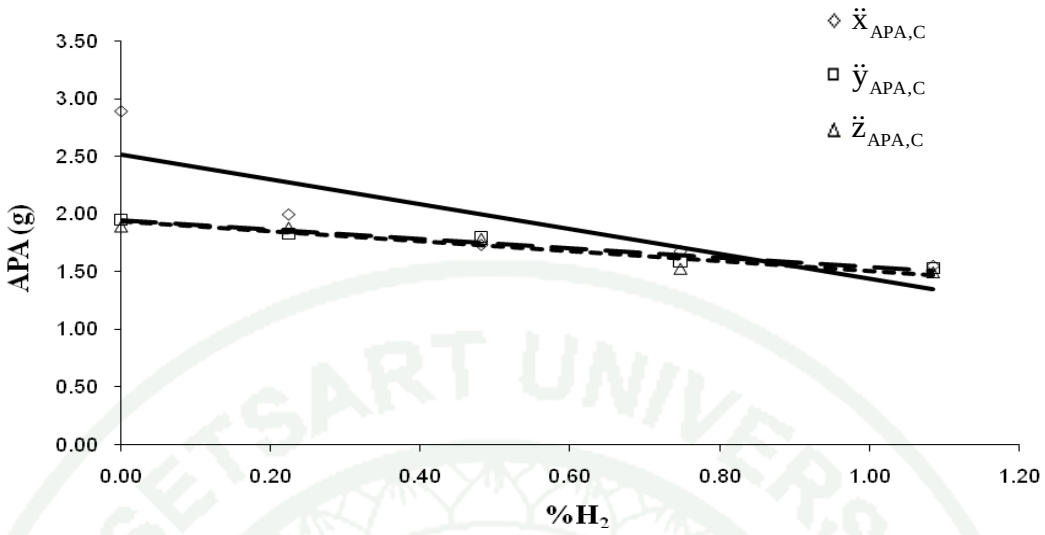

Figure 44 The correlation between APA at point C and $\%H_2$ (Exp. 2 and n = 1)

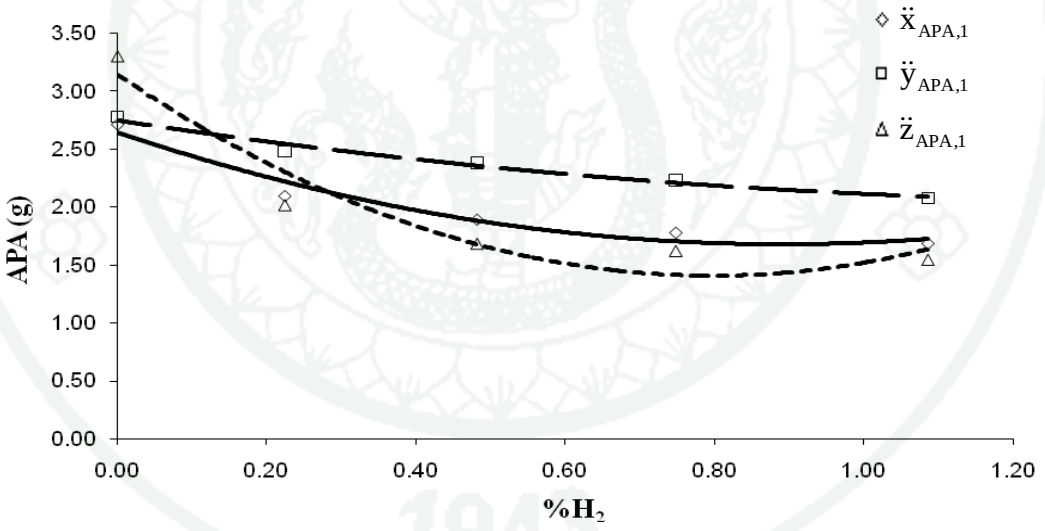

Figure 45 The correlation between APA at point 1 and $\%H_2$ (Exp. 2 and n = 2)

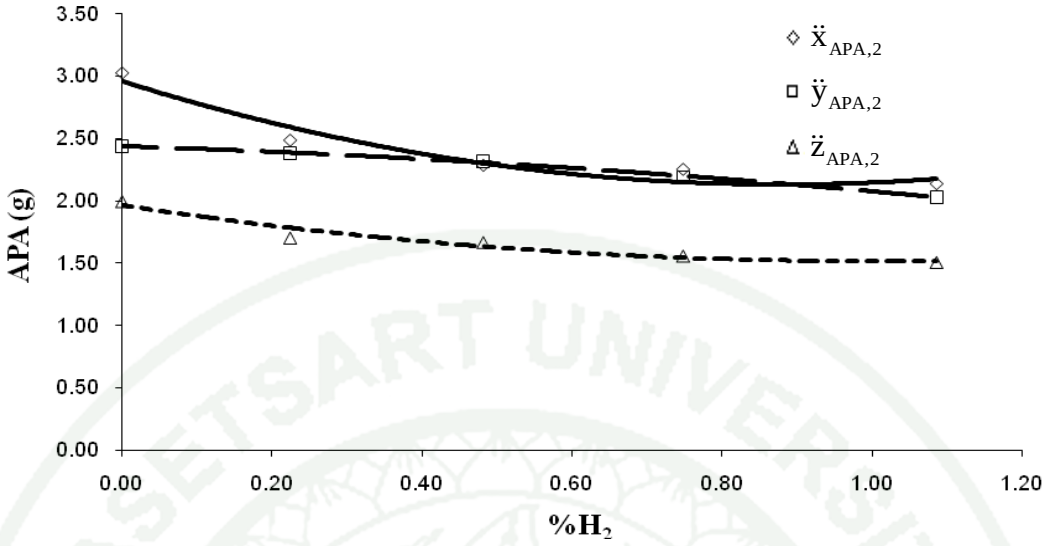

Figure 46 The correlation between APA at point 2 and $\%H_2$ (Exp. 2 and n = 2)

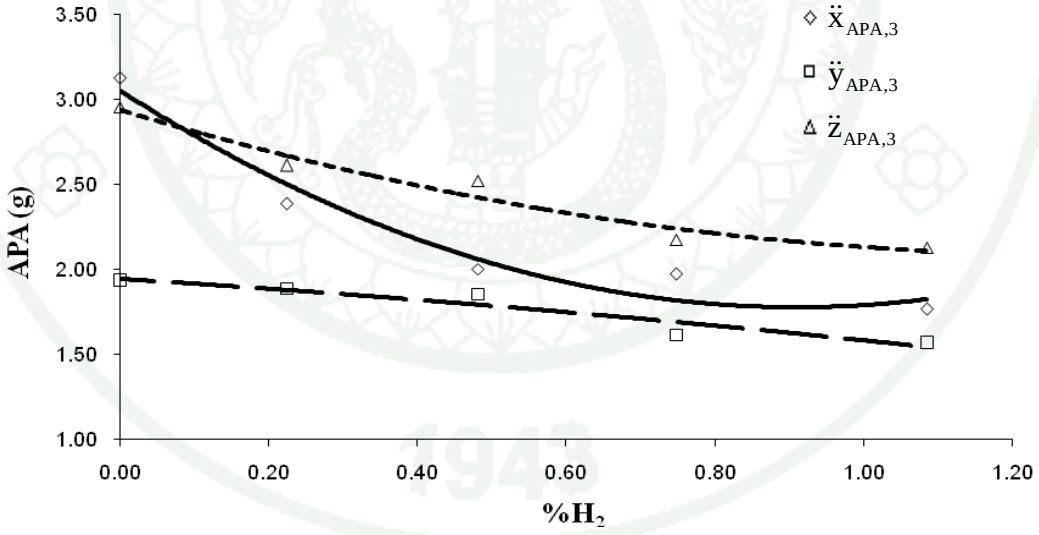

Figure 47 The correlation between APA at point 3 and $\%H_2$ (Exp. 2 and n = 2)

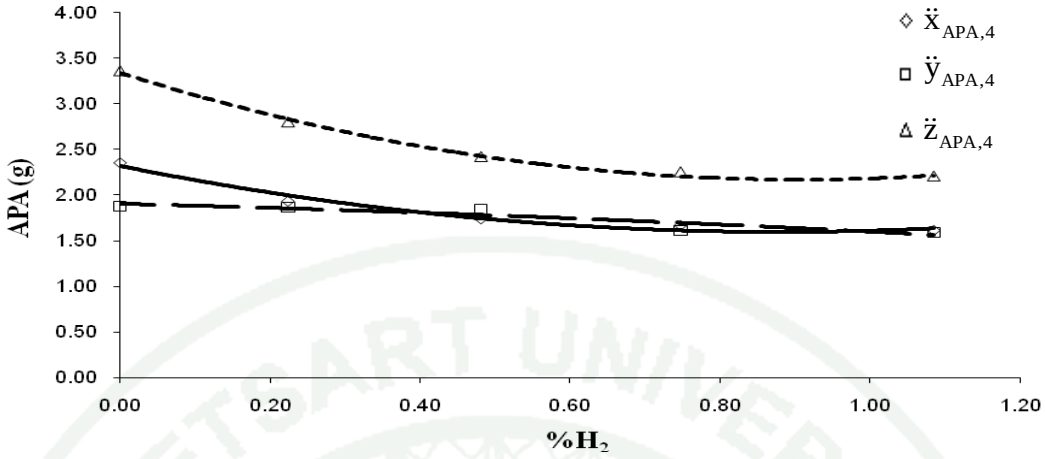

Figure 48 The correlation between APA at point 4 and $\%H_2$ (Exp. 2 and n = 2)

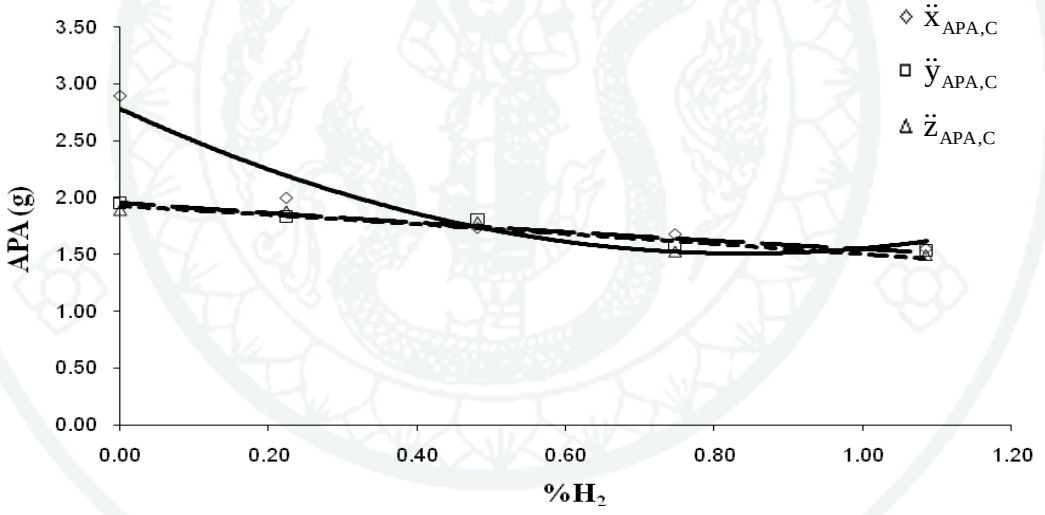

Figure 49 The correlation between APA at point C and $\%H_2$ (Exp. 2 and n = 2)

For the test condition Exp. 3 (N = 1,600 rpm, T = 50%) the average peak acceleration is plotted against the hydrogen percentage as shown in Figure 50 to Figure 59.

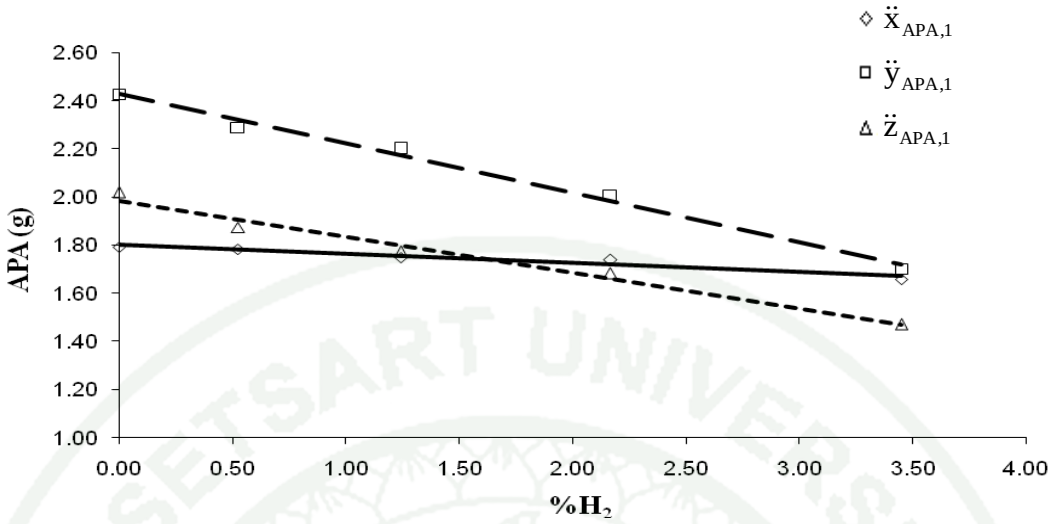

Figure 50 The correlation between APA at point 1 and $\%H_2$ (Exp. 3 and n = 1)

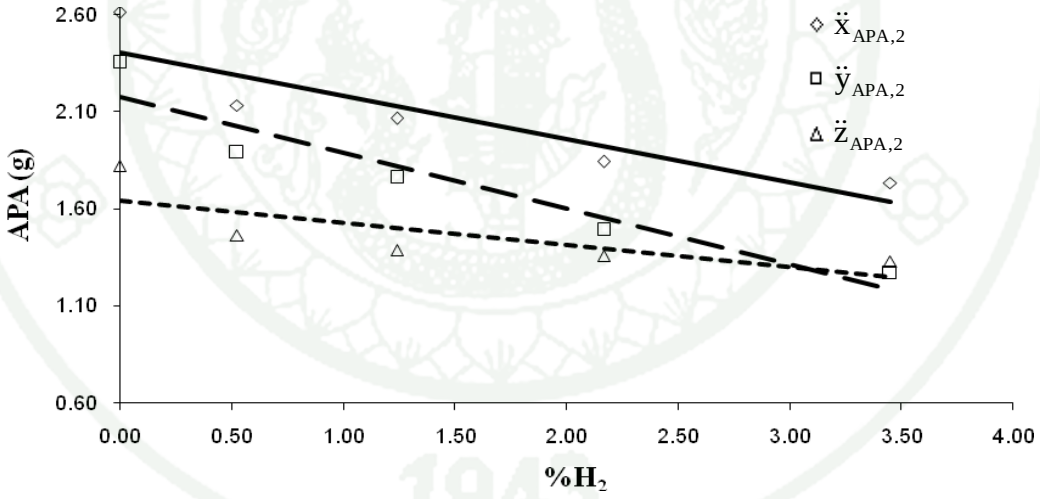

Figure 51 The correlation between APA at point 2 and $\%H_2$ (Exp. 3 and n = 1)

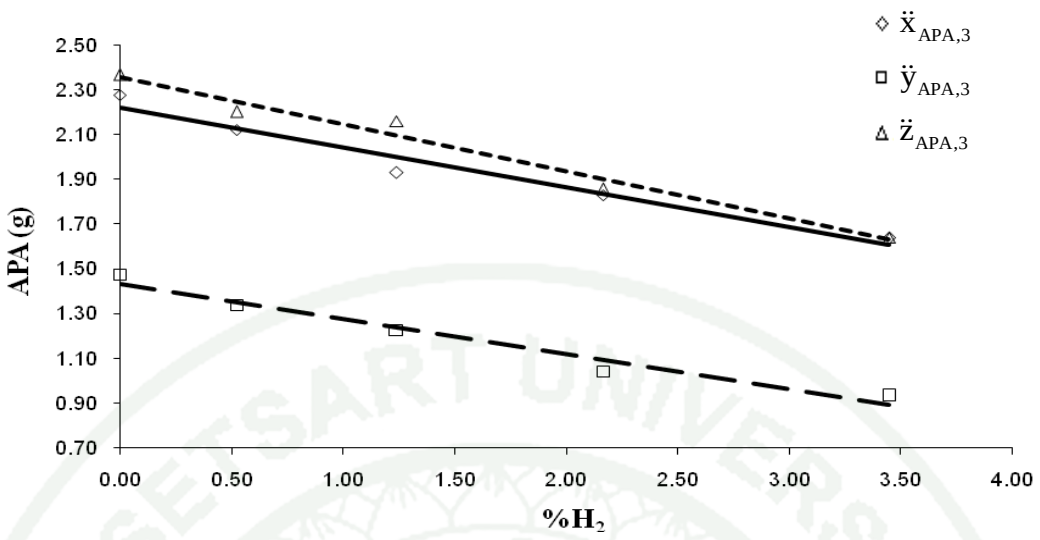

Figure 52 The correlation between APA at point 3 and $\%H_2$ (Exp. 3 and n = 1)

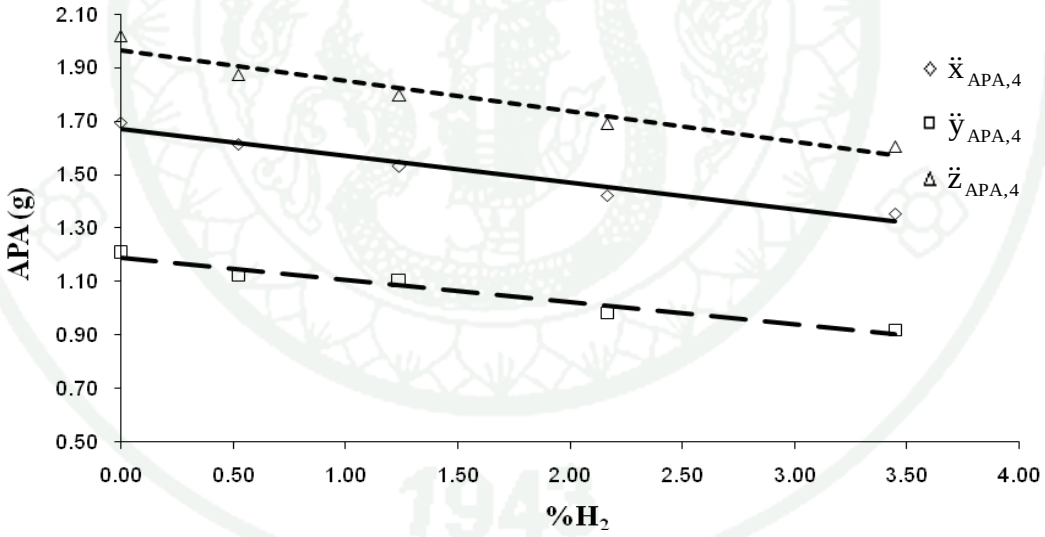

Figure 53 The correlation between APA at point 4 and $\%H_2$ (Exp. 3 and n = 1)

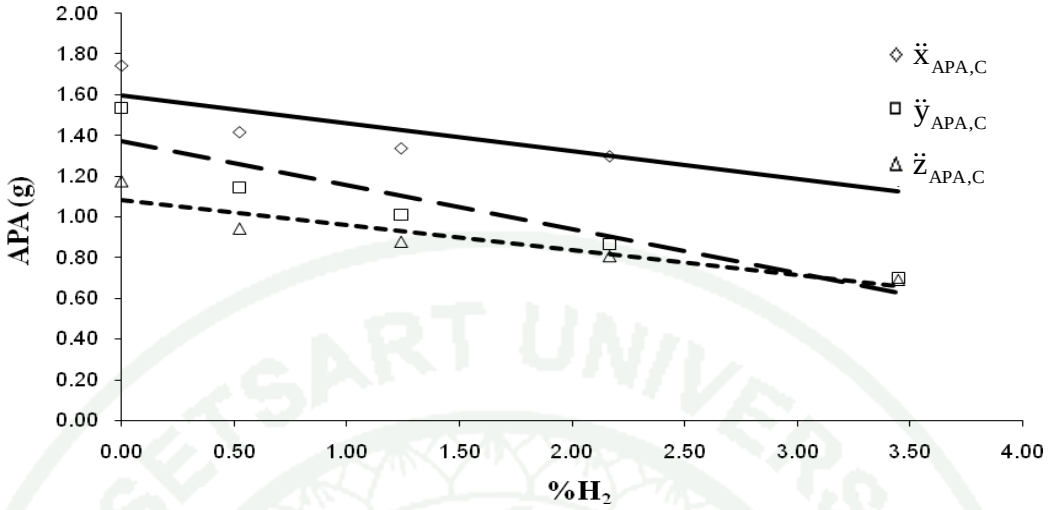

Figure 54 The correlation between APA at point C and $\%H_2$ (Exp. 3 and n = 1)

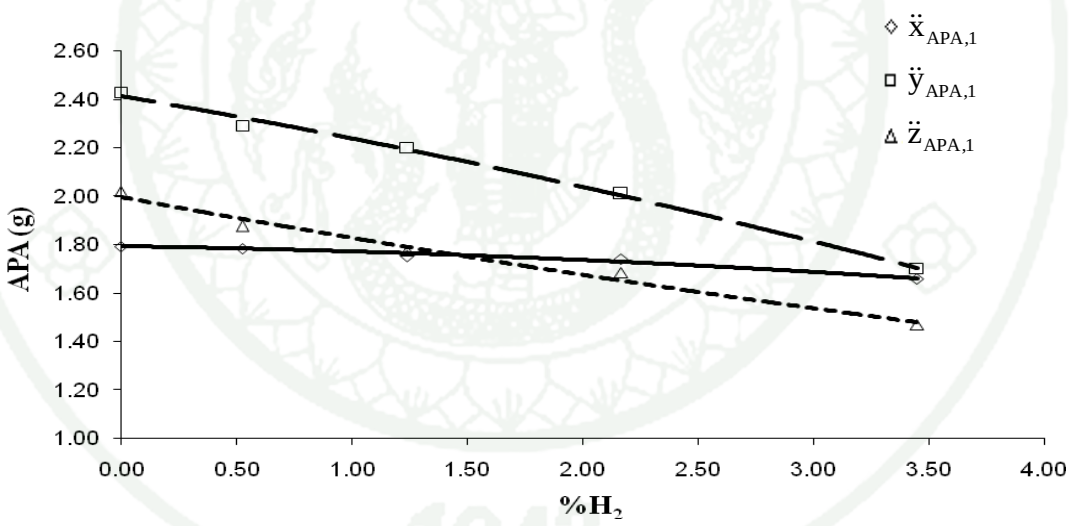

Figure 55 The correlation between APA at point 1 and $\%H_2$ (Exp. 3 and n = 2)

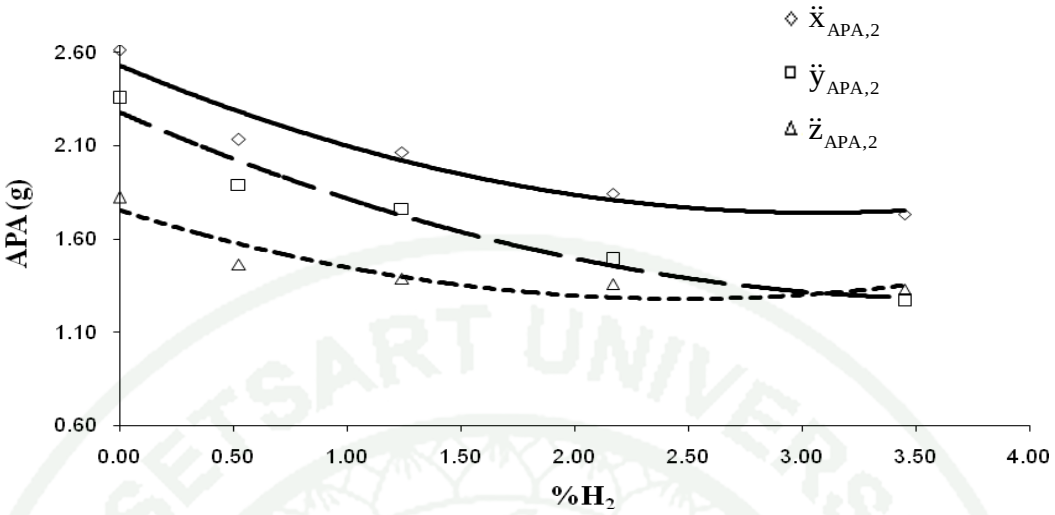

Figure 56 The correlation between APA at point 2 and $\%H_2$ (Exp. 3 and n = 2)

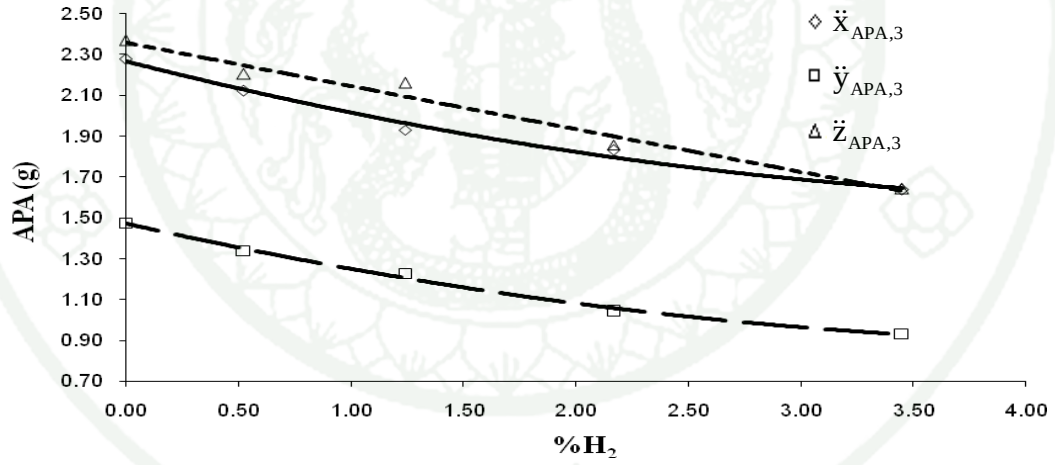

Figure 57 The correlation between APA at point 3 and $\%H_2$ (Exp. 3 and n = 2)

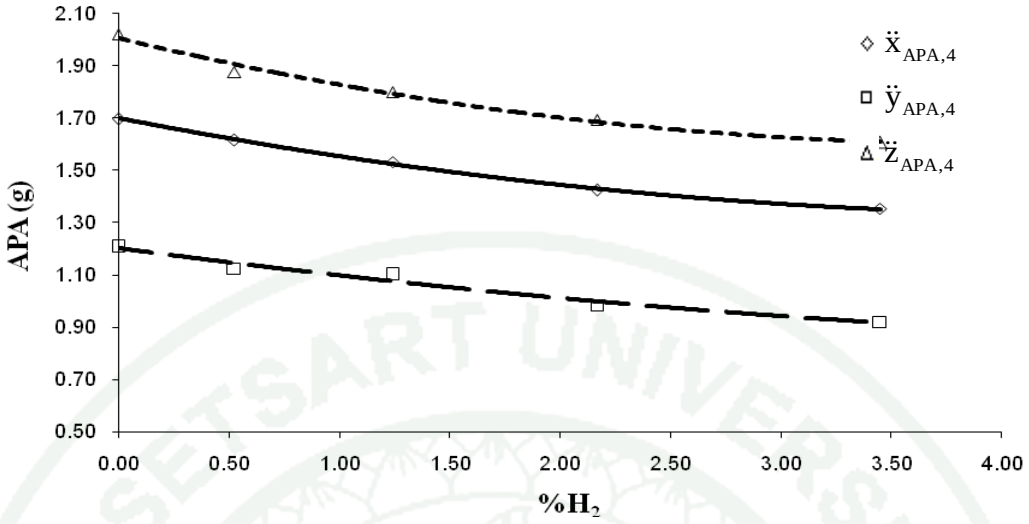

Figure 58 The correlation between APA at point 4 and $\%H_2$ (Exp. 3 and n = 2)

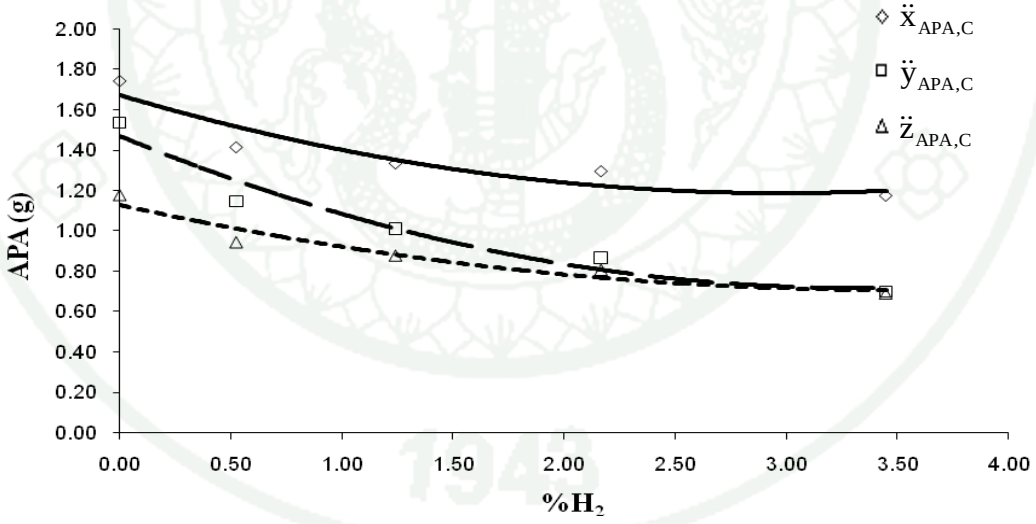

Figure 59 The correlation between APA at point C and $\%H_2$ (Exp. 3 and n = 2)

For the test condition Exp. 4 (N = 1,600, T = 25%) the the average peak acceleration is plotted against hydrogen percentage as shown in Figure 60 to Figure 69.

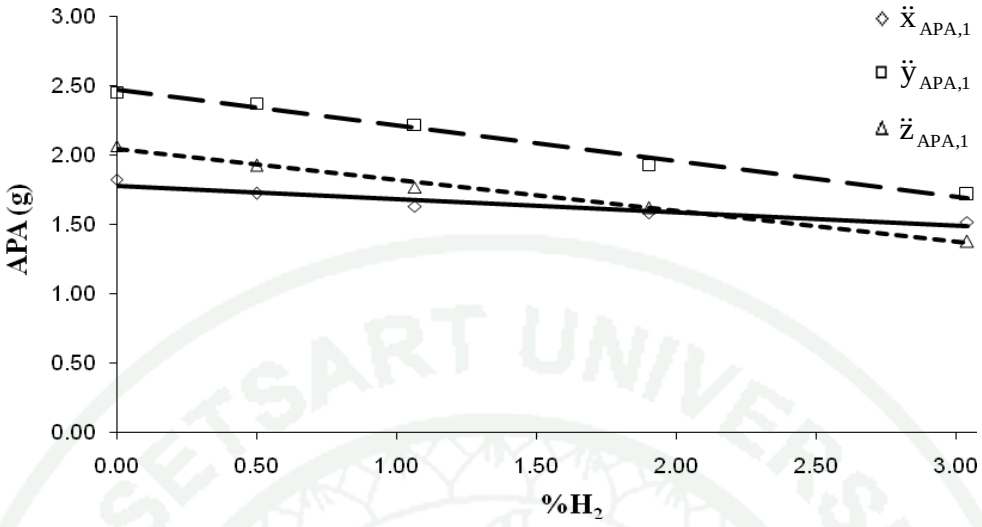

Figure 60 The correlation between APA at point 1 and $\%H_2$ (Exp. 4 and n = 1)

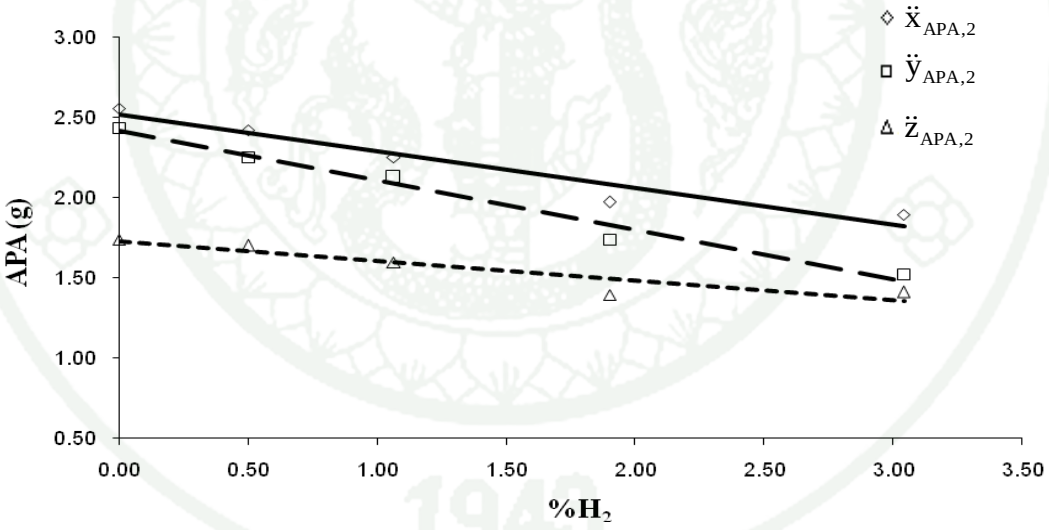

Figure 61 The correlation between APA at point 2 and $\%H_2$ (Exp. 4 and n = 1)

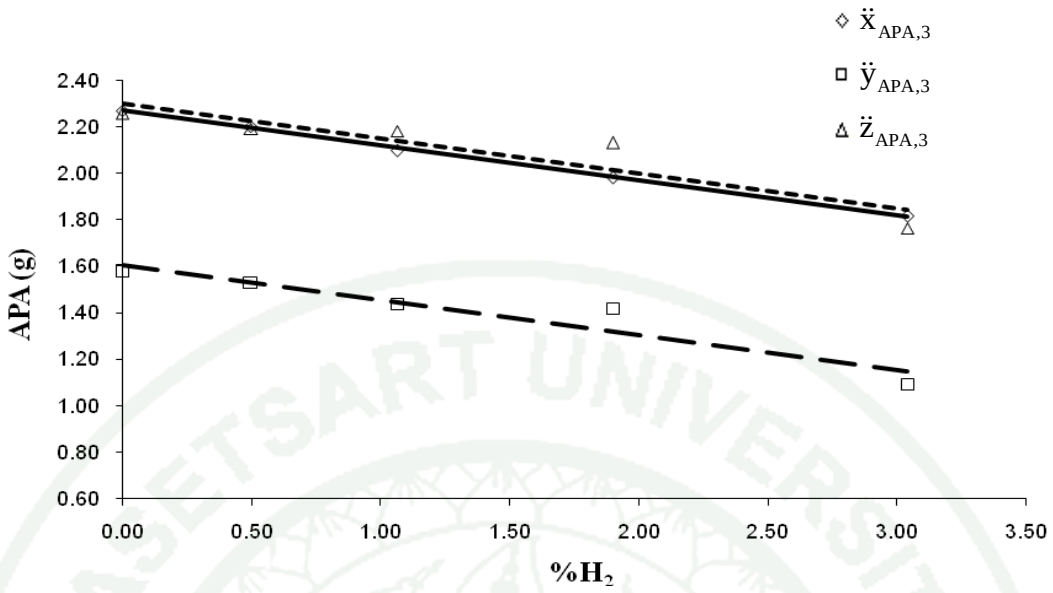

Figure 62 The correlation between APA at point 3 and $\%H_2$ (Exp. 4 and n = 1)

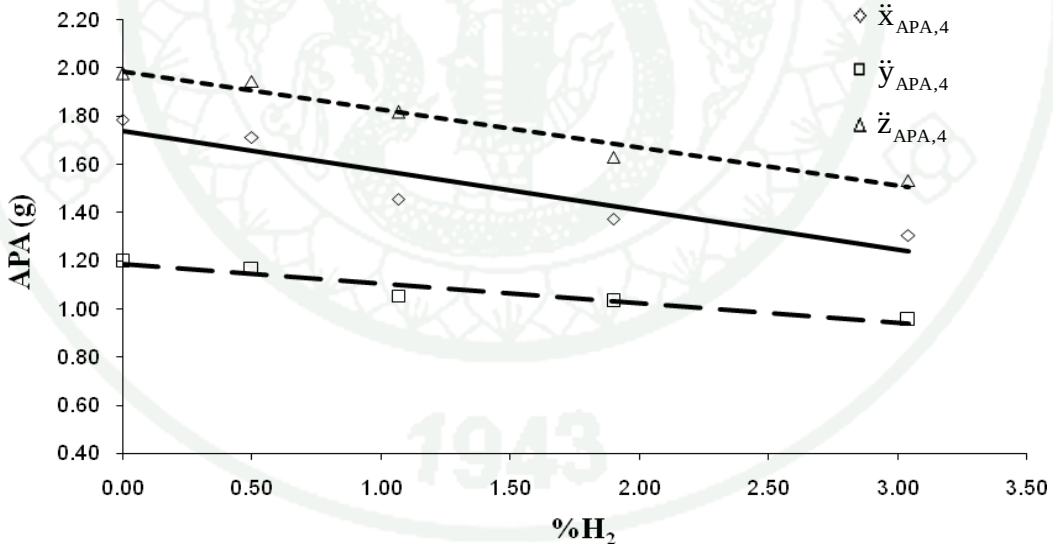

Figure 63 The correlation between APA at point 4 and $\%H_2$ (Exp. 4 and n = 1)

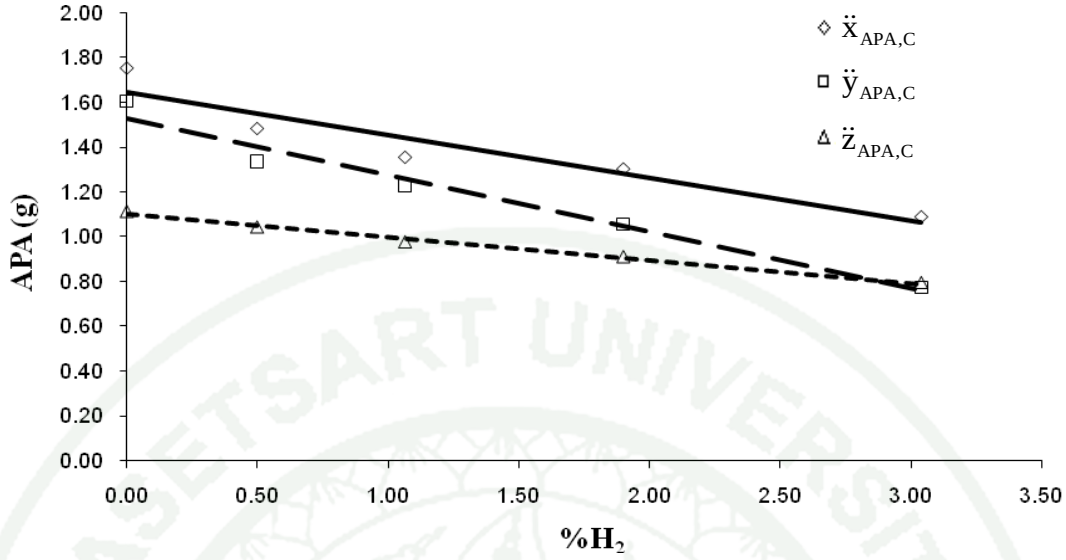

Figure 64 The correlation between APA at point C and $\%H_2$ (Exp. 4 and n = 1)

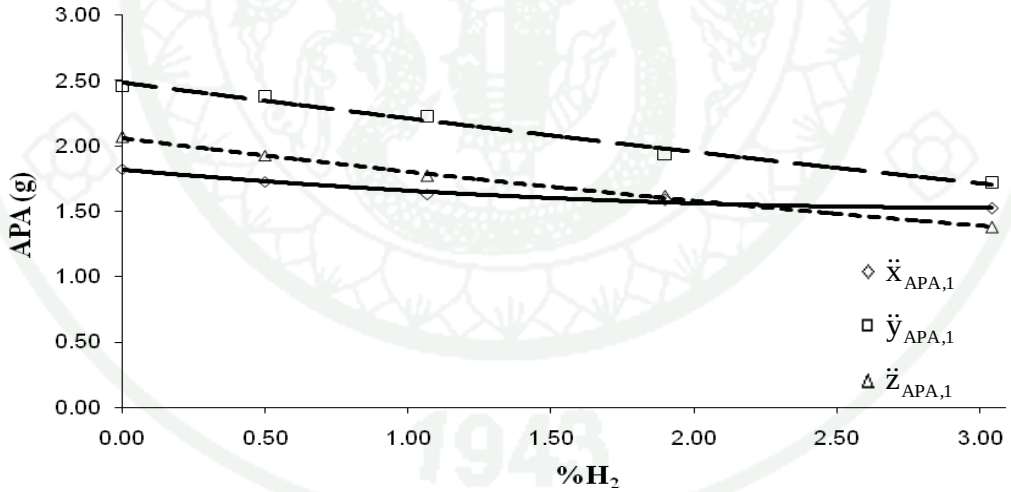

Figure 65 The correlation between APA at point 1 and $\%H_2$ (Exp. 4 and n = 2)

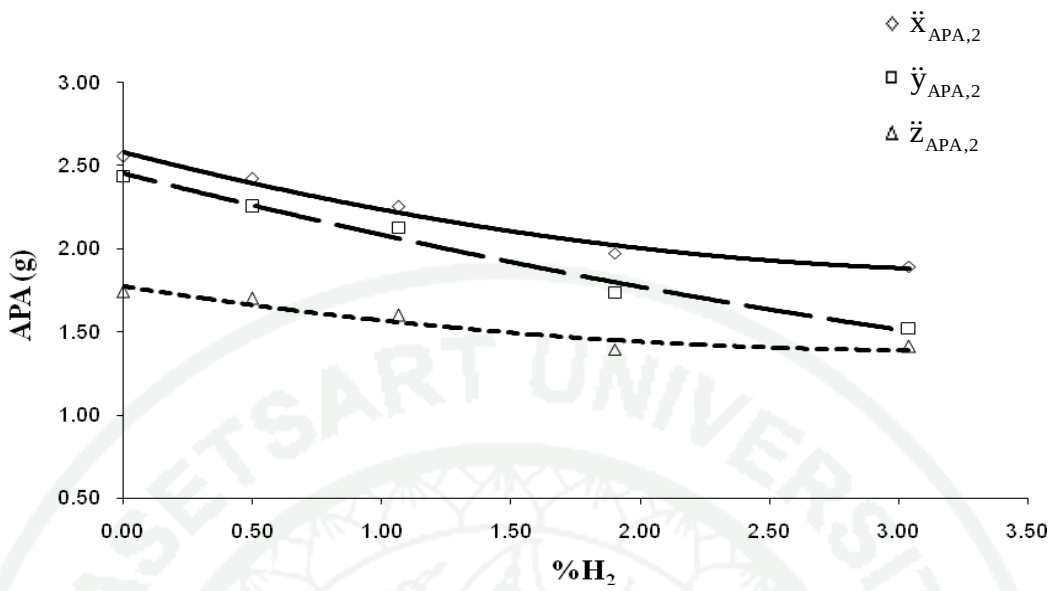

Figure 66 The correlation between APA at point 2 and $\%H_2$ (Exp. 4 and n = 2)

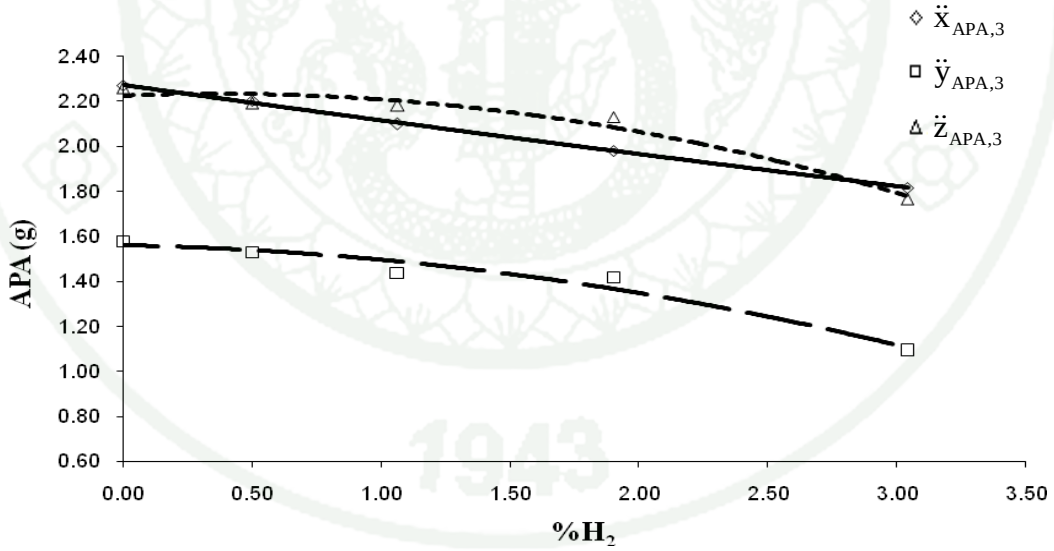

Figure 67 The correlation between APA at point 3 and $\%H_2$ (Exp. 4 and n = 2)

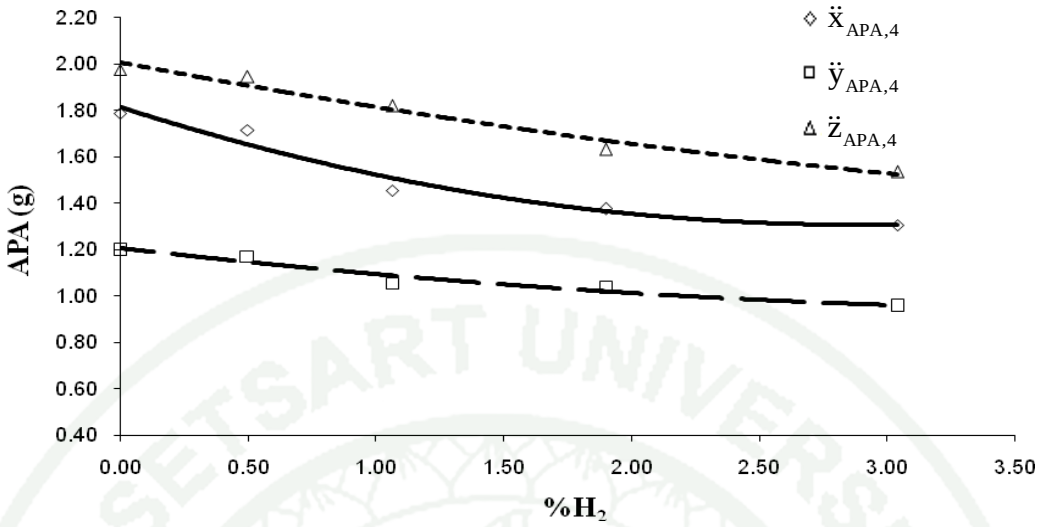

Figure 68 The correlation between APA at point 4 and $\%H_2$ (Exp. 4 and n = 2)

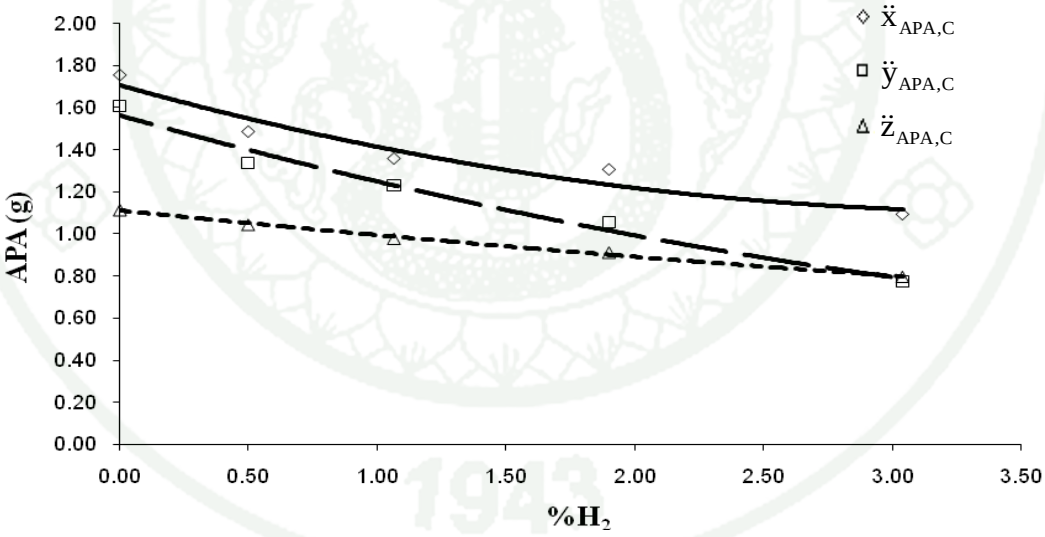

Figure 69 The correlation between APA at point C and $\%H_2$ (Exp. 4 and n = 2)

By using Equation (61) and Equation (65), the relationships between the average peak acceleration and hydrogen percentage in first (n=1) and second (n=2) orders generate the correlation constants for regression analysis numerated in Table 13.

Table 13 Correlation constants for the relation between APA and $\%H_2$

n	APA	a	b	c	R^2
1	Exp. 1				
	$\ddot{x}_{APA,1}$	-0.4877	2.3831		0.9872
	$\ddot{y}_{APA,1}$	-0.5169	2.033		0.9704
	$\ddot{z}_{APA,1}$	-0.2766	1.8642		0.883
	$\ddot{x}_{APA,2}$	-0.4465	2.7325		0.8541
	$\ddot{y}_{APA,2}$	-0.3572	1.7786		0.99
	$\ddot{z}_{APA,2}$	-0.3864	1.9701		0.9248
	$\ddot{x}_{APA,3}$	-0.5408	2.3065		0.9356
	$\ddot{y}_{APA,3}$	-0.264	1.3505		0.7798
	$\ddot{z}_{APA,3}$	-0.6471	2.1324		0.8097
	$\ddot{x}_{APA,4}$	-0.6716	2.1822		0.8604
	$\ddot{y}_{APA,4}$	-0.5078	1.959		0.9745
	$\ddot{z}_{APA,4}$	-0.1241	1.9317		0.9963
	$\ddot{x}_{APA,CG}$	-0.7019	2.2799		0.8988
	$\ddot{y}_{APA,CG}$	-0.2835	1.3563		0.941
	$\ddot{z}_{APA,CG}$	-0.3385	1.5143		0.9395
1	Exp.2				
	$\ddot{x}_{APA,1}$	-0.8476	2.4619		0.7863
	$\ddot{y}_{APA,1}$	-0.6036	2.6952		0.9461
	$\ddot{z}_{APA,1}$	-1.3849	2.7375		0.6545
	$\ddot{x}_{APA,2}$	-0.7194	2.8017		0.7649
	$\ddot{y}_{APA,2}$	-0.3779	2.4622		0.9756
	$\ddot{z}_{APA,2}$	-0.407	1.8919		0.8262
	$\ddot{x}_{APA,3}$	-1.1268	2.8221		0.7997
	$\ddot{y}_{APA,3}$	-0.3736	1.9607		0.9051
	$\ddot{z}_{APA,3}$	-0.7617	2.8652		0.9179
	$\ddot{x}_{APA,4}$	-0.6273	2.1823		0.7904
	$\ddot{y}_{APA,4}$	-0.3129	1.9156		0.8385
	$\ddot{z}_{APA,4}$	-1.0253	3.1255		0.8295
	$\ddot{x}_{APA,CG}$	-1.0728	2.5158		0.716
	$\ddot{y}_{APA,CG}$	-0.3984	1.9453		0.9397
	$\ddot{z}_{APA,CG}$	-0.4312	1.9354		0.897

Table 13 (Continued)

n	APA	a	b	c	R^2
1	Exp.3				
	$\ddot{x}_{APA,1}$	-0.0377	1.8016		0.9437
	$\ddot{y}_{APA,1}$	-0.2051	2.4294		0.9914
	$\ddot{z}_{APA,1}$	-0.1491	1.9851		0.9808
	$\ddot{x}_{APA,2}$	-0.2237	2.4075		0.8119
	$\ddot{y}_{APA,2}$	-0.2873	2.1771		0.9065
	$\ddot{z}_{APA,2}$	-0.1132	1.6397		0.5887
	$\ddot{x}_{APA,3}$	-0.1785	2.2233		0.9643
	$\ddot{y}_{APA,3}$	-0.1572	1.4359		0.9679
	$\ddot{z}_{APA,3}$	-0.2104	2.3572		0.9758
	$\ddot{x}_{APA,4}$	-0.0996	1.6707		0.9659
	$\ddot{y}_{APA,4}$	-0.082	1.1879		0.962
	$\ddot{z}_{APA,4}$	-0.1138	1.9668		0.9393
	$\ddot{x}_{APA,CG}$	-0.1355	1.5946		0.7573
	$\ddot{y}_{APA,CG}$	-0.2154	1.3701		0.8639
	$\ddot{z}_{APA,CG}$	-0.1223	1.0807		0.8624
1	Exp.4				
	$\ddot{x}_{APA,1}$	-0.0945	1.7796		0.9057
	$\ddot{y}_{APA,1}$	-0.2561	2.4717		0.9875
	$\ddot{z}_{APA,1}$	-0.223	2.0416		0.993
	$\ddot{x}_{APA,2}$	-0.2286	2.5169		0.9384
	$\ddot{y}_{APA,2}$	-0.309	2.4181		0.9784
	$\ddot{z}_{APA,2}$	-0.1242	1.7316		0.858
	$\ddot{x}_{APA,3}$	-0.1504	2.2697		0.9985
	$\ddot{y}_{APA,3}$	-0.1504	1.608		0.9052
	$\ddot{z}_{APA,3}$	-0.1496	2.3003		0.8417
	$\ddot{x}_{APA,4}$	-0.1637	1.74		0.8638
	$\ddot{y}_{APA,4}$	-0.0804	1.1866		0.9275
	$\ddot{z}_{APA,4}$	-0.1581	1.9861		0.9643
	$\ddot{x}_{APA,CG}$	-0.1923	1.6486		0.8972
	$\ddot{y}_{APA,CG}$	-0.254	1.5312		0.9707
	$\ddot{z}_{APA,CG}$	-0.1023	1.101		0.9923

Table 13 (Continued)

n	APA	a	b	c	R^2
2	Exp.1				
	$\ddot{x}_{APA,1}$	0.0938	-0.6374	2.4125	0.995
	$\ddot{y}_{APA,1}$	0.1651	-0.7802	2.0848	0.9916
	$\ddot{z}_{APA,1}$	-0.1646	-0.0141	1.8126	0.9497
	$\ddot{x}_{APA,2}$	-0.1688	-0.1773	2.6796	0.8801
	$\ddot{y}_{APA,2}$	-0.022	-0.3221	1.7717	0.9908
	$\ddot{z}_{APA,2}$	0.157	-0.6367	2.0193	0.9573
	$\ddot{x}_{APA,3}$	0.2888	-1.0015	2.397	0.9925
	$\ddot{y}_{APA,3}$	0.1712	-0.537	1.4042	0.8498
	$\ddot{z}_{APA,3}$	0.6458	-1.677	2.3349	0.9818
	$\ddot{x}_{APA,4}$	0.4868	-1.4479	2.3349	0.9569
	$\ddot{y}_{APA,4}$	0.0639	-0.6098	1.9791	0.9778
	$\ddot{z}_{APA,4}$	-0.0045	-0.1168	1.9303	0.9965
	$\ddot{x}_{APA,CG}$	0.4489	-1.4178	2.4206	0.9772
	$\ddot{y}_{APA,CG}$	0.0829	-0.4158	1.3823	0.9582
	$\ddot{z}_{APA,CG}$	0.1032	-0.5031	1.5466	0.9581
2	Exp.2				
	$\ddot{x}_{APA,1}$	1.2233	-2.1782	2.6434	0.9592
	$\ddot{y}_{APA,1}$	0.3426	-0.9763	2.746	0.9783
	$\ddot{z}_{APA,1}$	2.7438	-4.3693	3.1448	0.9257
	$\ddot{x}_{APA,2}$	1.071	-1.8843	2.9607	0.9439
	$\ddot{y}_{APA,2}$	-0.1754	-0.1871	2.4362	0.9978
	$\ddot{z}_{APA,2}$	0.4602	-0.9076	1.9603	0.9378
	$\ddot{x}_{APA,3}$	1.5375	-2.7992	3.0503	0.9569
	$\ddot{y}_{APA,3}$	-0.0902	-0.2755	1.9473	0.9107
	$\ddot{z}_{APA,3}$	0.5082	-1.3145	2.9407	0.9611
	$\ddot{x}_{APA,4}$	0.932	-1.6411	2.3207	0.9746
	$\ddot{y}_{APA,4}$	-0.1024	-0.2015	1.9004	0.848
	$\ddot{z}_{APA,4}$	1.4129	-2.5622	3.3353	0.9959
	$\ddot{x}_{APA,CG}$	1.8152	-3.0472	2.7852	0.9325
	$\ddot{y}_{APA,CG}$	0.0509	-0.4537	1.9529	0.9414
	$\ddot{z}_{APA,CG}$	-0.0407	-0.3869	1.9294	0.8978

Table 13 (Continued)

n	APA	a	b	c	R2
2	Exp.3				
	$\ddot{x}_{APA,1}$	-0.0067	-0.0145	1.792	0.9739
	$\ddot{y}_{APA,1}$	-0.0125	-0.1616	2.4113	0.9952
	$\ddot{z}_{APA,1}$	0.0074	-0.175	1.9959	0.9832
	$\ddot{x}_{APA,2}$	0.0839	-0.515	2.5289	0.9279
	$\ddot{y}_{APA,2}$	0.0717	-0.5363	2.2807	0.9638
	$\ddot{z}_{APA,2}$	0.0765	-0.379	1.7503	0.8619
	$\ddot{x}_{APA,3}$	0.029	-0.2791	2.2652	0.9901
	$\ddot{y}_{APA,3}$	0.0264	-0.2489	1.4741	0.9956
	$\ddot{z}_{APA,3}$	0.001	-0.214	2.3587	0.9758
	$\ddot{x}_{APA,4}$	0.0181	-0.1625	1.6969	0.9984
	$\ddot{y}_{APA,4}$	0.0088	-0.1126	1.2006	0.9733
	$\ddot{z}_{APA,4}$	0.0257	-0.2032	2.004	0.9882
	$\ddot{x}_{APA,CG}$	0.0546	-0.3252	1.6736	0.8823
	$\ddot{y}_{APA,CG}$	0.0685	-0.4534	1.4692	0.9527
	$\ddot{z}_{APA,CG}$	0.0348	-0.2434	1.1312	0.9335
2	Exp.4				
	$\ddot{x}_{APA,1}$	0.0319	-0.1927	1.8165	0.9875
	$\ddot{y}_{APA,1}$	0.0084	-0.2821	2.4815	0.9884
	$\ddot{z}_{APA,1}$	0.0166	-0.274	2.0607	0.9974
	$\ddot{x}_{APA,2}$	0.0567	-0.4031	2.5824	0.9841
	$\ddot{y}_{APA,2}$	0.0282	-0.3958	2.4507	0.9848
	$\ddot{z}_{APA,2}$	0.0384	-0.2423	1.7759	0.923
	$\ddot{x}_{APA,3}$	0.0037	-0.1619	2.274	0.999
	$\ddot{y}_{APA,3}$	-0.0414	-0.0229	1.5601	0.9597
	$\ddot{z}_{APA,3}$	-0.0638	0.0466	2.2266	0.963
	$\ddot{x}_{APA,4}$	0.0612	-0.3522	1.8107	0.9597
	$\ddot{y}_{APA,4}$	0.0151	-0.1268	1.204	0.9534
	$\ddot{z}_{APA,4}$	0.0162	-0.2078	2.0048	0.9723
	$\ddot{x}_{APA,CG}$	0.0484	-0.3412	1.7045	0.9423
	$\ddot{y}_{APA,CG}$	0.0289	-0.3429	1.5646	0.9806
	$\ddot{z}_{APA,CG}$	0.0067	-0.1229	1.1087	0.9957

The graphs of the correlations between the average peak acceleration and the maximum cylinder pressure for the test condition Exp. 1 (N = 2,000 rpm and T = 25%) are shown in Figure 70 to Figure 79.

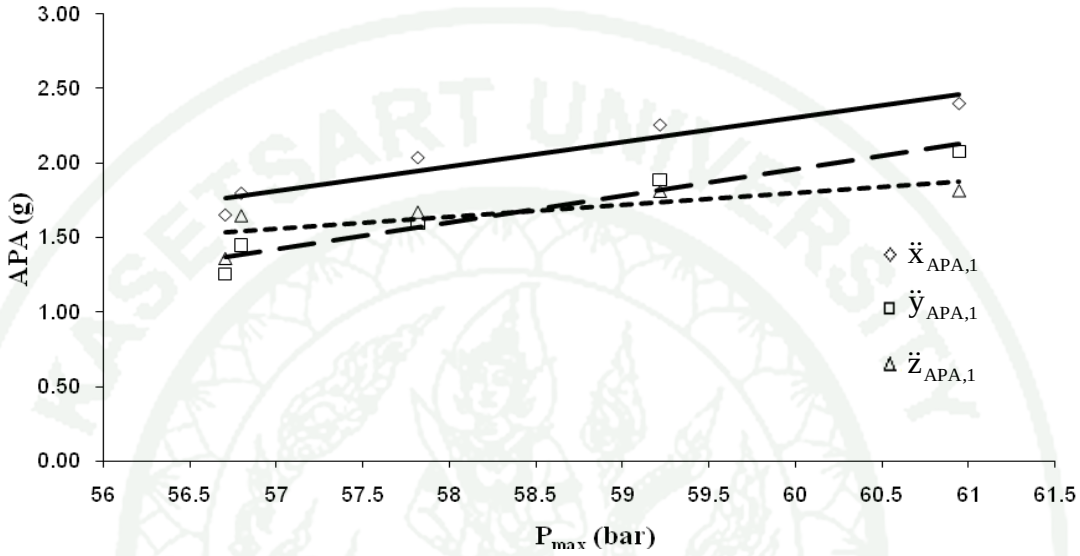

Figure 70 The correlation between APA at point 1 and P_{max} (Exp. 1 and n = 1)

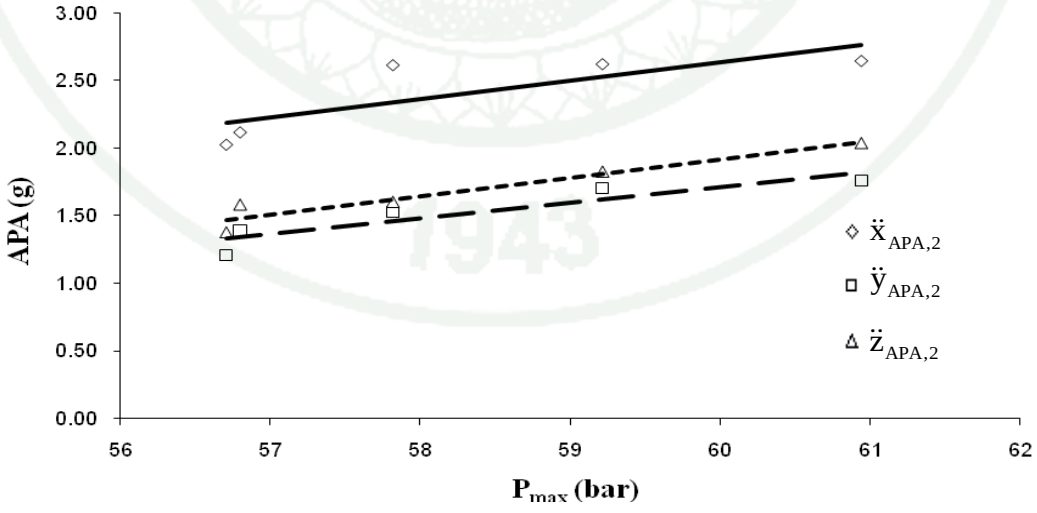

Figure 71 The correlation between APA at point 2 and P_{max} (Exp. 1 and n = 1)

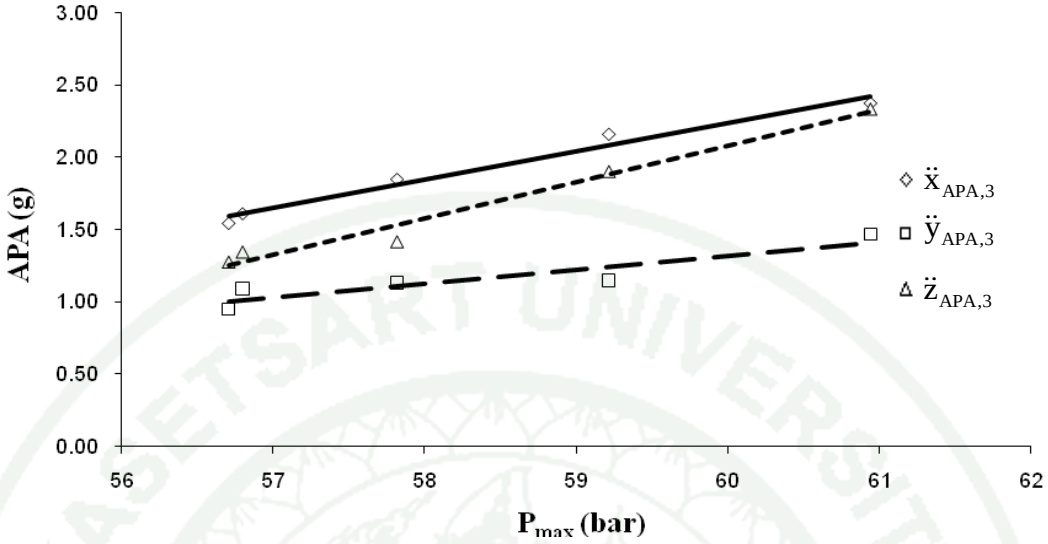

Figure 72 The correlation between APA at point 3 and P_{max} (Exp. 1 and n = 1)

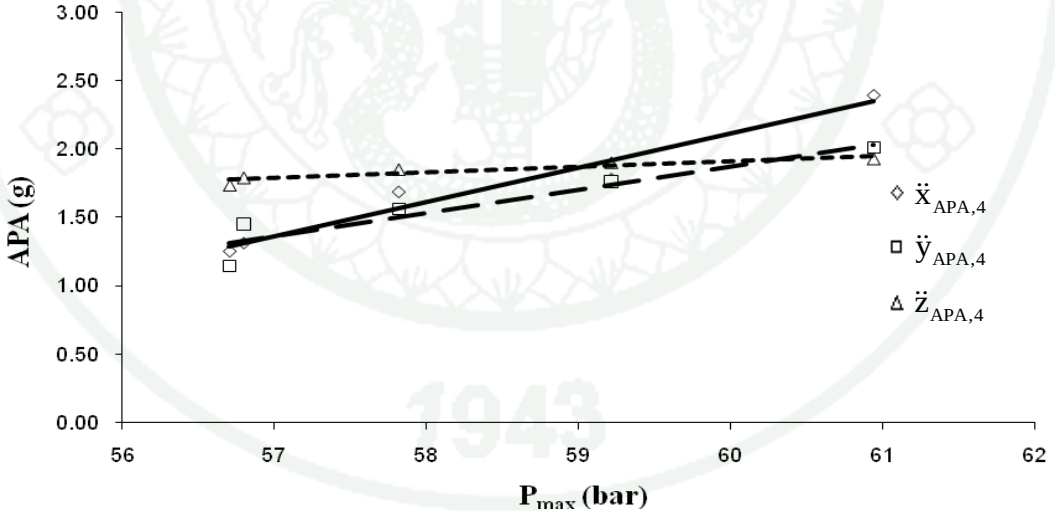

Figure 73 The correlation between APA at point 4 and P_{max} (Exp. 1 and n = 1)

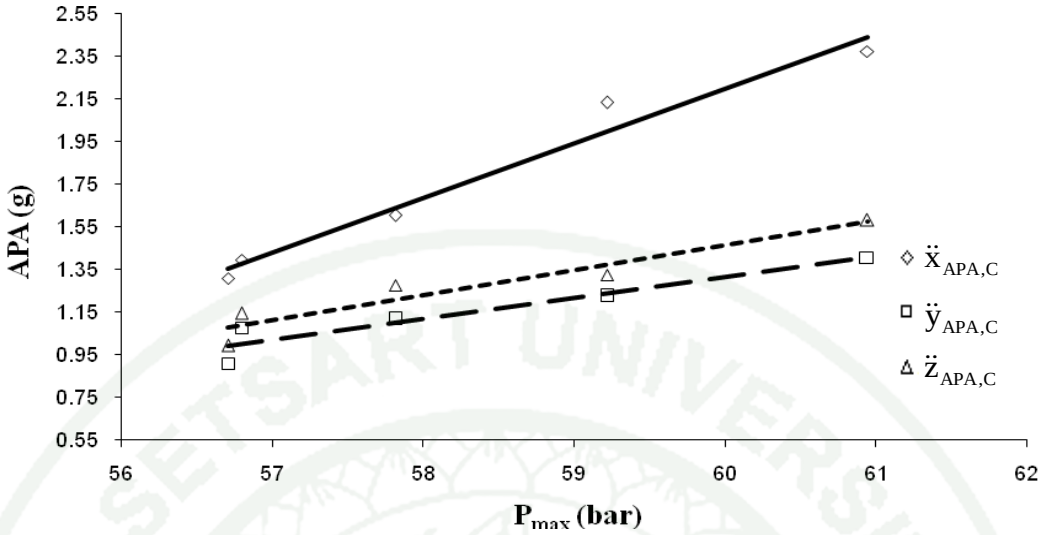

Figure 74 The correlation between APA at point C and P_{max} (Exp. 1 and n = 1)

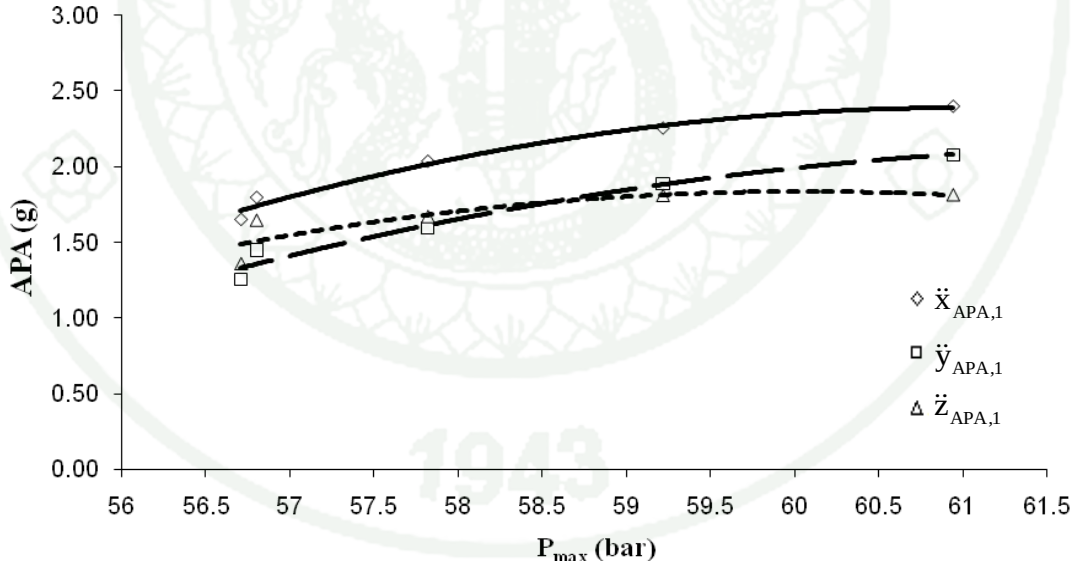

Figure 75 The correlation between APA at point 1 and P_{max} (Exp. 1 and n = 2)

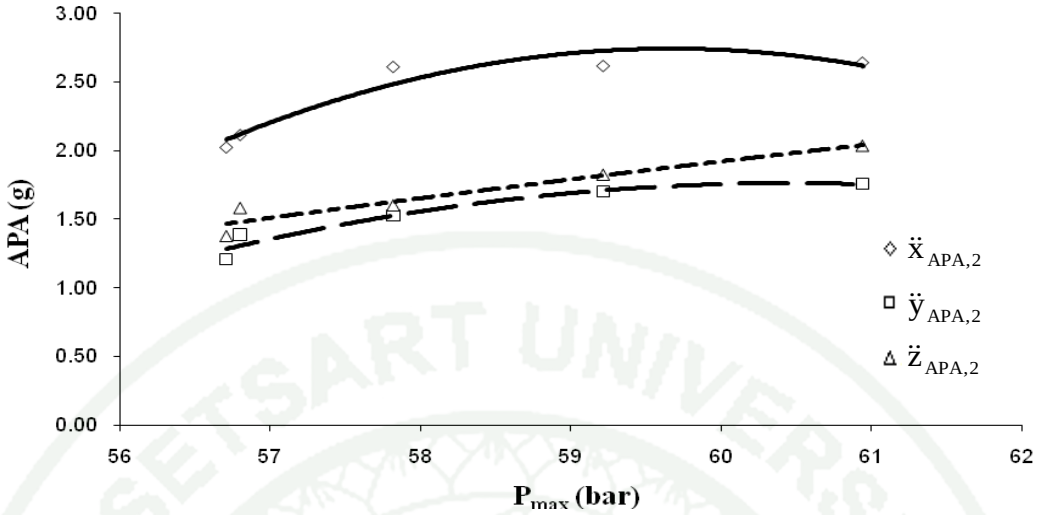

Figure 76 The correlation between APA at point 2 and P_{max} (Exp. 1 and n = 2)

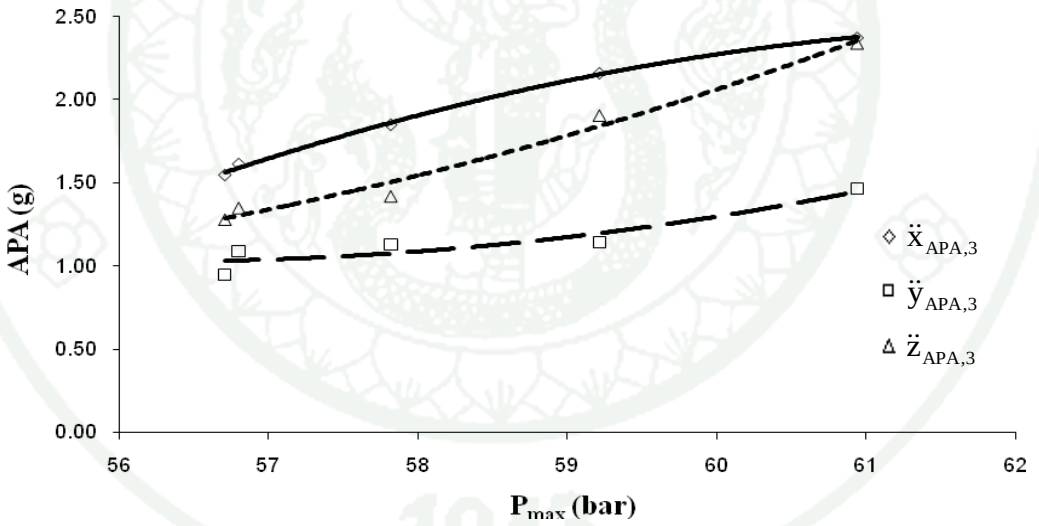

Figure 77 The correlation between APA at point 3 and P_{max} (Exp. 1 and n = 2)

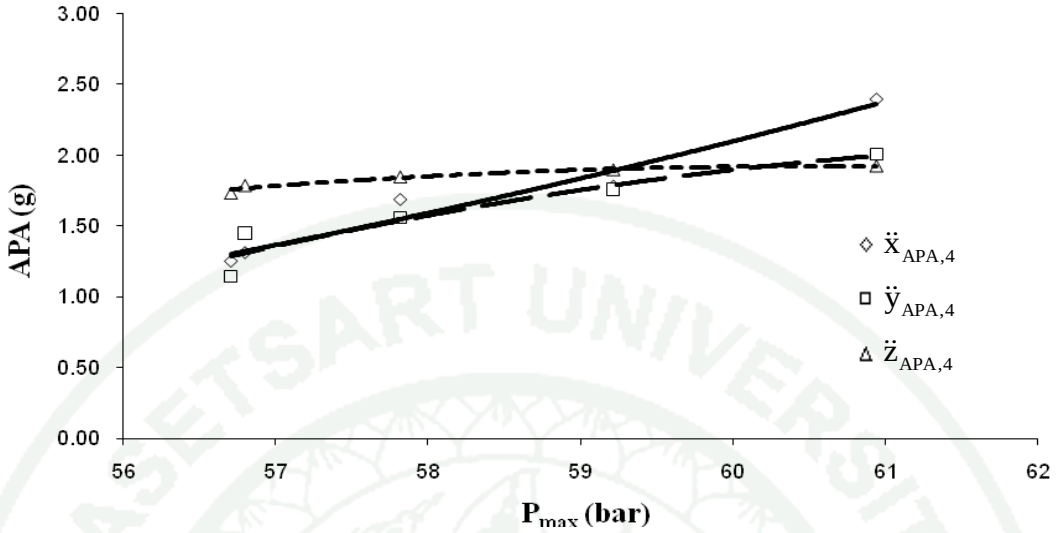

Figure 78 The correlation between APA at point 4 and P_{max} (Exp. 1 and n = 2)

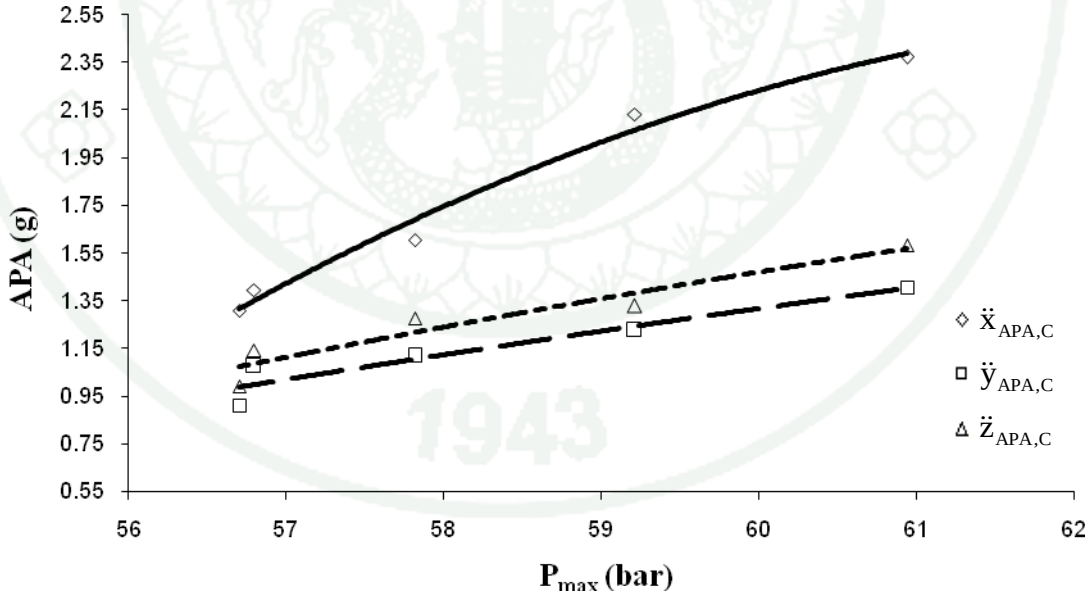

Figure 79 The correlation between APA at point C and P_{max} (Exp. 1 and n = 2)

For the test condition Exp. 2 (N = 2,000 rpm, T = 50%) the average peak acceleration is plotted against the maximum cylinder pressure as shown in Figure 80 to Figure 89.

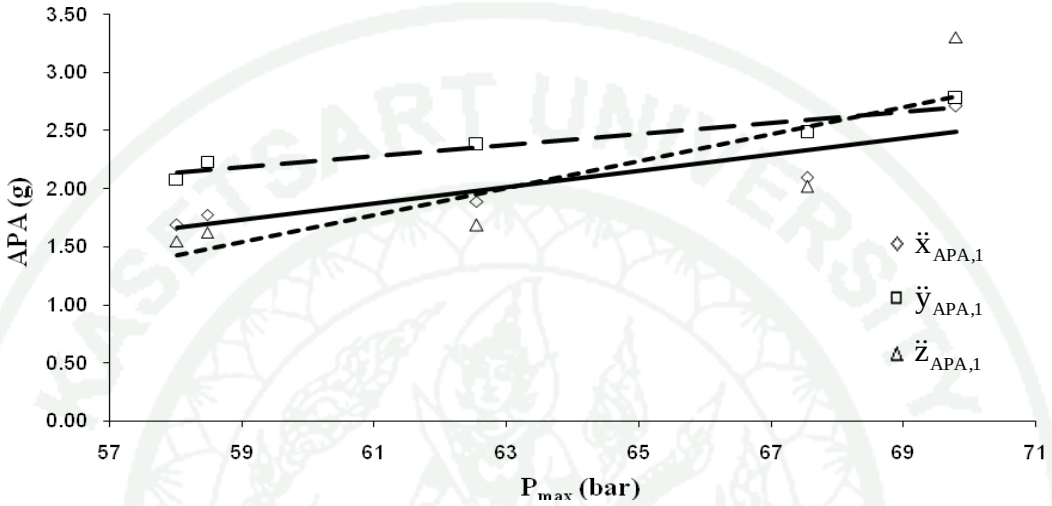

Figure 80 The correlation between APA at point 1 and P_{max} (Exp. 2 and n = 1)

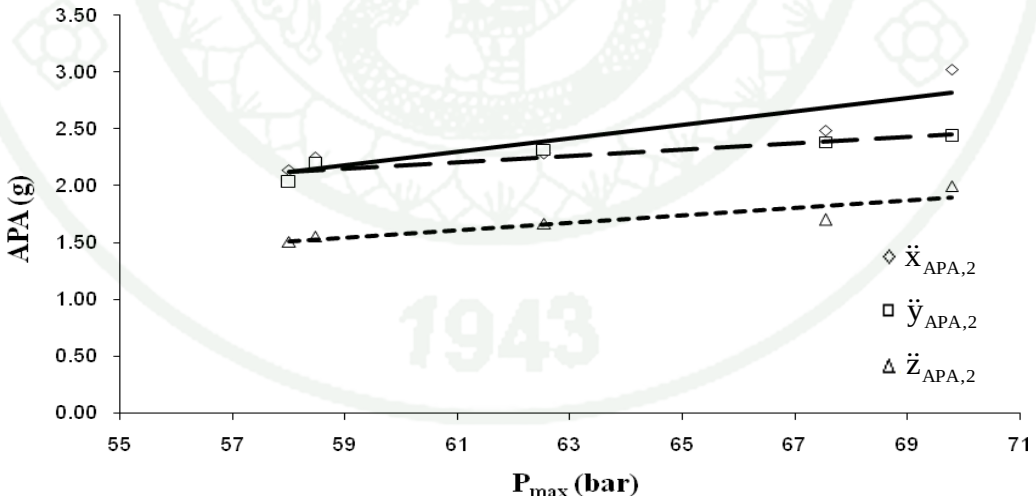

Figure 81 The correlation between APA at point 2 and P_{max} (Exp. 2 and n = 1)

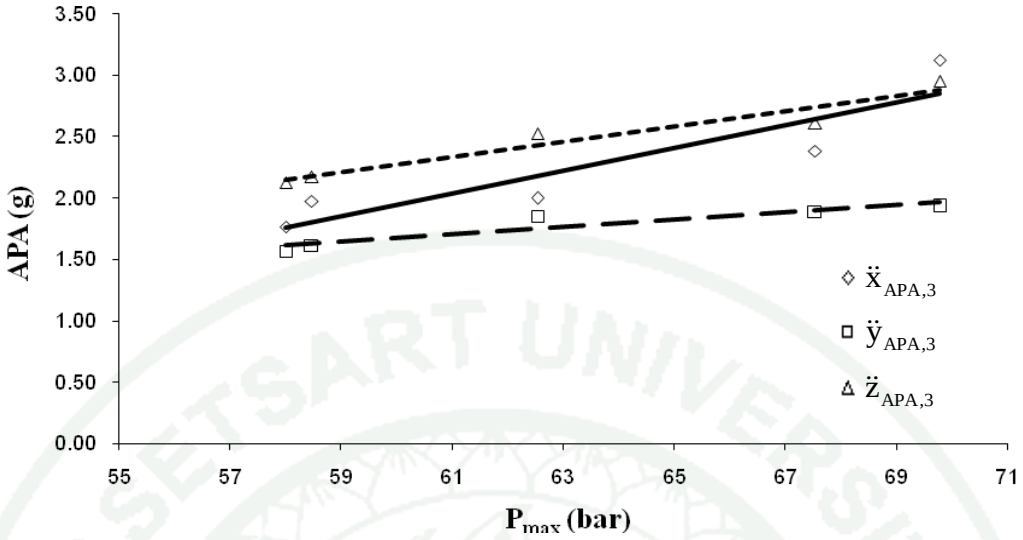

Figure 82 The correlation between APA at point 3 and P_{max} (Exp. 2 and n = 1)

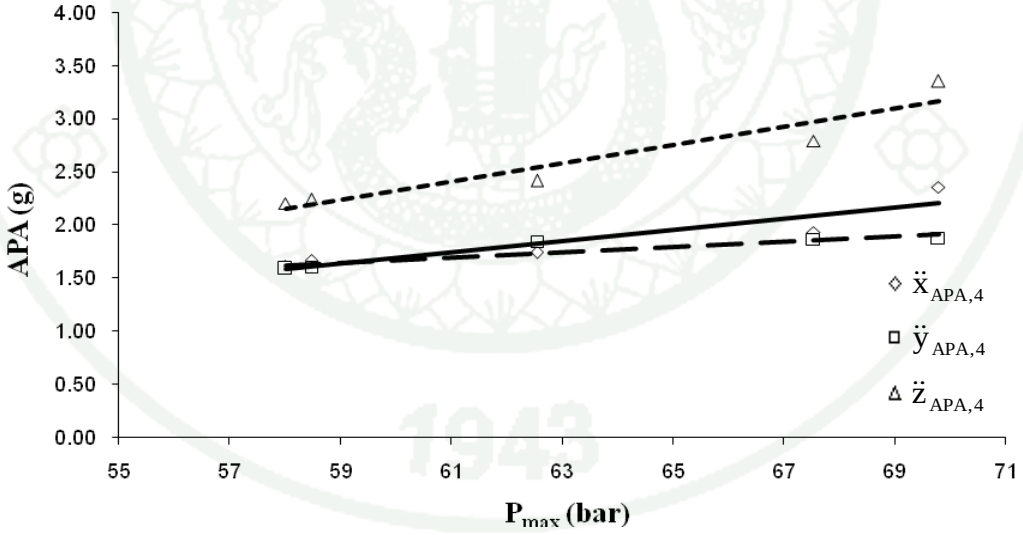

Figure 83 The correlation between APA at point 4 and P_{max} (Exp. 2 and n = 1)

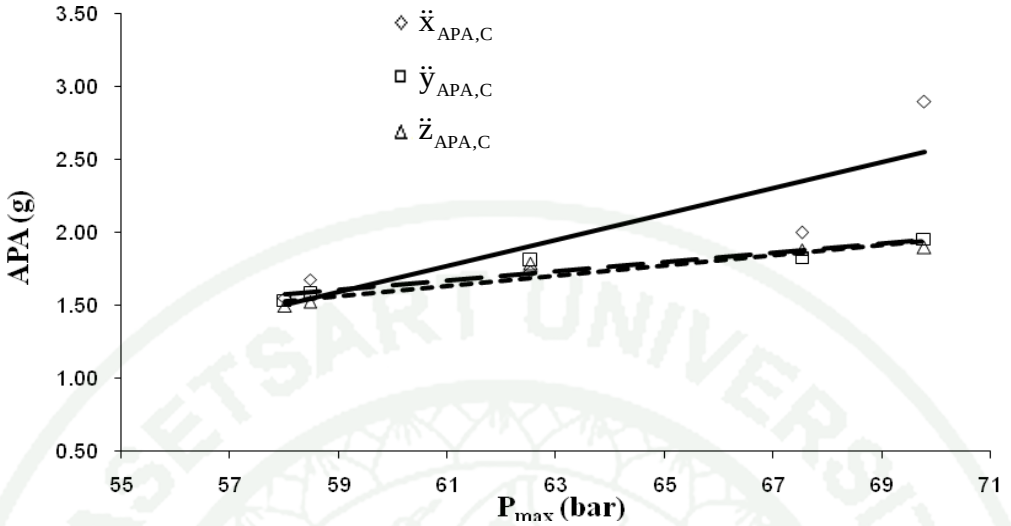

Figure 84 The correlation between APA at point C and P_{max} (Exp. 2 and n = 1)

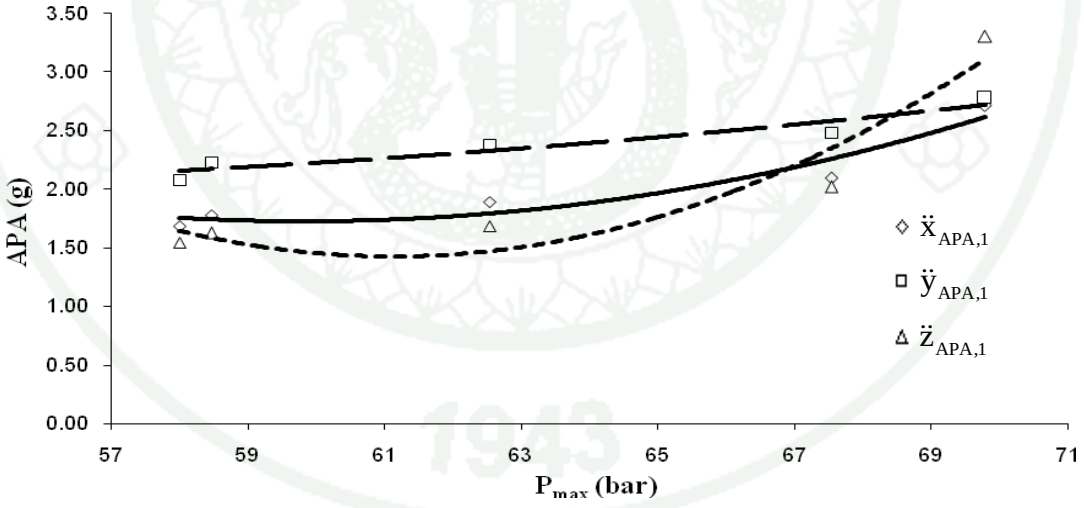

Figure 85 The correlation between APA at point 1 and P_{max} (Exp. 2 and n = 2)

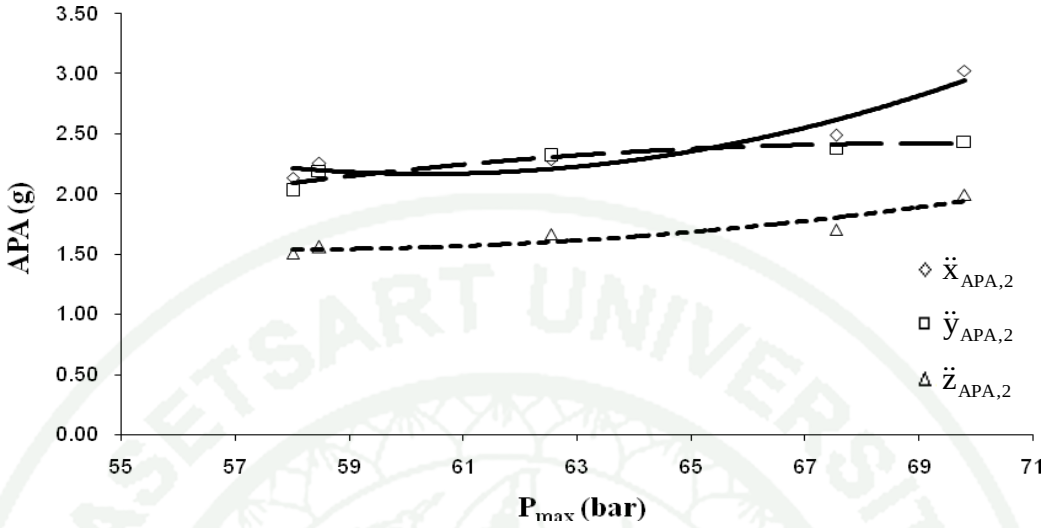

Figure 86 The correlation between APA at point 2 and P_{max} (Exp. 2 and n = 2)

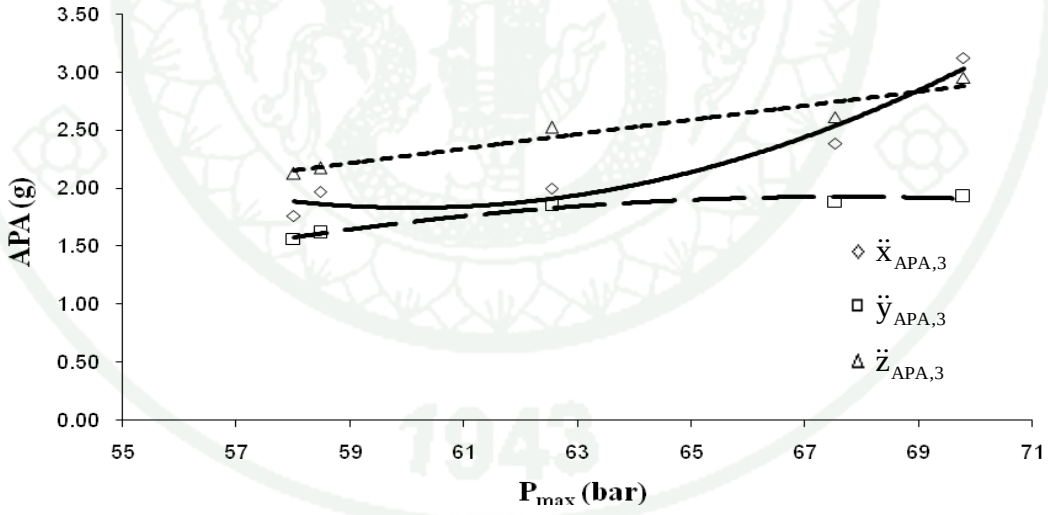

Figure 87 The correlation between APA at point 3 and $\%H_2$ (Exp. 2 and n = 2)

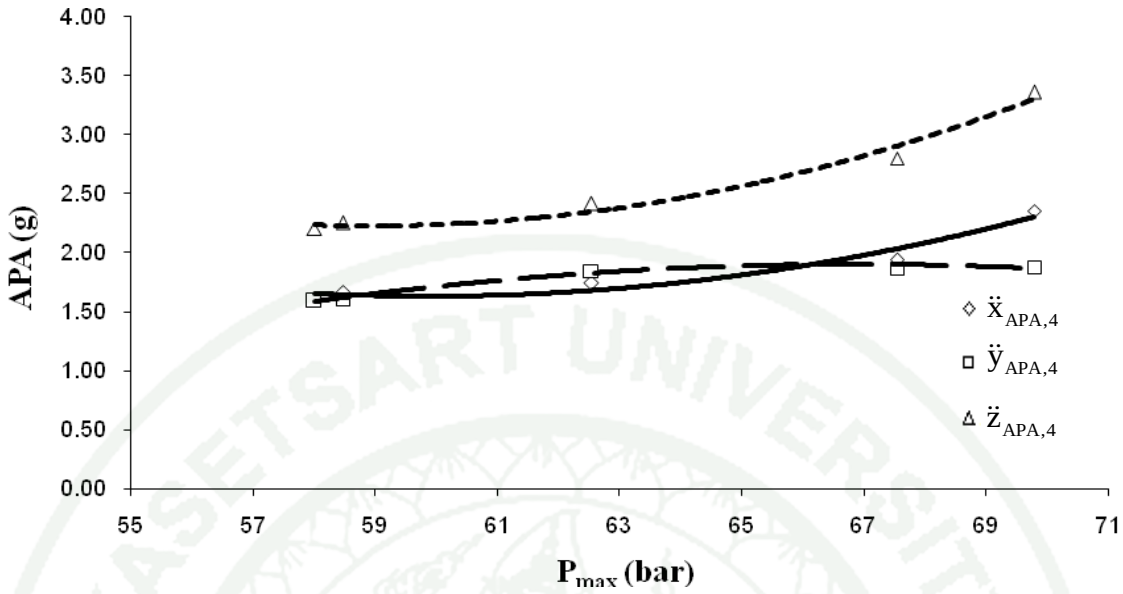

Figure 88 The correlation between APA at point 4 and P_{max} (Exp. 2 and n = 2)

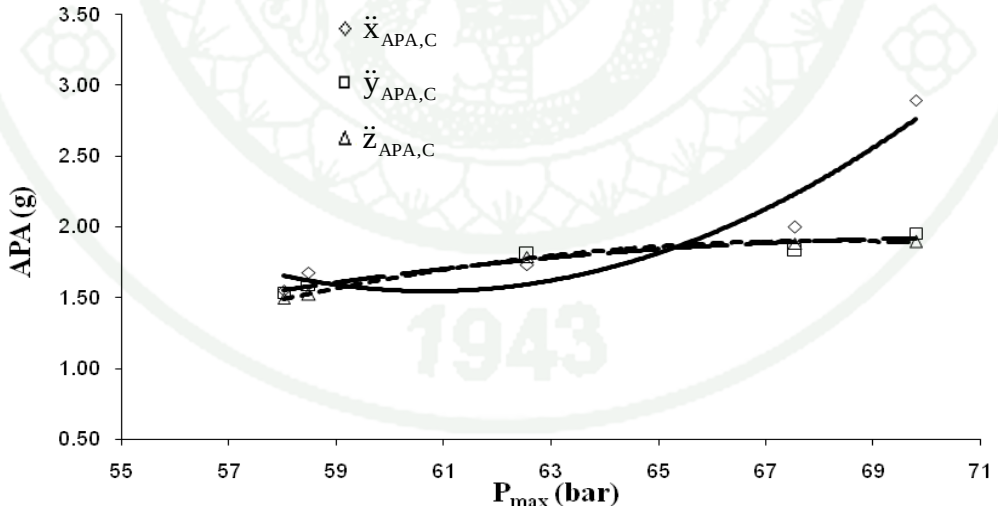

Figure 89 The correlation between APA at point C and P_{max} (Exp. 2 and n = 2)

For the test condition Exp. 3 (N = 1,600 rpm, T = 15%) the average peak acceleration is plotted against the maximum cylinder pressure as shown in Figure 89 to Figure 98.

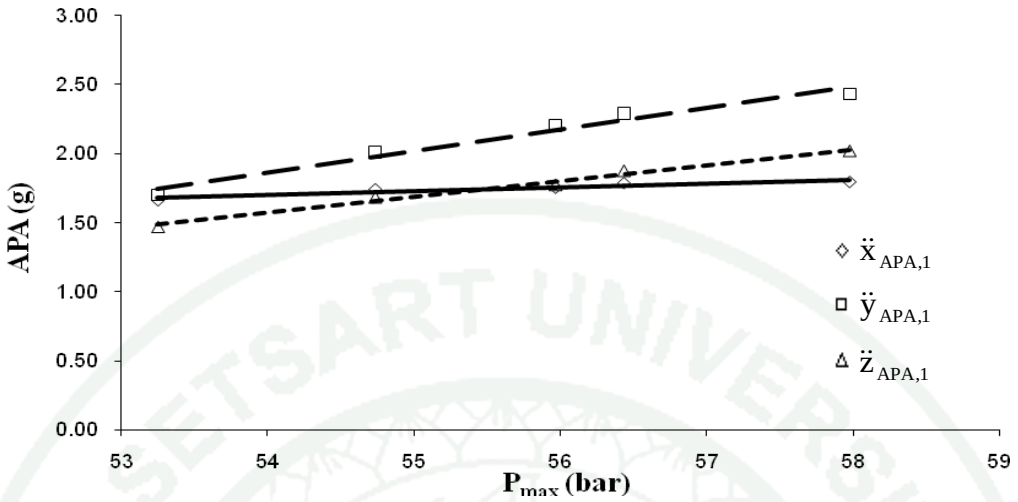

Figure 90 The correlation between APA at point 1 and P_{max} (Exp. 3 and n = 1)

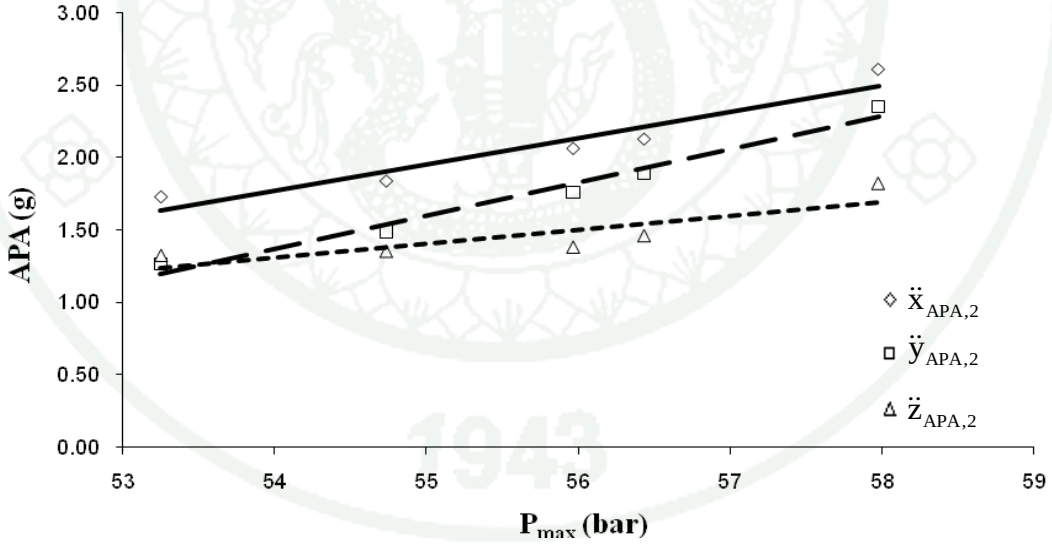

Figure 91 The correlation between APA at point 2 and P_{max} (Exp. 3 and n = 1)

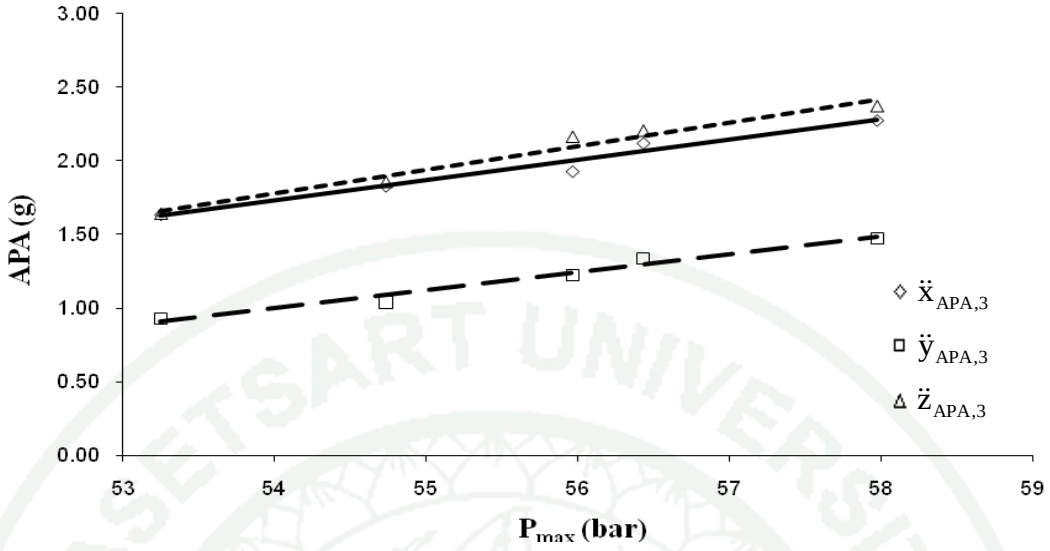

Figure 92 The correlation between APA at point 3 and P_{max} (Exp. 3 and n = 1)

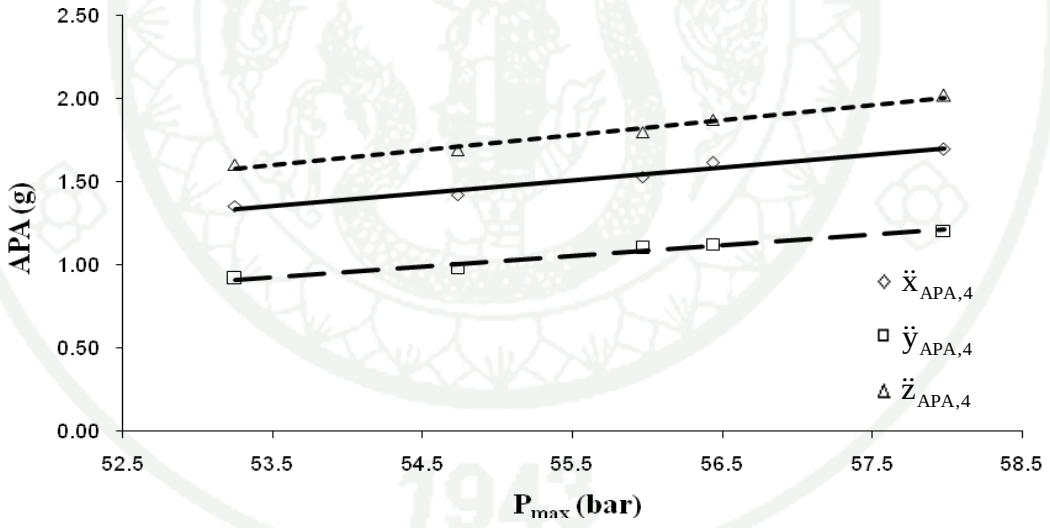

Figure 93 The correlation between APA at point 4 and P_{max} (Exp. 3 and n = 1)

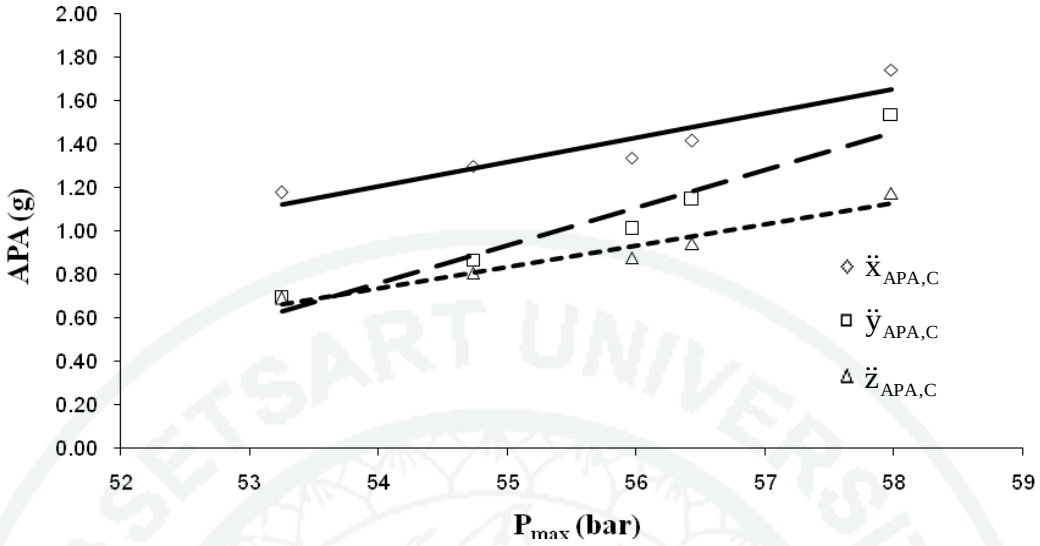

Figure 94 The correlation between APA at point C and P_{max} (Exp. 3 and n = 1)

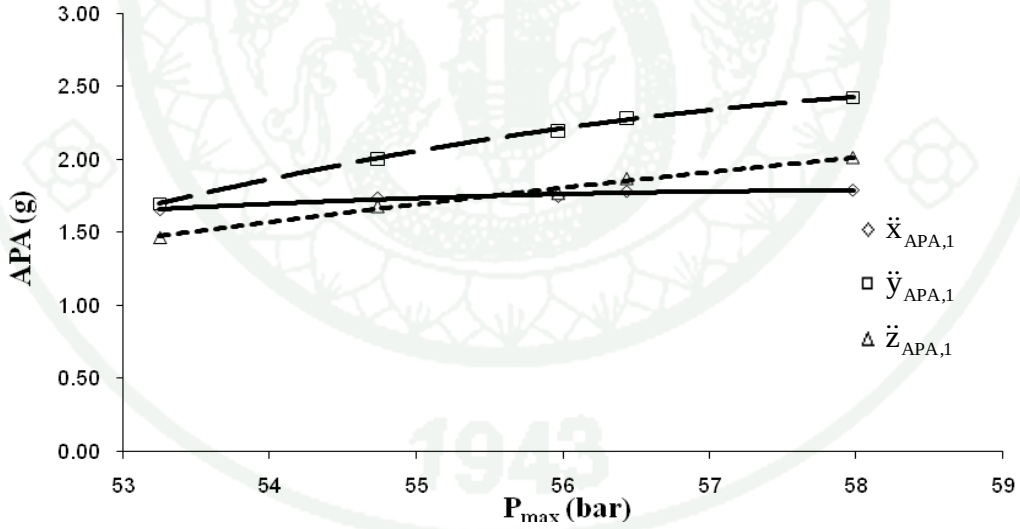

Figure 95 The correlation between APA at point 1 and P_{max} (Exp. 3 and n = 2)

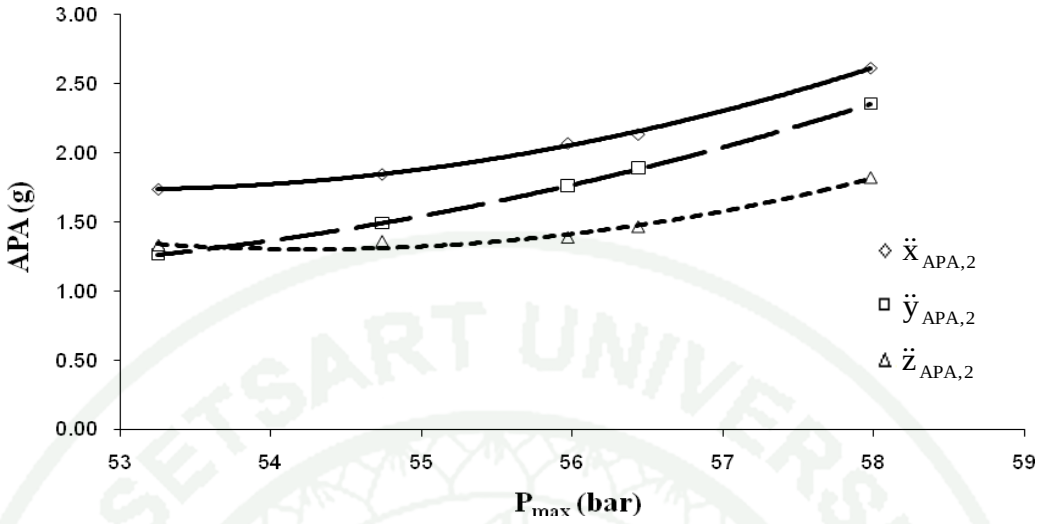

Figure 96 The correlation between APA at point 2 and P_{max} (Exp. 3 and n = 2)

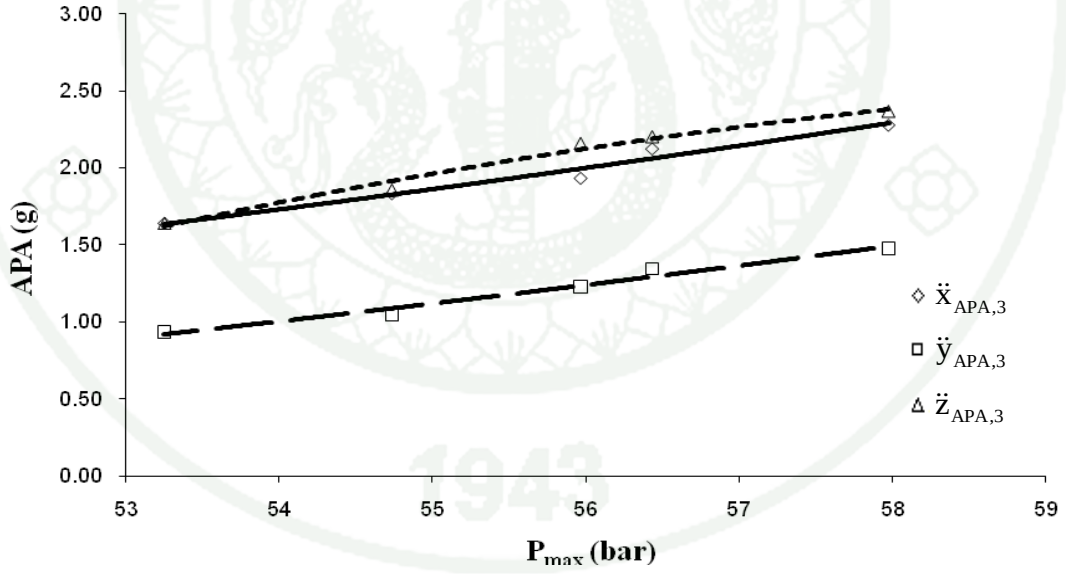

Figure 97 The correlation between APA at point 3 and P_{max} (Exp. 3 and n = 2)

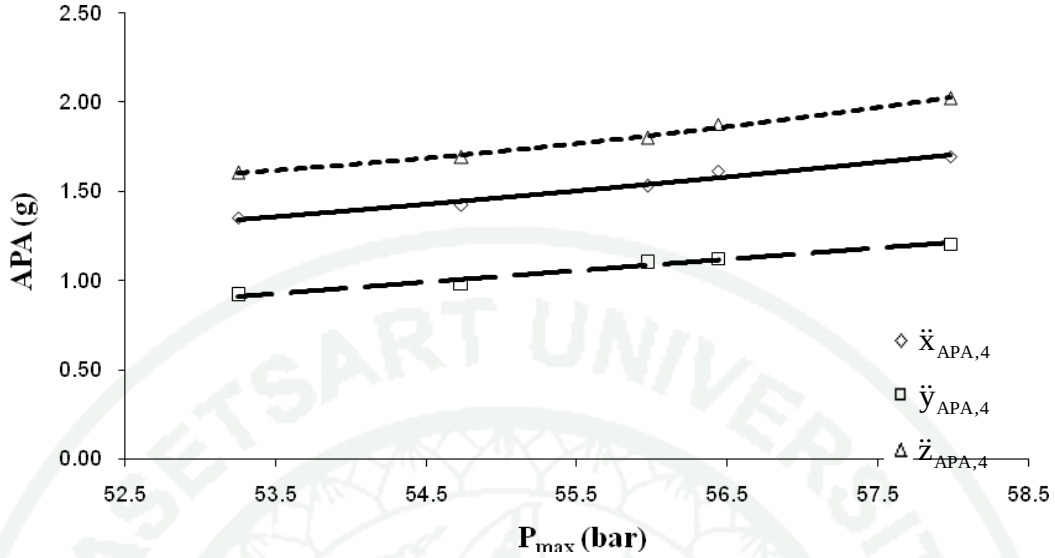

Figure 98 The correlation between APA at point 4 and P_{max} (Exp. 3 and n = 2)

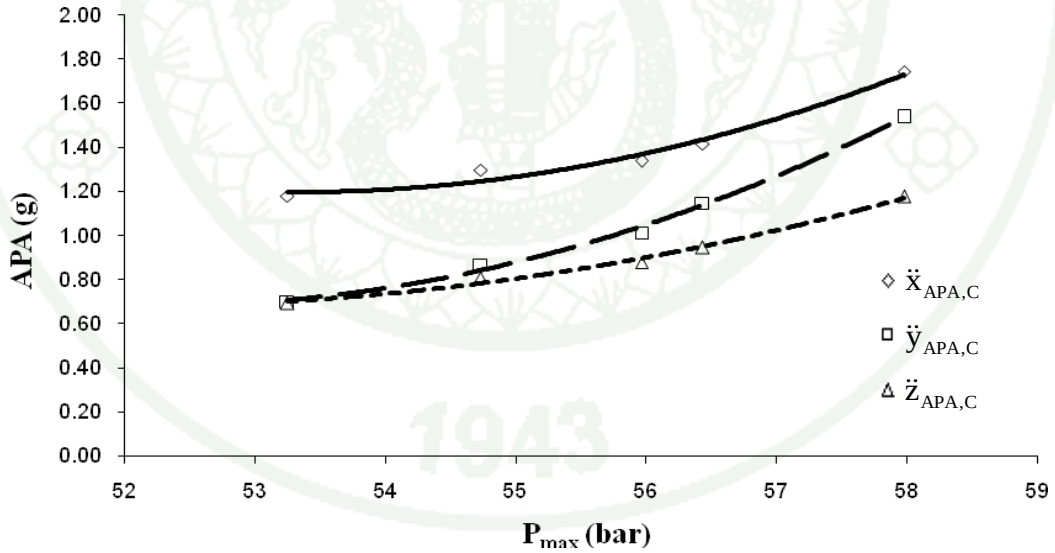

Figure 99 The correlation between APA at point C and P_{max} (Exp. 3 and n = 2)

For the test condition Exp. 4 (N = 1,600, T = 25%) the hydrogen percentage is plotted against the average peak acceleration as shown in Figure 100 to Figure 109.

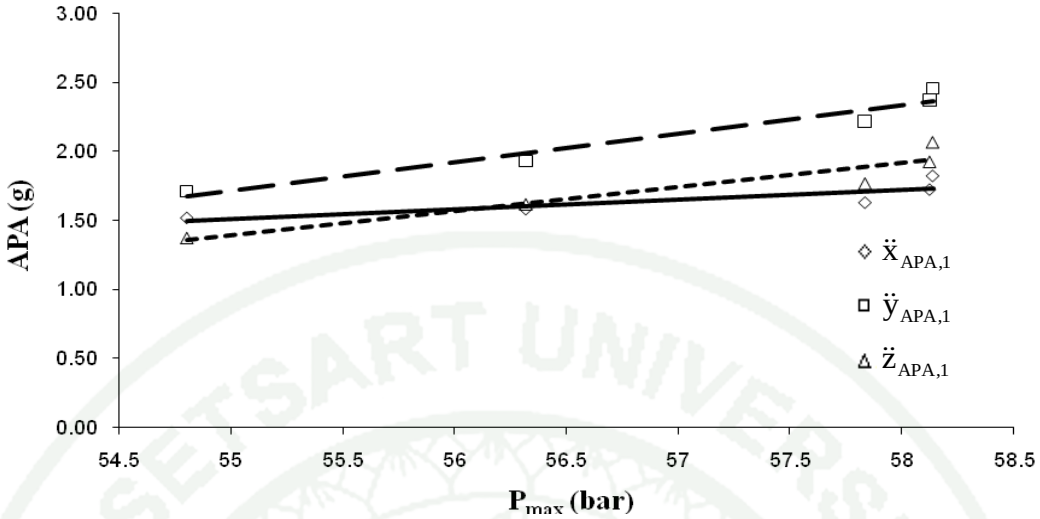

Figure 100 The correlation between APA at point 1 and P_{max} (Exp. 4 and n = 1)

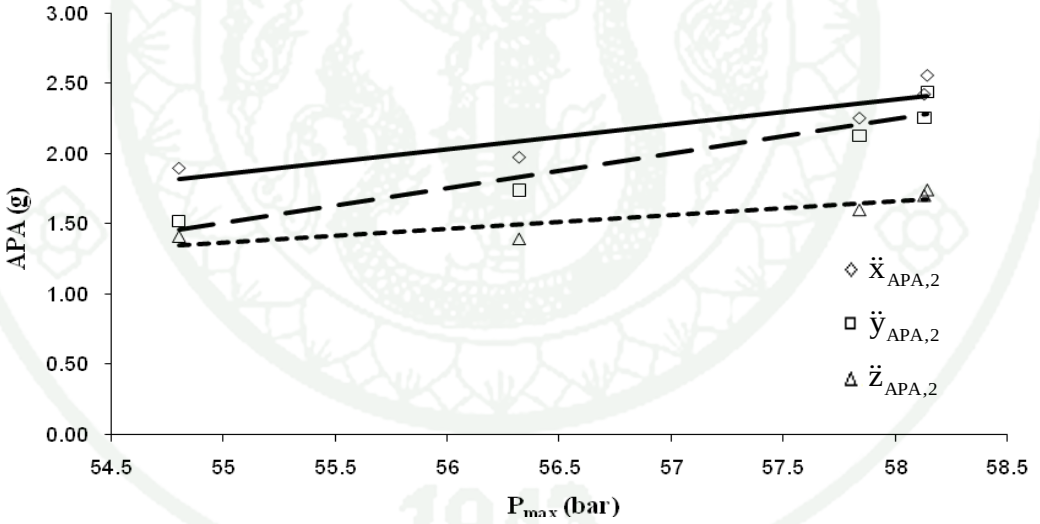

Figure 101 The correlation between APA at point 2 and P_{max} (Exp. 4 and n = 1)

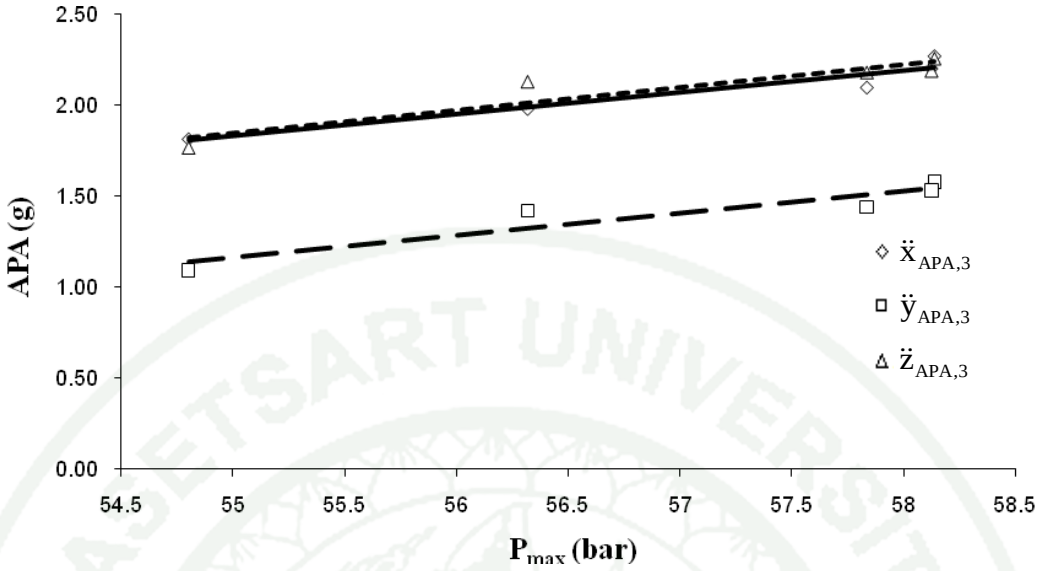

Figure 102 The correlation between APA at point 3 and P_{max} (Exp. 4 and n = 1)

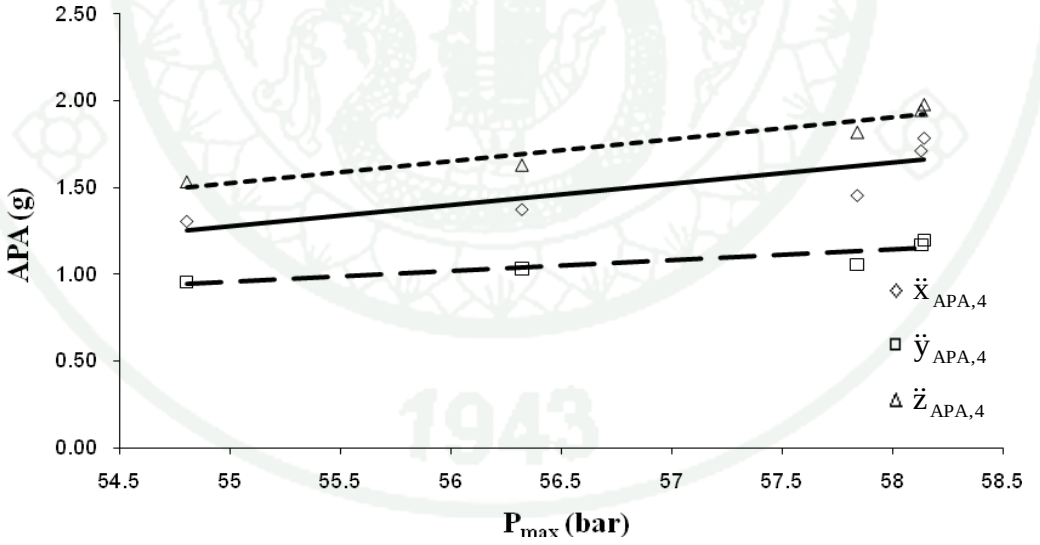

Figure 103 The correlation between APA at point 4 and P_{max} (Exp. 4 and n = 1)

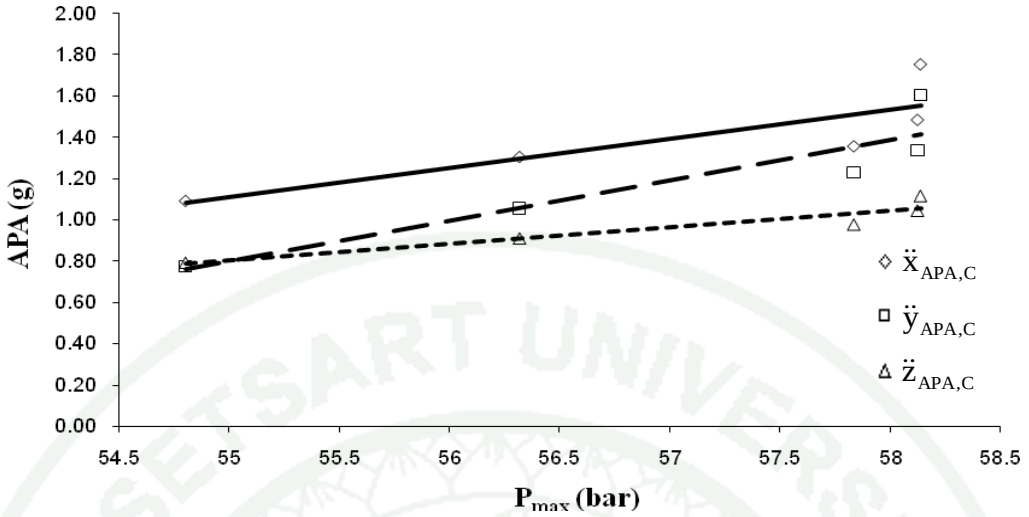

Figure 104 The correlation between APA at point C and P_{max} (Exp. 4 and n = 1)

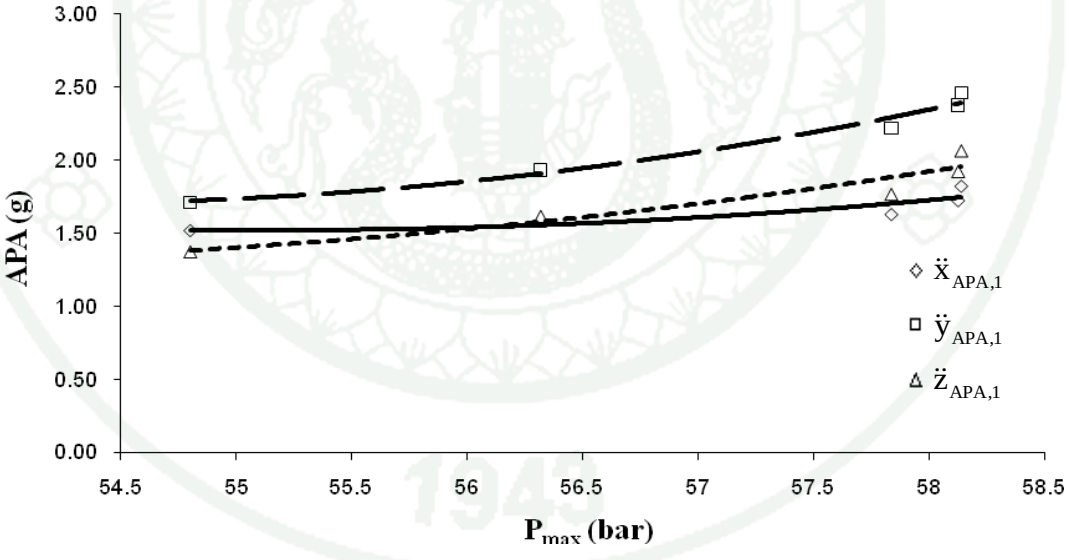

Figure 105 The correlation between APA at point 1 and P_{max} (Exp. 4 and n = 2)

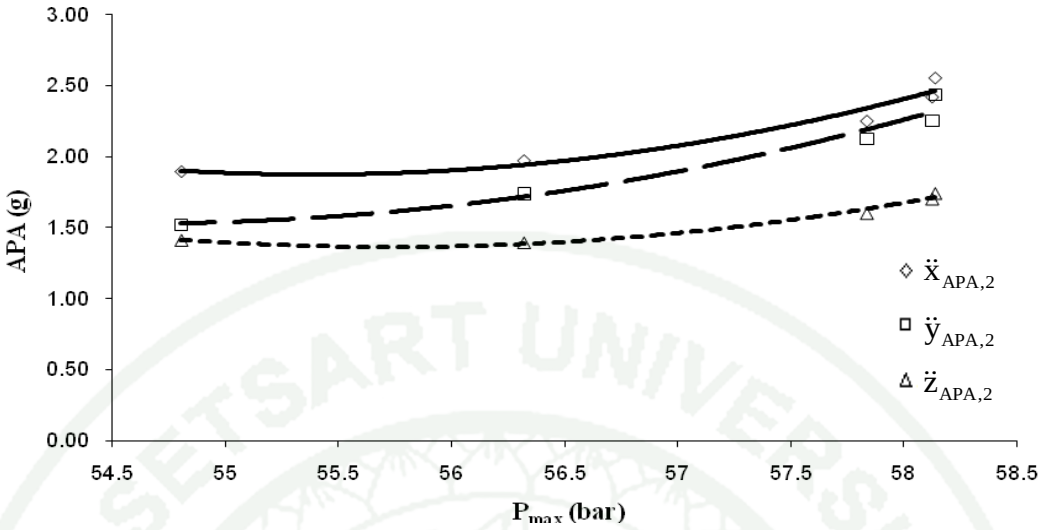

Figure 106 The correlation between APA at point 2 and P_{max} (Exp. 4 and n = 2)

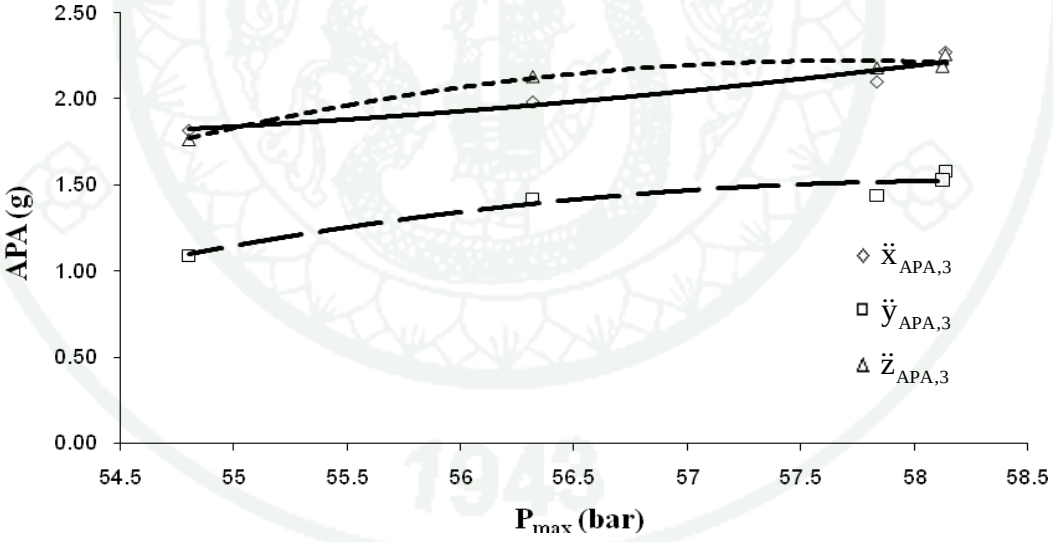

Figure 107 The correlation between APA at point 3 and P_{max} (Exp. 4 and n = 2)

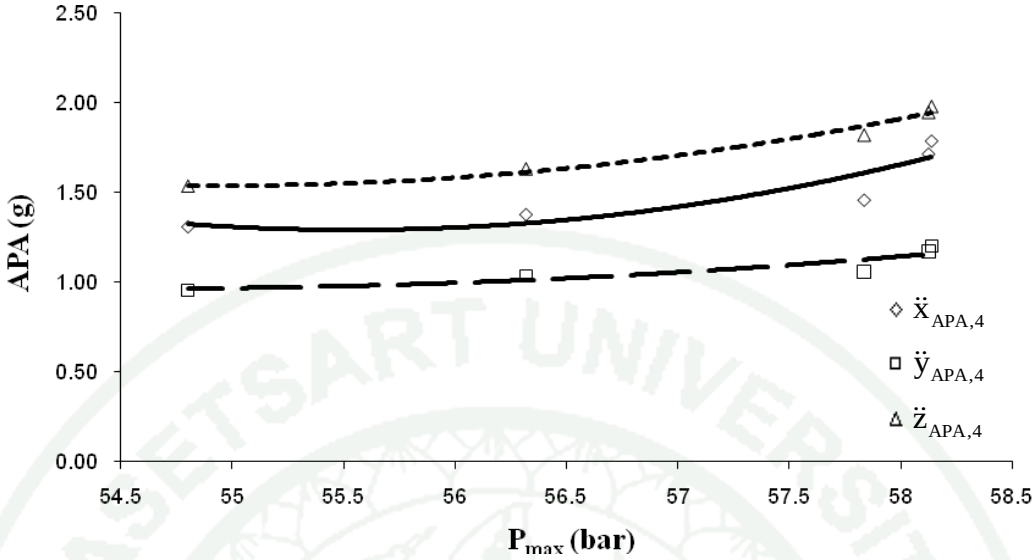

Figure 108 The correlation between APA at point 4 and P_{max} (Exp. 4 and n = 2)

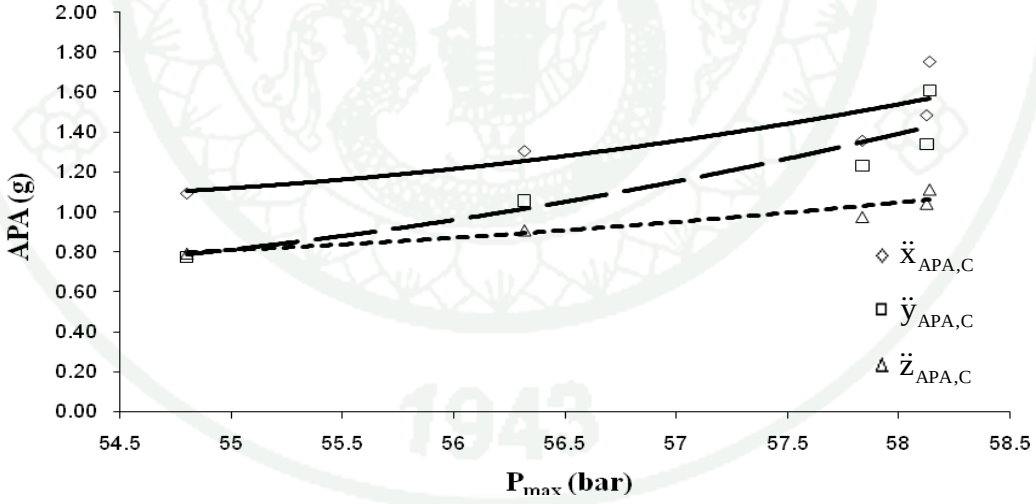

Figure 109 The correlation between APA at point C and P_{max} (Exp. 4 and n = 2)

By using Equation (62) and Equation (66), the correlation constants of the relations between the average peak acceleration and the maximum cylinder pressure are shown in Table 14.

Table 14 Correlation constants for the relation between APA and P_{max}

n	APA	a	b	c	R^2
1	Exp. 1				
	$\ddot{x}_{A,1}$	0.1657	-7.636		0.9197
	$\ddot{y}_{A,1}$	0.1794	-8.8044		0.9432
	$\ddot{z}_{A,1}$	0.0812	-3.0706		0.6136
	$\ddot{x}_{A,2}$	0.137	-5.5855		0.6494
	$\ddot{y}_{A,2}$	0.116	-5.2482		0.8429
	$\ddot{z}_{A,2}$	0.136	-6.2438		0.9248
	$\ddot{x}_{A,3}$	0.1945	-9.4315		0.9767
	$\ddot{y}_{A,3}$	0.0968	-4.4878		0.8461
	$\ddot{z}_{A,3}$	0.2501	-12.926		0.9764
	$\ddot{x}_{A,4}$	0.2493	-12.846		0.9569
	$\ddot{y}_{A,4}$	0.1705	-8.3571		0.8869
	$\ddot{z}_{A,4}$	0.0405	-0.5201		0.8565
	$\ddot{x}_{A,CG}$	0.2567	-13.199		0.9697
	$\ddot{y}_{A,CG}$	0.098	-4.5636		0.9068
	$\ddot{z}_{A,CG}$	0.1173	-5.573		0.9106
1	Exp.2				
	$\ddot{x}_{A,1}$	0.0699	-2.3904		0.8196
	$\ddot{y}_{A,1}$	0.0476	-0.6246		0.903
	$\ddot{z}_{A,1}$	0.1161	-5.3132		0.7056
	$\ddot{x}_{A,2}$	0.059	-1.2977		0.7894
	$\ddot{y}_{A,2}$	0.0284	0.4725		0.8457
	$\ddot{z}_{A,2}$	0.0329	-0.3939		0.8261
	$\ddot{x}_{A,3}$	0.0924	-3.5983		0.8251
	$\ddot{y}_{A,3}$	0.0296	-0.1003		0.8698
	$\ddot{z}_{A,3}$	0.062	-1.4456		0.9332
	$\ddot{x}_{A,4}$	0.0523	-1.4433		0.8413
	$\ddot{y}_{A,4}$	0.025	0.1725		0.8234
	$\ddot{z}_{A,4}$	0.0864	-2.8636		0.9038
	$\ddot{x}_{A,CG}$	0.0887	-3.6392		0.75
	$\ddot{y}_{A,CG}$	0.0316	-0.255		0.9054
	$\ddot{z}_{A,CG}$	0.035	-0.5002		0.9079

Table 14 (Continued)

n	APA	a	b	c	R^2
1	Exp.3				
	$\ddot{x}_{A,1}$	0.0279	0.1907		0.8792
	$\ddot{y}_{A,1}$	0.1559	-6.5507		0.9709
	$\ddot{z}_{A,1}$	0.1149	-4.6302		0.9868
	$\ddot{x}_{A,2}$	0.1826	-8.0914		0.9176
	$\ddot{y}_{A,2}$	0.2289	-10.988		0.9747
	$\ddot{z}_{A,2}$	0.0966	-3.9042		0.7263
	$\ddot{x}_{A,3}$	0.1372	-5.6806		0.9666
	$\ddot{y}_{A,3}$	0.1211	-5.5401		0.9743
	$\ddot{z}_{A,3}$	0.1612	-6.9305		0.9713
	$\ddot{x}_{A,4}$	0.0766	-2.7421		0.9699
	$\ddot{y}_{A,4}$	0.0636	-2.4759		0.9815
	$\ddot{z}_{A,4}$	0.0893	-3.1722		0.9802
	$\ddot{x}_{A,CG}$	0.1116	-4.819		0.871
	$\ddot{y}_{A,CG}$	0.1731	-8.5821		0.945
	$\ddot{z}_{A,CG}$	0.0985	-4.5851		0.948
1	Exp.4				
	$\ddot{x}_{A,1}$	0.0695	-2.3091		0.7239
	$\ddot{y}_{A,1}$	0.2064	-9.6345		0.9475
	$\ddot{z}_{A,1}$	0.1741	-8.1804		0.8948
	$\ddot{x}_{A,2}$	0.1779	-7.9306		0.8398
	$\ddot{y}_{A,2}$	0.2468	-12.065		0.9228
	$\ddot{z}_{A,2}$	0.098	-4.0213		0.7901
	$\ddot{x}_{A,3}$	0.1193	-4.7291		0.9283
	$\ddot{y}_{A,3}$	0.122	-5.547		0.8799
	$\ddot{z}_{A,3}$	0.1249	-5.0217		0.8673
	$\ddot{x}_{A,4}$	0.1211	-5.3832		0.6988
	$\ddot{y}_{A,4}$	0.061	-2.3954		0.7872
	$\ddot{z}_{A,4}$	0.1267	-5.4447		0.9146
	$\ddot{x}_{A,CG}$	0.141	-6.6442		0.7129
	$\ddot{y}_{A,CG}$	0.1955	-9.9539		0.8501
	$\ddot{z}_{A,CG}$	0.0798	-3.5839		0.8926

Table 14 (Continued)

n	APA	a	b	c	R^2
2	Exp.1				
	$\ddot{x}_{A,1}$	-0.0366	4.47	-133.99	0.9803
	$\ddot{y}_{A,1}$	-0.0244	3.0495	-93.055	0.9668
	$\ddot{z}_{A,1}$	-0.0312	3.7504	-110.78	0.7362
	$\ddot{x}_{A,2}$	-0.0755	9.0096	-266.04	0.9153
	$\ddot{y}_{A,2}$	-0.0341	4.1221	-122.85	0.9411
	$\ddot{z}_{A,2}$	-0.0028	0.4596	-15.742	0.9253
	$\ddot{x}_{A,3}$	-0.0247	3.1014	-94.761	0.998
	$\ddot{y}_{A,3}$	0.019	-2.1385	61.13	0.8901
	$\ddot{z}_{A,3}$	0.0181	-1.8729	49.395	0.9833
	$\ddot{x}_{A,4}$	0.0091	-0.82	18.545	0.9586
	$\ddot{y}_{A,4}$	-0.0188	2.3803	-73.222	0.9015
	$\ddot{z}_{A,4}$	-0.0116	1.4058	-40.598	0.9516
	$\ddot{x}_{A,CG}$	-0.0266	3.3871	-105.09	0.9838
	$\ddot{y}_{A,CG}$	-0.0022	0.3614	-12.295	0.9074
	$\ddot{z}_{A,CG}$	-0.0037	0.5485	-18.23	0.9118
2	Exp.2				
	$\ddot{x}_{A,1}$	0.009	-1.0771	33.944	0.9218
	$\ddot{y}_{A,1}$	0.0014	-0.1336	5.1175	0.909
	$\ddot{z}_{A,1}$	0.0225	-2.754	85.609	0.905
	$\ddot{x}_{A,2}$	0.0088	-1.0646	34.296	0.9217
	$\ddot{y}_{A,2}$	-0.0027	0.3689	-10.313	0.9018
	$\ddot{z}_{A,2}$	0.0028	-0.3203	10.795	0.8702
	$\ddot{x}_{A,3}$	0.0127	-1.5245	47.625	0.9419
	$\ddot{y}_{A,3}$	-0.0038	0.5101	-15.323	0.9761
	$\ddot{z}_{A,3}$	-0.0001	0.0811	-2.0503	0.9333
	$\ddot{x}_{A,4}$	0.0068	-0.8158	26.056	0.9487
	$\ddot{y}_{A,4}$	-0.004	0.5324	-15.899	0.9798
	$\ddot{z}_{A,4}$	0.009	-1.0632	33.554	0.9778
	$\ddot{x}_{A,CG}$	0.0149	-1.8106	56.528	0.9092
	$\ddot{y}_{A,CG}$	-0.0022	0.3111	-9.1106	0.9382
	$\ddot{z}_{A,CG}$	-0.004	0.5463	-16.696	0.9973

Table 14 (Continued)

n	APA	a	b	c	R^2
2	Exp.3				
	$\ddot{x}_{A,1}$	-0.0055	0.6354	-16.676	0.9611
	$\ddot{y}_{A,1}$	-0.017	2.0406	-58.885	0.9989
	$\ddot{z}_{A,1}$	-0.0036	0.5141	-15.716	0.9892
	$\ddot{x}_{A,2}$	0.0347	-3.6745	99.013	0.9982
	$\ddot{y}_{A,2}$	0.0236	-2.392	61.788	0.9999
	$\ddot{z}_{A,2}$	0.0367	-3.978	109.24	0.9808
	$\ddot{x}_{A,3}$	0.003	-0.1987	3.6489	0.9678
	$\ddot{y}_{A,3}$	0.0024	-0.1462	1.8843	0.9752
	$\ddot{z}_{A,3}$	-0.0115	1.4373	-42.364	0.9833
	$\ddot{x}_{A,4}$	0.002	-0.147	3.4667	0.9716
	$\ddot{y}_{A,4}$	-0.0003	0.0943	-3.3272	0.9815
	$\ddot{z}_{A,4}$	0.0066	-0.643	17.161	0.9932
	$\ddot{x}_{A,CG}$	0.0247	-2.6303	71.317	0.9745
	$\ddot{y}_{A,CG}$	0.0258	-2.6898	70.913	0.9959
	$\ddot{z}_{A,CG}$	0.0135	-1.404	37.135	0.9914
2	Exp.4				
	$\ddot{x}_{A,1}$	0.0247	-2.7279	76.729	0.783
	$\ddot{y}_{A,1}$	0.0425	-4.6033	126.26	0.9735
	$\ddot{z}_{A,1}$	0.0233	-2.4648	66.378	0.9052
	$\ddot{x}_{A,2}$	0.0771	-8.5437	238.49	0.9415
	$\ddot{y}_{A,2}$	0.0628	-6.8532	188.54	0.9613
	$\ddot{z}_{A,2}$	0.0601	-6.6986	188.01	0.9816
	$\ddot{x}_{A,3}$	0.0145	-1.5201	41.588	0.9371
	$\ddot{y}_{A,3}$	-0.0361	4.204	-120.88	0.9296
	$\ddot{z}_{A,3}$	-0.054	6.2284	-177.47	0.9716
	$\ddot{x}_{A,4}$	0.06	-6.6623	186.27	0.8092
	$\ddot{y}_{A,4}$	0.015	-1.6371	45.582	0.818
	$\ddot{z}_{A,4}$	0.0396	-4.35	121.04	0.9721
	$\ddot{x}_{A,CG}$	0.0217	-2.3132	62.696	0.7237
	$\ddot{y}_{A,CG}$	0.0227	-2.3763	62.712	0.8575
	$\ddot{z}_{A,CG}$	0.0088	-0.9201	24.666	0.8997

5. The magnitude of the difference between the acceleration vector summation at the engine supports with the hydrogen percentage of i% and the hydrogen percentage of 0% (Δa)

The Equation of Δa at the engine supports (at points P_1, P_2, P_3, and P_4) can be written as Equation (67)

$$\Delta a = \sqrt{(\ddot{x}_i - \ddot{x}_0)^2 + (\ddot{y}_i - \ddot{y}_0)^2 + (\ddot{z}_i - \ddot{z}_0)^2} \quad (67)$$

where:

$\ddot{x}_i$ = the average acceleration at the engine supports in x direction with the hydrogen percentage of i%

$\ddot{y}_i$ = the average acceleration at the engine supports in y direction with the hydrogen percentage of i%

$\ddot{z}_i$ = the average acceleration at the engine supports in z direction with the hydrogen percentage of i%

$\ddot{x}_0$, $\ddot{y}_0$, and $\ddot{z}_0$ = the average acceleration at the engine supports in x, y, and z direction with the hydrogen percentage of 0%

The average acceleration at the engine supports in x, y, and z direction can be determined from the Equations (68) to the Equations (70)

$$\ddot{x}_i = \frac{\sum_{j=1}^{4} \ddot{x}_{P_j,i}}{4} \quad (68)$$

$$\ddot{y}_i = \frac{\sum_{j=1}^{4} \ddot{y}_{P_j,i}}{4} \quad (69)$$

$$\ddot{z}_i = \frac{\sum_{j=1}^{4} \ddot{z}_{P_j,i}}{4} \quad (70)$$

where:

$\ddot{x}_{P_j,i}$ = the acceleration at point P_j in x direction with the hydrogen percentage of i%

$\ddot{y}_{P_j,i}$ = the acceleration at point P_j in y direction with the hydrogen percentage of i%

$\ddot{z}_{P_j,i}$ = the acceleration at point P_j in z direction with the hydrogen percentage of i%

Figure 113 shows the graph of the magnitude of the acceleration vector summation at the engine supports with the hydrogen percentage of 0% (a_0).

$$a_0 = \sqrt{\ddot{x}_0^2 + \ddot{y}_0^2 + \ddot{z}_0^2}$$

where:

a_0 = the magnitude of the acceleration vector summation at the engine supports with the hydrogen percentage of 0%

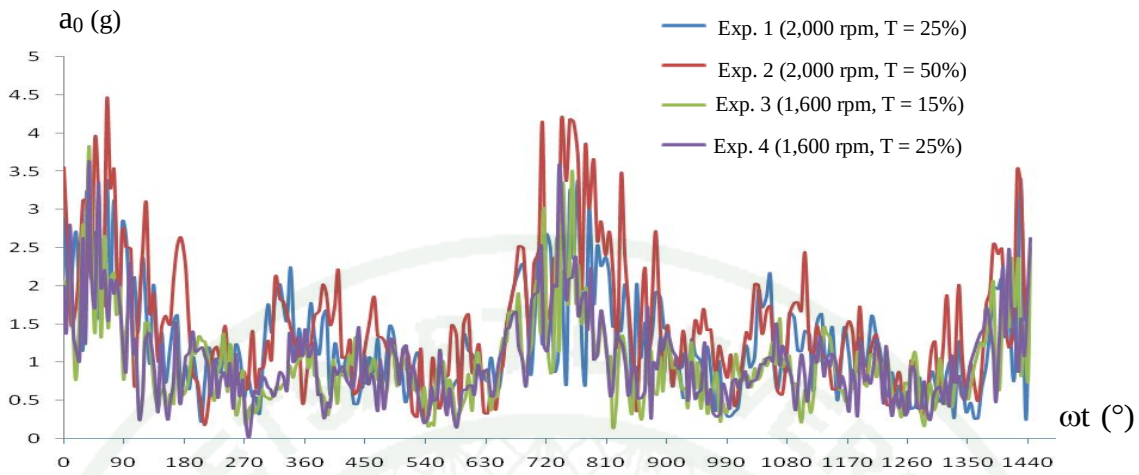

Figure 110 The a_0 for all test conditions

The graphs of the Δa for all test conditions are shown in Figure 111 to Figure 114

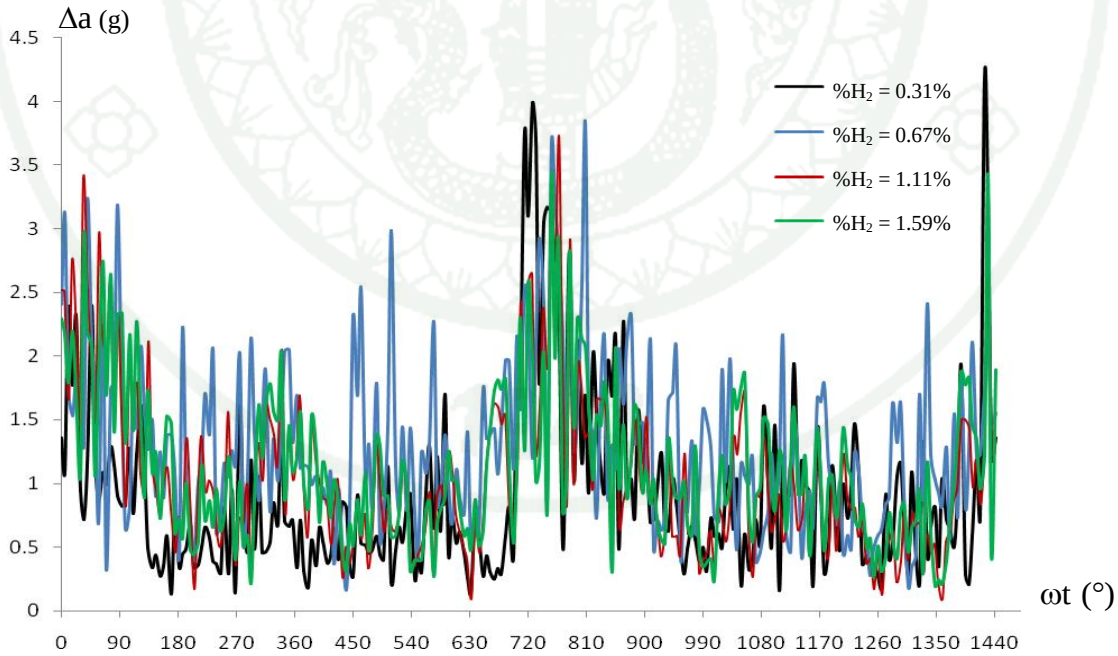

Figure 111 The Δa for the test condition Exp. 1 (2,000 rpm and T = 25%)

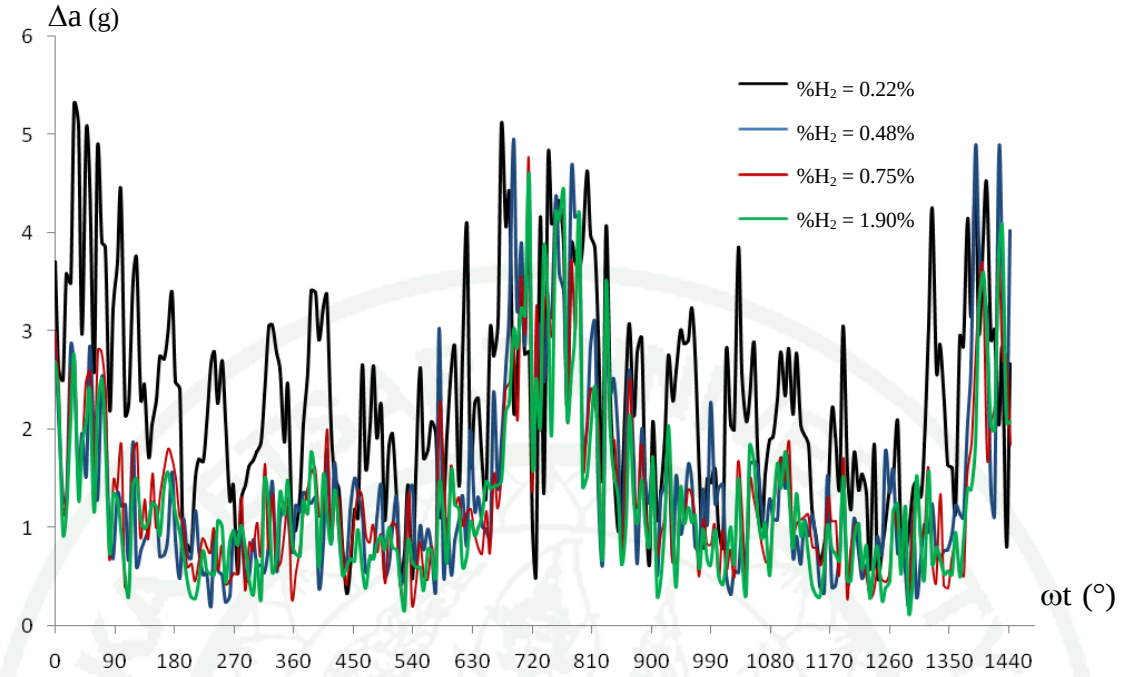

Figure 112 The Δa for the test condition Exp. 2 (2,000 rpm and T = 50%)

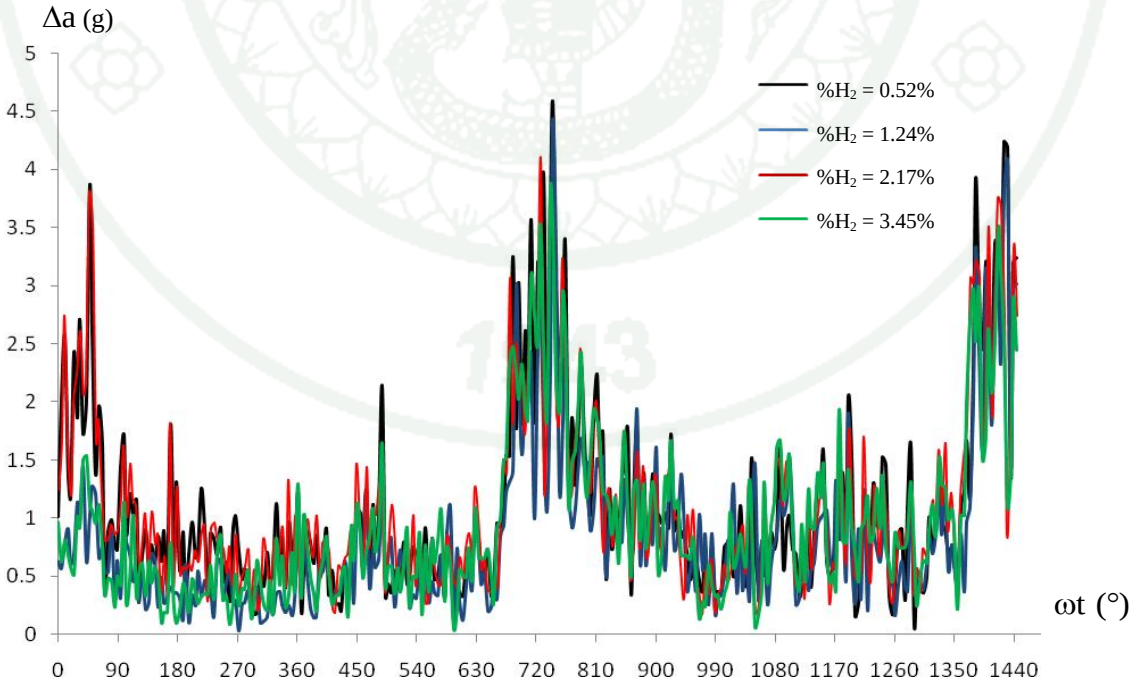

Figure 113 The Δa for the test condition Exp. 3 (1,600 rpm and T = 15%)

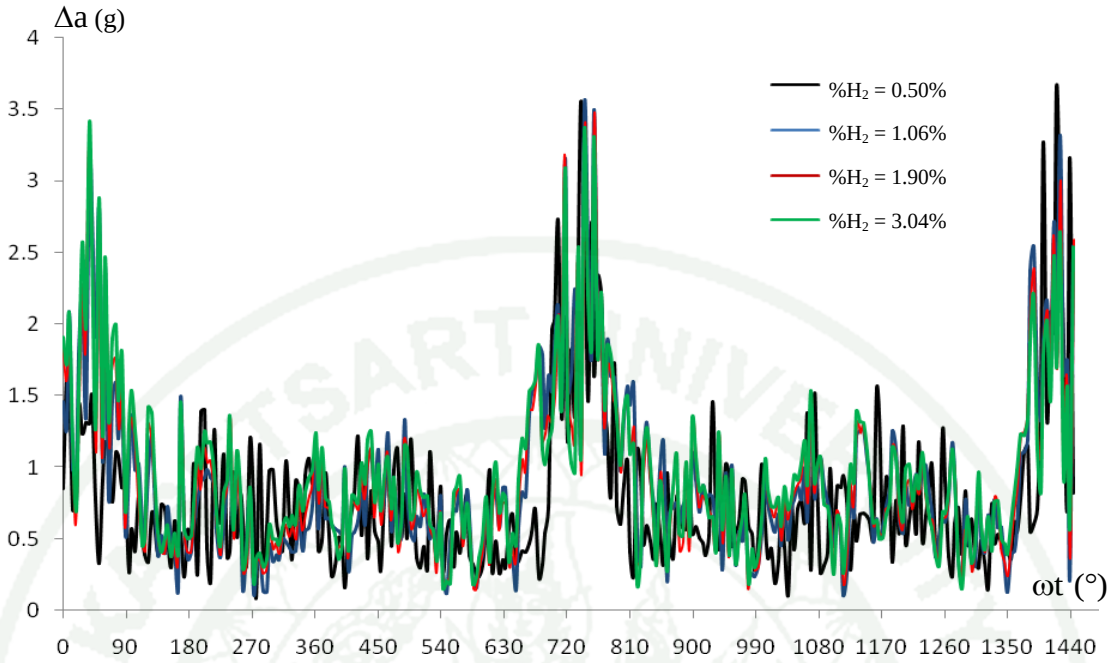

Figure 114 The Δa for the test condition Exp. 4 (1,600 rpm and T = 25%)

From Figure 110 to Figure 113, The peak of the Δa are shown in Table 15.

Table 15 The peak of the Δa (Δa_{peak})

	Exp. 1		Exp. 2		Exp. 3		Exp. 4	
H_2 lpm	$\%H_2$	Δa_{peak} (g)	$\%H_2$	Δa_{peak} (g)	$\%H_2$	Δa_{peak} (g)	$\%H_2$	Δa_{peak} (g)
5	0.31	4.12	0.22	5.31	0.52	56.43	4.56	3.66
10	0.67	3.83	0.48	4.95	1.24	55.97	4.11	3.53
15	1.11	3.73	0.75	4.75	2.17	54.73	4.08	3.47
20	1.59	3.43	1.09	4.58	3.45	53.25	3.84	3.41

The graphs of the Δa_{peak} versus $\%H_2$ with n = 1 and n = 2 are shown in Figure 115 and Figure 118. By using regression analysis, the correlation constants for the relation between Δa_{peak} and $\%H_2$ are listed in Table 16.

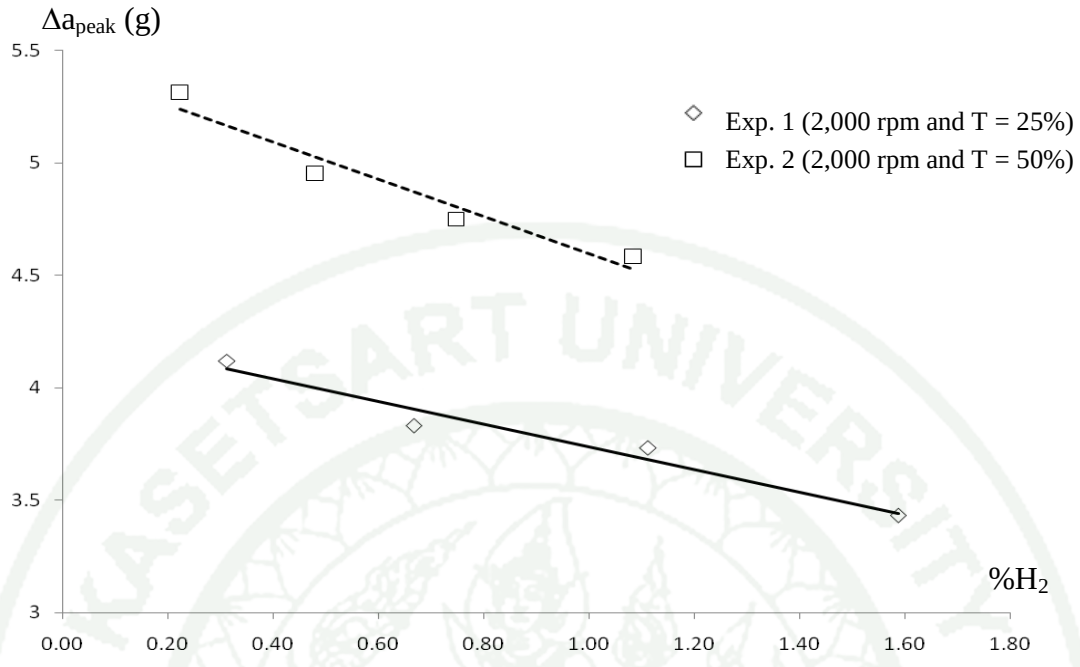

Figure 115 The Δa_{peak} versus $\%H_2$ (Exp. 1 and Exp. 2 with n = 1)

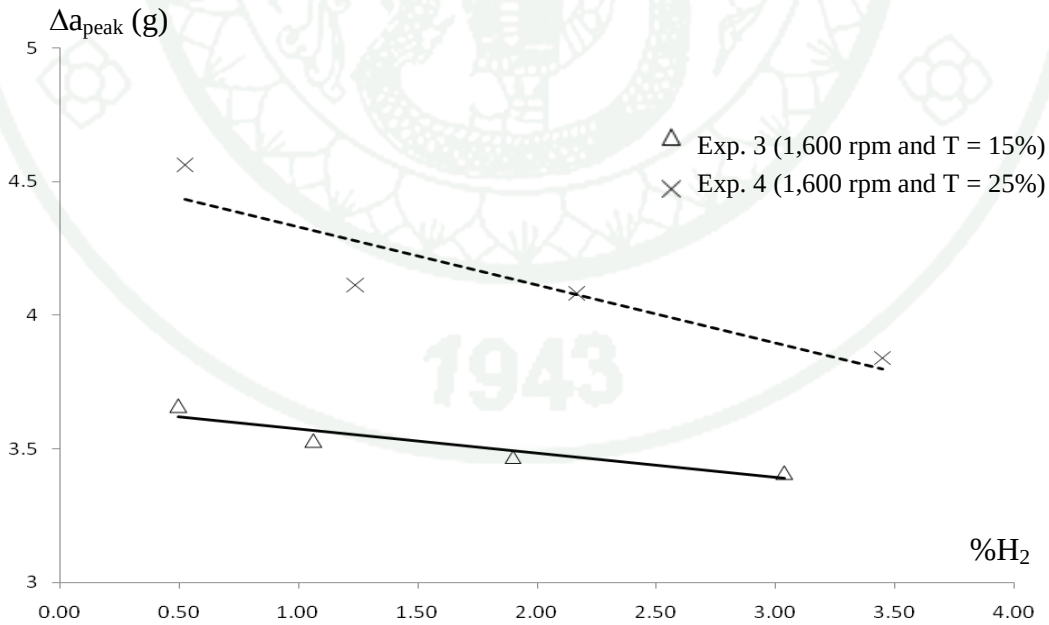

Figure 116 The Δa_{peak} versus $\%H_2$ (Exp. 3 and Exp. 4 with n = 1)

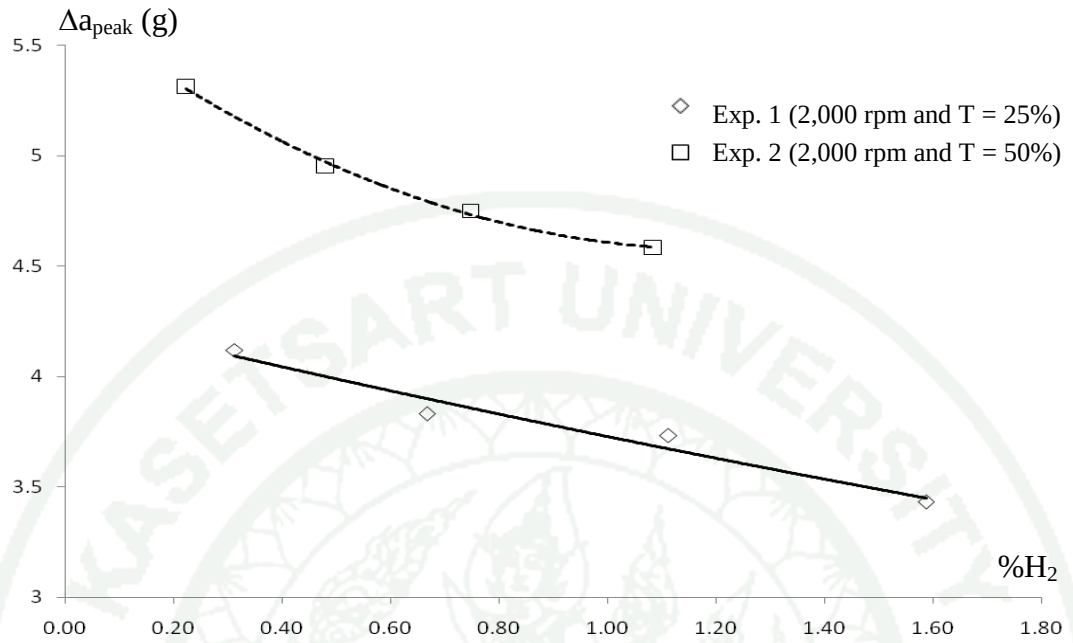

Figure 117 The Δa_{peak} versus $\%H_2$ (Exp. 1 and Exp. 2 with n = 2)

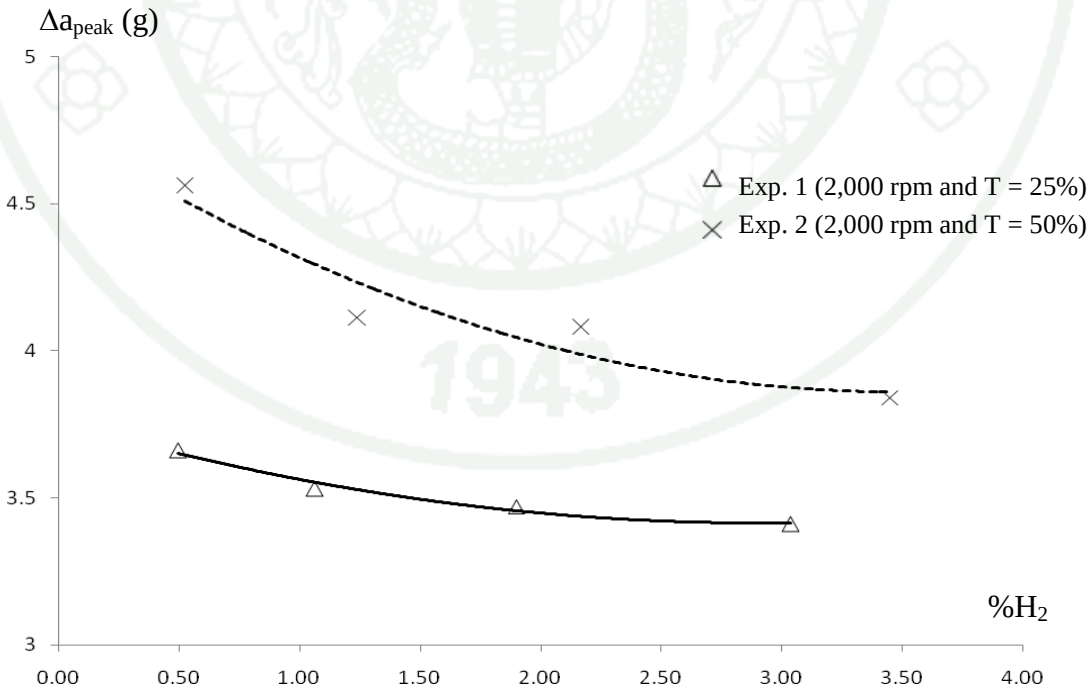

Figure 118 The Δa_{peak} versus $\%H_2$ (Exp. 3 and Exp. 4 with n = 2)

Table 16 Correlation constants for the relation between Δa_{peak} and $\%H_2$

n	TPA_{peak}	a	b	c	R^2
1	Exp. 1	-0.505	4.242		0.960
	Exp. 2	-0.826	5.421		0.943
	Exp. 3	-0.090	3.665		0.882
	Exp. 4	-0.826	0.882		0.943
2	Exp. 1	0.044	-0.589	4.272	0.961
	Exp. 2	0.758	-1.826	5.673	0.997
	Exp. 3	0.040	-0.236	3.757	0.975
	Exp. 4	0.074	-0.516	4.758	0.902

Discussion

The experimental results in Figure 21 have shown that the maximum cylinder pressure obtained from this engine occurred after the engine top dead center for all the test conditions. It has seen from Figure 22 that when higher hydrogen percentages were added, the combustion shifted toward later crank angles while maintaining the same area under the pressure-crank angle thus, the same output as set in Table 1. It is obvious in the Figure 22 that the maximum cylinder pressure decreased as the hydrogen percentages were added.

The results of the maximum cylinder pressure are different from several research work. Mostly, the results have been found that the maximum cylinder pressure increase by hydrogen addition (Szwaja *et al.*, 2009; Lilik *et al.*, 2010; Miyamoto *et al.*, 2011; Shin *et al.*, 2011) because the conditions of the performance testing of the engines are different from this study. In the performance testing of the engines, the speed and torque are not set as this work such as only constant brake torque. Meanwhile, this study set the speed and torque constant yielding a constant work per cycle. However, Lata *et al.* (2012) found that the maximum cylinder pressure increased at low hydrogen addition and decreased at high hydrogen addition. By the fumigation, the hydrogen and the air are mixed as the homogeneous mixture and it has smooth combustion by the increasing of the hydrogen. By this reason, the maximum cylinder pressure can decrease by hydrogen addition. The graphs of the cylinder pressure versus the crankshaft angle expand on the both side with the same area under the p-θ curves.

The reducing maximum cylinder pressure traces were confirmedly plotted against hydrogen percentage, shown in Figure 23 and Figure 24 with the first and second order correlations, respectively. It is found that the lower engine loads gave lower maximum cylinder pressures at constant speed. The added hydrogen percentages show eminent effects at higher load and speed; this can be observed by the sharp slope in maximum cylinder pressure reduction both in Figure 23 and Figure 24.

The results of the maximum cylinder pressure-hydrogen percentage correlations in Table 6 show better curve fittings by second order correlation ($R^2 \rightarrow 1$) compared to the first order correlation for all the test conditions. Though, the linear correlation is apparently adequate for the two parameters. The averaged values of R^2 are 0.9261 and 0.9808 for linear (first order) equation and parabola (second order) polynomial equations, respectively. All curves are the decreasing function and P_{max} can decrease by increasing hydrogen percentage.

In Figure 25 and Figure 26, the plots of the coefficient of variation of the maximum cylinder pressure ($COV_{P_{max}}$) against hydrogen percentage, respectively for the first and second order correlations show the increase in variation of maximum cylinder pressure when the hydrogen percentage increased for all conditions tested. The values of $COV_{P_{max}}$ are in the level of less than 1.6 in majority. Acceptingly, the test condition Exp. 2 which is at high speed and high load is found to give a prominent increase in $COV_{P_{max}}$ even when only subtle amount of hydrogen percentages were added. This can be observed by the sharp slope of $COV_{P_{max}}$ increase both in Figure 25 and 26.

The results of the $COV_{P_{max}}$ -hydrogen percentage correlations in Table 7 show better curve fittings by second order correlation ($R^2 \rightarrow 1$) compared to the first order correlation for all the test conditions. Though, the linear correlation is apparently adequate for the two parameters. The averaged values of R^2 are 0.8654 and 0.9340 for linear (first order) equation and parabola (second order) polynomial equations, respectively. All curves are the increasing function and $COV_{P_{max}}$ values increase by increasing hydrogen percentage.

In Figure 30 to Figure 69, the plots of the average peak acceleration against hydrogen percentage for the first and second order correlations show the reduction of the average peak acceleration in all directions ($\ddot{x}_A, \ddot{y}_A, \ddot{z}_A$) when the hydrogen percentage increased for all conditions tested. Table 13 show better curve fittings by second order correlation ($R^2 \rightarrow 1$) compared to the first order correlation for all the test conditions. Though, the linear correlation is apparently adequate for the two

parameters. The averaged values of R^2 are 0.8973 and 0.9592 for linear (first order) equation and parabola (second order) polynomial equations, respectively.

The results of the average peak acceleration can be explained by using Equation (18) and Equation (71) for the m-k system of this work.

$$\ddot{x}+\omega_n^2 x=\frac{1}{m}F(t)) \tag{18}$$

When F(t) is the shaking force in Equation (71)

$$\vec{S}=\vec{F}_{0_4}+\vec{F}_{B_3}=\vec{R}_1+\vec{R}_2 \tag{71}$$

The Equation (71) can be written

$$S=(m_4+m_B)a_B \tag{72}$$

By substitution S in Equation (18)

$$\ddot{x}+\omega_n^2 x=\frac{1}{m}(m_4+m_B)a_B \tag{73}$$

and

$$a_B=R\omega^2[\cos\theta+\frac{R}{\ell}\cos 2\theta] \tag{74}$$

when

R = the length of the crank (m)

The Equation (74) can be written

$$\ddot{x}+\omega_n^2 x=\frac{1}{m}(m_4+m_B)R\omega^2[\cos\theta+\frac{R}{\ell}\cos 2\theta] \tag{75}$$

Because ω and θ are the function of the cylinder pressure, the engine vibration is therefore the function of the cylinder pressure. The maximum amplitude of the engine vibration decreases when the maximum amplitude of the right term in Equation (75) decreased. From this reason, the average peak acceleration decreases when the maximum cylinder pressure decreased.

In Figure 70 to Figure 109, the plots of the average peak acceleration against the maximum cylinder pressure for the first and second order correlations show the increase of the average peak acceleration in all directions when the maximum cylinder is increased. Table 14 show better curve fittings by second order correlation ($R^2 \rightarrow 1$) compared to the first order correlation for all the test conditions. Though, the linear correlation is apparently adequate for the two parameters. The averaged values of R^2 are 0.8757 and 0.9368 for linear (first order) equation and parabola (second order) polynomial equations, respectively.

In Figure 114 to Figure 117 show the correlations between the Δa_{peak} and the hydrogen percentage for the first and second order. The results found that the Δa_{peak} decrease by the hydrogen addition for all test conditions. Table 15 show the better curve fitting by second order ($R^2 \rightarrow 1$) compared to the first order correlation for all the test conditions. Though, the linear correlation is apparently adequate for the two parameters. The averaged values of R^2 are 0.9320 and 0.9587 for linear (first order) equation and parabola (second order) polynomial equations, respectively.

For overall discussions of the effects of the hydrogen addition on the P_{max}, the APA, and the Δa_{peak}, the maximum cylinder pressure decreases when the hydrogen is added and it lowers the amplitude of the right term of the Equation (75). Because the amplitude of the engine vibration is directly varied with the amplitude of the right term of the Equation (75), by this reason, the APA and the Δa_{peak} decrease by hydrogen addition.

CONCLUSION AND RECOMENDATION

Conclusion

From the experimental results and discussion of this study can draw the conclusions as the followings.

1. The maximum cylinder pressure obtained from this engine occurred after the engine top dead center. When higher hydrogen percentages is added, the combustion shifted toward later crank angles. The maximum cylinder pressure decreases as the hydrogen percentages is added. Because the diesel engine is tested with the constant torque and the constant engine speed for all of the test conditions, the work per cycle must be constant. By the fumigation, the hydrogen and the air are mixed as the homogeneous mixture and it has smooth combustion by the increasing of the hydrogen. By this reason, the maximum cylinder pressure can decrease by hydrogen addition. The graphs of the cylinder pressure versus the shaft angle expand on the both side with the same area under the graph of p-θ.

2. The added hydrogen percentages show eminent effects at higher load and speed that can be observed by the sharp slope in maximum cylinder pressure reduction.

3. The maximum cylinder pressure - hydrogen percentage correlations show better curve fittings by second order correlation compared to the first order correlation for all the test conditions. However, the relation between the maximum cylinder pressure and hydrogen percentage is the linear equation because the graphs of the maximum cylinder pressure versus hydrogen percentage have the good fitting when using n = 1.

4. The plots of the coefficient of variation of the maximum cylinder pressure against hydrogen percentage show the increase in variation of maximum cylinder pressure when the hydrogen percentage increased for all conditions tested. The values

of $COV_{P_{max}}$ are in the level of less than 1.6 in majority, accept the test condition at high speed and high load which is prominent increase in $COV_{P_{max}}$. That mean the maximum cylinder pressure can become unstable when the hydrogen is added. The engine knocking may occurs if the hydrogen addition reaches to the critical point. The maximum pressure will increases with little hydrogen addition and may cause the engine knocking.

5. The coefficient of variation of the maximum cylinder pressure-hydrogen percentage correlations show better curve fittings by second order correlation compared to the first order correlation for all the test conditions. However, the relation between the coefficient of variation of the maximum cylinder pressure and hydrogen percentage is the linear equation because the graphs of the coefficient of variation of the maximum cylinder pressure versus hydrogen percentage have the good fitting when using n = 1.

6. The average peak acceleration and hydrogen correlation shows the decrease of the average peak acceleration in all directions when the hydrogen percentage increased for all conditions tested. Because the amplitude of the engine vibration (the maximum displacement, the maximum velocity, and the maximum acceleration) is varies directly with the maximum cylinder pressure. The maximum cylinder pressure decreases with the hydrogen addition. By this reason, The average peak acceleration will decreases when the hydrogen is added.

7. The average peak acceleration-hydrogen percentage correlations show better curve fittings by second order correlation compared to the first order correlation for all the test conditions. However, the relation between the average peak acceleration and hydrogen percentage is the linear equation because the graphs of the average peak acceleration versus hydrogen percentage have the good fitting when using n = 1.

8. The average peak acceleration and the maximum cylinder pressure correlation shows the increase of the average peak acceleration in all directions when the maximum cylinder pressure increased for all test conditions. Because the

amplitude of the engine vibration (the maximum displacement, the maximum velocity, and the maximum acceleration) is varies directly with the maximum cylinder pressure.

9. The average peak acceleration - the maximum cylinder pressure correlations show better curve fittings by second order correlation compared to the first order correlation for all the test conditions. However, the relation between the average peak acceleration and hydrogen percentage is the linear equation because the graphs of the average peak acceleration versus the maximum cylinder pressure have the good fitting when using n = 1.

10. The peak of the magnitude of the different between the acceleration vector summation at the engine supports with the hydrogen percentage of i% and the hydrogen percentage of 0% decrease by hydrogen addition for all test conditions. The reason for explain this phenomena is the same reason in the section 6th of the conclusion. Although the Δa_{peak} is the magnitude of the acceleration vector summation, the cylinder pressure can transfer to the engine supports as the shaking forces and the shaking torque and it directly affect the engine vibration in all directions. When the hydrogen is added, the maximum pressure decreases and directly affect the Δa_{peak} decreasing.

12. The Δa_{peak} and the hydrogen percentage correlations show better curve fittings by second order correlation compared to the first order correlation for all the test conditions. However, the relation between the Δa_{peak} and hydrogen percentage is the linear equation because the graphs of the Δa_{peak} versus hydrogen percentage have the good fitting when using n = 1.

Recommendation

In the future work, the optimization between the engine vibration decreasing and the maximum pressure variation is the interesting work. When the hydrogen is added, the engine vibration and the maximum cylinder pressure is decrease but the variation of maximum cylinder pressure is increase. If hydrogen is added until the

critical point, the maximum pressure and the engine vibration will be increased by slight hydrogen addition.

LITERATURE CITED

Apostolescu, N. and R. Chiriac. 1996 A study of combustion of hydrogen-enriched gasoline in a spark ignition engine. **SAE.** Paper No. 960603.

Abbas, H. F. and W.M.A. Wan Daud. 2010. Hydrogen production by methane decomposition: A review. **International Journal of Hydrogen.** 35: 1160-1190

Ahmed, S. and M. Krumpelt. 2001. Hydrogen from hydrocarbon fuels for fuel cells. **International Journal of Hydrogen Energy.** 26: 291 – 301.

Antunes, J.M. G., A. R. Mikalsen and A.P. Roskilly. 2009. An experimental study of a direct injection compression ignition hydrogen engine. **International Journal of Hydrogen Energy.** 34: 2009.

Badr, O., G.A. Karim, and B. Liu. 1999. An examination of the flame spread limits in a dual fuel engine. **Applied Thermal Engineering.** 19: 1071-1080.

Balachandran, B. and E. B. Magrab. 2004. **Vibrations.** Thomson Learning, Inc. USA.

Barelli, L., G. Bidini, C. Buratti and R. Mariani. 2009. Diagnosis of internal combustion engine through vibration and acoustic pressure non-intrusive measurements. **Applied Thermal Engineering.** 29: 1707-1713.

Bohn, C., A. Cortabarria, V. H.artel and K. Kowalczyk. 2004. Active control of engine-induced vibrations in automotive vehicles using disturbance observer gain scheduling. **Control Engineering Practice.** 12: 1029-1039.

Bose, P. K. and D. Maji. 2009. An experimental investigation on engine performance and emissions of a single cylinder diesel engine using hydrogen as inducted fuel and diesel as injected fuel with exhaust gas recirculation. **International Journal of Hydrogen Energy.** 34: 4847-4854.

Jeon, B. H., M. Ajovalasit and J. Giacomin. 2009. Effects of gender differences on the subjective perceived intensity of steering wheel rotational vibration based on a multivariate regression model Byung-Ho. **International Journal of Industrial Ergonomics.** 39: 736-743

Cai, J., G. Wang and G. Pan. 2012. Hydrogen production from butyrate by a marine mixed phototrophic bacterial consort. **International Journal of Hydrogen Energy.** 37: 4057-4067.

Cheng, Y., J. Tang, S. Ji and M. Huang. 2012. Combustion timing determination based on vibration velocity in HCCI engines. **Mechanism and Machine Theory.** 58: 20-28.

Cox, K.E. and K.D. Williamson. 1977. **Hydrogen: its technology and implications volume I: hydrogen production technology.** CRC Press, Ohio.

Demirci, U.B., O. Akdim and P. Miele. 2009. Ten-year efforts and a no-go recommendation for sodium borohydride for on-board automotive hydrogen storage. **International Journal of Hydrogen Energy.** 34: 2638-2645.

Dincer, I. and C. Zamfirescu. 2012. Sustainable hydrogen production options and the role of IAHE. **International Journal of Hydrogen Energy.** 1-21.

Eker, S. and F. Kargi. 2010. Hydrogen gas production from electrohydrolysis of industrial wastewater organics by using photovoltaic cells (PVC). **International Journal of Hydrogen Energy.** 35: 12761-12766.

Encyclopedia Britannica Inc. 2007. **Four strokes diesel engine.** Available Source: http://www.britannica.com/EBchecked/media/19423/Four-stroke-diesel-engine-The-typical-sequence-of-cycle-events, May 2, 2012.

Escalante, S. M.A. and A.M. Fernandez. 2010. A review on the technical adaptations for internal combustion engines to operate with gas/hydrogen mixtures**. International Journal of Hydrogen Energy.** 35: 2134-12140.

Ferguson, C.R. 1986. **Internal combustion engines: applied thermosciences.** John Wiley, Newyork.

Fireman, N. 1987. **Naval Education and Training Program Development Center.** Pensacola, Florida.

Fredrik, O. and H. T. Toivonen. 2008. Active torsional vibration control of reciprocating engines. **Control Engineering Practice** 16: 78–88.

Grenoble, D.C., M.M. Estadt and D.F. Ollis, 1981. The chemistry and catalysis of the water gas shift reaction: the kinetics over supported metal catalysts. **Journal of Catalysis.** 67: 90-102.

Hafidi, A. E., B. Martin, A. Loredo and E. Jego. 2010. Vibration reduction on city buses: Determination of optimal position of engine mounts. **Mechanical Systems and Signal Processing.** 24: 2198-2209.

Heywood, J.B. 1988. **Internal combustion engine fundamentals.** McGraw-Hill, Singapore.

Houseman, J. and Hoehn, F.W. (1974) A two-charge engine concept: hydrogen enrichment. **SAE Transaction.** 83 (4): 3522 – 3533, Paper No. 741169.

Jeon, B. H., M. Ajovalasit and J. Giacomin. 2009. Effects of gender differences on the subjective perceived intensity of steering wheel rotational vibration based on a multivariate regression model. **International Journal of Industrial Ergonomics.** 39: 736-743.

Ji, C. and S. Wang. 2009. Effect of hydrogen addition on the idle performance of a spark ignited gasoline engine at stoichiometric condition. **International Journal of Hydrogen.** 34: 3546-3556.

Kargi, F., E. C. Catalkaya and S. Uzuncar. 2011. Hydrogen gas production from waste anaerobic sludge by electrohydrolysis: Effects of applied DC voltage. **International Journal of Hydrogen Energy.** 36: 2049-2056.

Korakianitis, T., A.M. Namasivayam and R.J. Crookes. 2010. Hydrogen dual-fuelling of compression ignition engines with emulsified biodiesel as pilot fuel. **International Journal of Hydrogen.** 35: 13359-13344.

Langohr, D., S. Berthon-Fabry, J. Gonzalez-Aguilar, L. Fulcheri and P. Achard. 2007. Development of a volumetric method-experimental test bench for hydrogen storage characterisation. **International Journal of Hydrogen Energy.** 32: 1846-1854.

Lata, D.B., A. Misra and S. Medhekar. 2011. Investigations on the combustion parameters of a dual fuel diesel engine with hydrogen and LPG as secondary fuels**. International Journal of Hydrogen.** 35: 13808-13819.

Lata, D.B., A. Misra and S. Medhekar. 2012. Effect of hydrogen and LPG addition on the efficiency and emissions of a dual fuel diesel engine. **International Journal of Hydrogen.** 35: 13808-13819.

Li, H. and B.J. Stone. 1999. Time domain of a reciprocating engine. **Mechanical Systems and Signal Processing**. 13 (1): 169-178.

Li, W., F. Gu, A. D. Ball, A. Y. T. Leung and C. E. Phipps. 2001. A study of the noise from diesel engines using the independent component analysis. **Mechanical Systems and Signal Processing**. 15(6): 1165-1184.

Li, Z., S. Akishita and T. Kato. 1997. Engine failure diagnosis with sound signal using wavelet transform. **SAE**. 970034: 79-86.

Liew, C., H. Li, J. Nuszkowski, S. Liu, T. Gatts, R. Atkinson and N. Clark. 2010. An experimental investigation of the combustion process of a heavy-duty diesel engine enriched with H_2. **International Journal of Hydrogen.** 35: 11357-11365.

Lilik, G. K., H. Zhang, J. M. Herreros, D. C. Haworth and A. L. Boeh. 2010. Hydrogen assisted diesel combustion. **International Journal of Hydrogen.** 35: 4382-4398.

Loutridis, S., Th. Gialamas, I. Gravalos, D. Moshou, D. Kateris, P. Xyradakis and Z. Tsiropoulos. 2011. A study on the effect of electronic engine speed regulator on agricultural tractor ride vibration behavior. **Journal of Terramechanics** 48:139–147.

Luzan, S.M., H. Jung, H. Chun and A.V. Talyzin. 2009. Hydrogen storage in Co-and Zn-based metal-organic frameworks at ambient temperature. **International Journal of Hydrogen Energy.** 34: 9751-9759.

McWilliam, L. 2008. **Combined hydrogen diesel combustion: an experimental investigation into the effects of hydrogen addition on the exhaust gas emissions, particulate matter size distribution and chemical composition.** Ph.D. Thesis, Brunel University.

Mabie, H. H. and C. F. Reinholtz. 1987. **Mechanisims and dynamics of machinery.** John Wiley & Son, Inc. USA.

Morris, D. J., D.F. Bahr and M.J. Anderson. 2008. Displacement amplification in curved piezoelectric diaphragm transducers. **Sensors and Actuators.** 141: 262-265.

Miyamoto, T., H. Hasegawa, M. Mikami, N. Kojima, H. Kabashima and Y. Urata. 2011. Effect of hydrogen addition to intake gas on combustion and exhaust emission characteristics of a diesel engine. **International Journal of Hydrogen.** 36: 13138-13149.

Muradov, N. 2000. **Advances in hydrogen energy.** Kluwer Academic/Plenum Publishers, Newyork.

Profeti, L.P.R., E.A.Ticianelli and E.M. Assaf. 2009. Production of hydrogen via steam reforming of biofuels on Ni/CeO2–Al2O3 catalysts promoted by noble metals. **International Journal of Hydrogen Energy.** 34: 5049-5060.

Pukazhselvan, D., 2012. Effect of crystallite size of Al on the reversible hydrogen storage of NaAlH4 and few aspects of catalysts and catalysis. **International Journal of Hydrogen Energy.** 37: 9696-9705.

Williams, L.O. 1980. **Hydrogen power an introduction to hydrogen energy and its application.** Pergamon Press, Oxford.

Johnsson, R. 2006. Cylinder pressure reconstruction based on complex radial basis function networks from vibration and speed signals. **Mechanical Systems and Signal Processing.** 20: 1923-1940.

Saravanan. N., G. Nagarajan, C. Dhanasekaran, and K.M. Kalaiselvan. 2007. Experimental investigation of hydrogen port fuel injection in DI diesel engine. **International Journal of Hydrogen.** 35: 4071-4080.

Shin, B., Y. Cho, D. Han, S. Song, and K. M. Chun. 2011. Investigation of the effects of hydrogen on cylinder pressure in a split-injection diesel engine at heavy EGR. **International Journal of Hydrogen.** 36: 13158-13170.

Sun, Z., F.S. Liu, X.H. Liu, B.G. Sun and D.W. Sun. 2012. Research and development of hydrogen fuelled engines in China. **International Journal of Hydrogen Energy.** 37: 664-681.

Szwaja, S. and K. Grab-Rogalinski. 2009. Hydrogen combustion in a compression ignition diesel engine**. International Journal of Hydrogen Energy.** 37: 4413-4421.

Tomita, E., N. Kawahara, Z. Piao, S. Fujita, and Y. Hamamoto. 2001. Hydrogen combustion and exhaust emissions ignited with diesel oil in a dual fuel engine. **SAE.** Paper No. 2001-01-3503.

Tsolakis, A., A. Megaritis, and S.E. Golunski. 2005. Reaction profiles during exhaustassisted reforming of diesel engine fuels. **Energy & Fuels.** 19: 744-752.

Varde, K.S. and G.A. Frame GA. 1983. Hydrogen aspiration in direct injection type diesel engine-its effect on smoke and other engine performance parameters. **International Journal of Hydrogen.** 8: 549-555.

Wakui, s., A. Noda, T. Akiyama, and M. Takahashi. 2007. Development of velocity sensor with high frequency band and its application to a vibration isolate table. **Precision Engineering.** 31: 146-455.

Wang[1] , S., C. Ji and B. Z. 2010. Effect of hydrogen addition on combustion and emissions performance of a spark-ignited ethanol engine at idle and stoichiometric conditions. **International Journal of Hydrogen.** 35: 9205-9213.

Wang[2] , S., C. Ji, B. Zhang and X. Liu. 2012. Performance of a hydroxygen-blended gasoline engine at different hydrogen volume fractions in the hydroxygen. **International Journal of Hydrogen.** 37: 13209-13218.

Wu, H.W. and Z.Y. Wu. 2012. Investigation on combustion characteristics and emissions of diesel/hydrogen mixtures by using energy-share method in a diesel engine. **Applied Thermal Engineering.** 42: 154-162.

YANG, S. and R.F GIBSON. 1996. Vibration characteristic and comparisons of automotive engine valves made from conventional and non-conventional materials. **Journal of Sound and Vibration**. 191(5): 986-992.

Züttel, A. 2003. Materials for hydrogen storage. **Materials Today.** 6 (9): 24 – 33.

Xu, J., X. Zhang, J. Liu and L. Fan. 2010. Experimental study of a single-cylinder engine fueled with natural gas–hydrogen mixtures. **International Journal of Hydrogen.** 35: 2009-2914.

APPENDIX

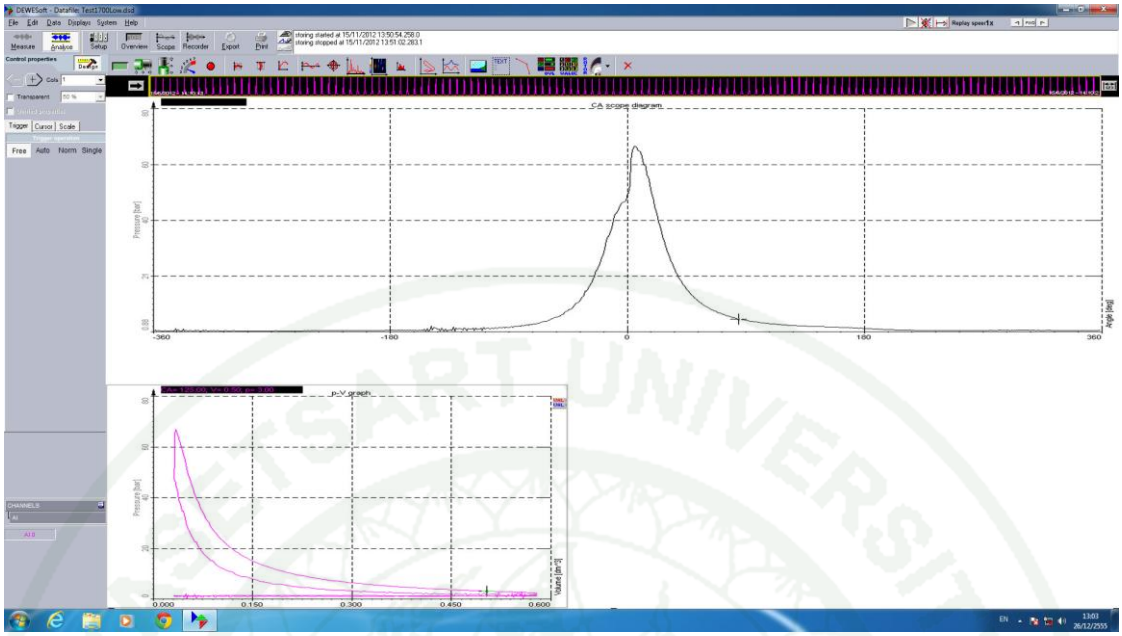

Appendix Figure 1 DEWESoft software for cylinder pressure measurement

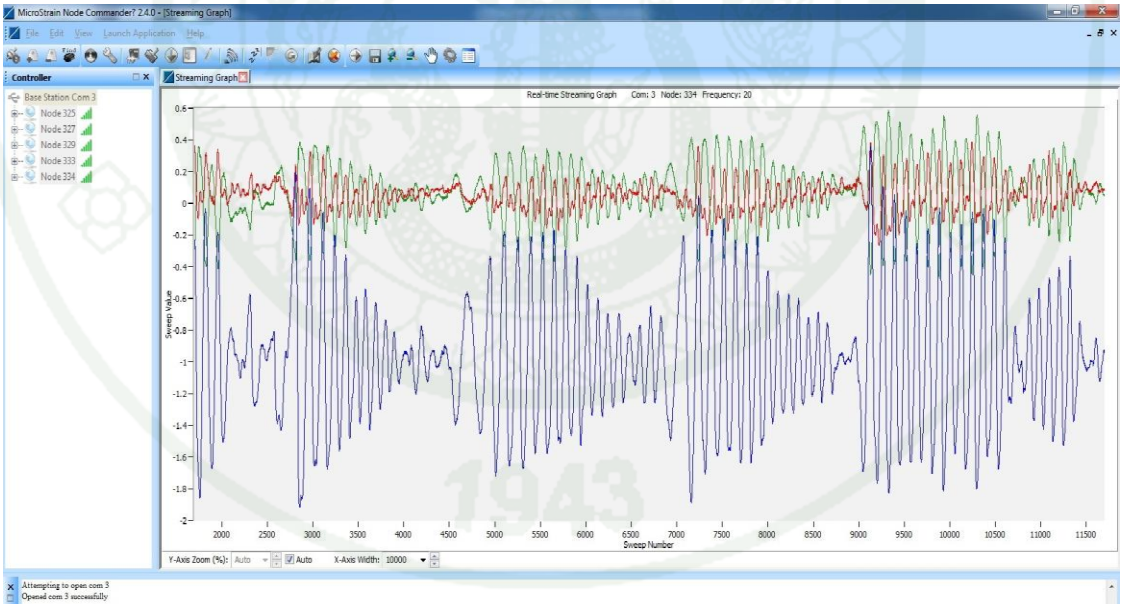

Appendix Figure 2 Node Commander software for engine vibration measurement

Appendix Figure 3 Hydrogen inlet at intake manifold

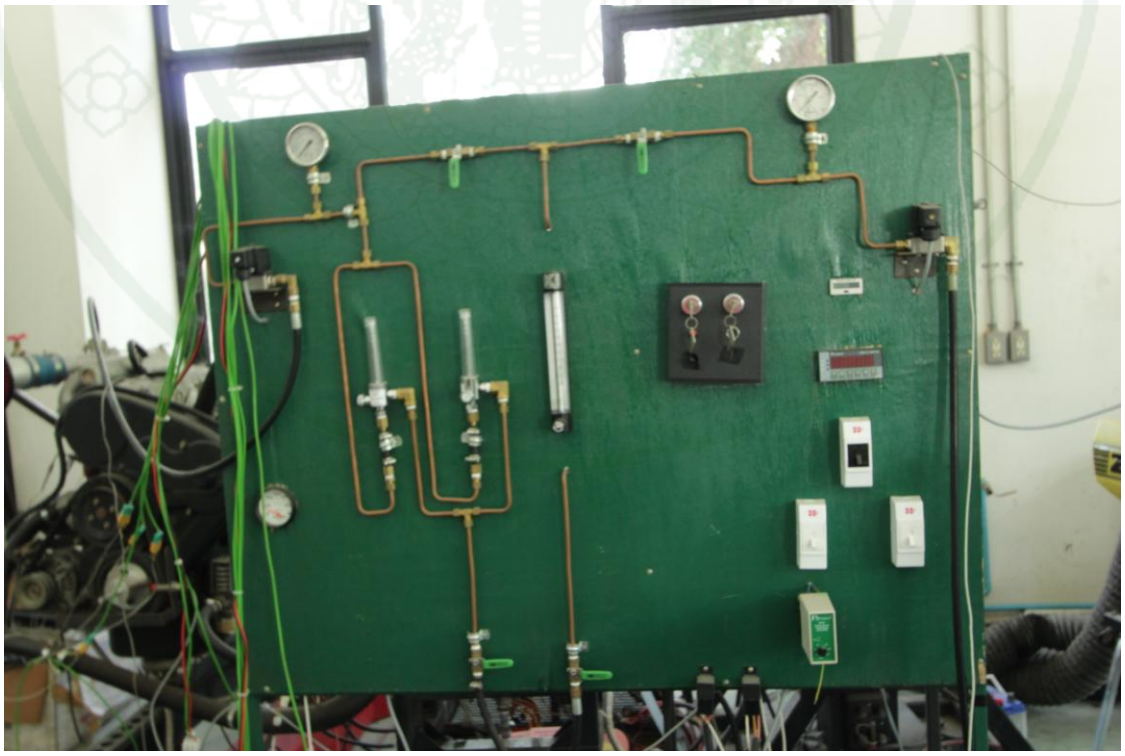

Appendix Figure 4 Hydrogen flow meter and control valves

Appendix Figure 5 Hydrogen cylinders

CURRICULUM VITAE

NAME : Mr. Boonthum Wonchai

BIRTH DATE : July 15, 1975

BIRTH PLACE : Phayao, Thailand

EDUCATION :

YEAR	INSTITUTE	DEGREE/DIPLOMA
1997	Chiang Mai Univ.	B.Eng. (Mechanical Engineering)
2004	Kasetsart Univ.	M.Eng. (Mechanical Engineering)